HOLLOW CYLINDER DYNAMIC PRESSURIZATION AND RADIAL FLOW THROUGH PERMEABILITY TESTS FOR CEMENTITIOUS MATERIALS

A Thesis

by

CHRISTOPHER ANDREW JONES

Submitted to the Office of Graduate Studies of
Texas A&M University
in partial fulfillment of the requirements for the degree of

MASTER OF SCIENCE

August 2008

Major Subject: Civil Engineering

HOLLOW CYLINDER DYNAMIC PRESSURIZATION AND RADIAL FLOW THROUGH PERMEABILITY TESTS FOR CEMENTITIOUS MATERIALS

A Thesis

by

CHRISTOPHER ANDREW JONES

Submitted to the Office of Graduate Studies of
Texas A&M University
in partial fulfillment of the requirements for the degree of

MASTER OF SCIENCE

Approved by:

Chair of Committee,	Zachary C. Grasley
Committee Members,	K. Ted Hartwig
	Robert L. Lytton
Head of Department,	David Rosowsky

August 2008

Major Subject: Civil Engineering

ABSTRACT

Hollow Cylinder Dynamic Pressurization and Radial Flow Through Permeability Tests for Cementitious Materials. (August 2008)

Christopher Andrew Jones, B.S., Texas A&M University; B.A., Southwestern University

Chair of Advisory Committee: Dr. Zachary C. Grasley

Saturated permeability is likely a good method for characterizing the susceptibility of portland cement concrete to various forms of degradation; although no widely accepted test exists to measure this property. The hollow cylinder dynamic pressurization test is a potential solution for measuring concrete permeability. The hollow cylinder dynamic pressurization (HDP) test is compared with the radial flow through (RFT) test and the solid cylinder dynamic pressurization (SDP) test to assess the accuracy and reliability of the HDP test.

The three test methods, mentioned above, were used to measure the permeability of Vycor glass and portland cement paste and the results of the HDP test were compared with the results from the SDP and RFT tests. When the HDP and RFT test results were compared, the measured difference between the mean values of the two tests was 40% for Vycor glass and 47% for cement paste. When the HDP and SDP tests results were compared, the measured difference with Vycor glass was 53%. The cement paste

permeability values could not be compared in the same manner since they were tested at various ages to show the time dependency of permeability in cement paste.

The results suggest good correlation between the HDP test and both the SDP and RFT tests. Furthermore, good repeatability was shown with low coefficients of variation in all test permutations. Both of these factors suggest that the new HDP test is a valid tool for measuring the permeability of concrete materials.

DEDICATION

To Lauren and the girls.

ACKNOWLEDGEMENTS

I would like to thank my committee chair, Dr. Grasley, for teaching me and for helping me to gain a more complete understanding of the materials field. His help and guidance has been invaluable in this process. Furthermore, I appreciate the sacrifice of my committee members who supported me through the revision process.

Thanks also go to my friends and coworkers without whom I would surely have gone crazy. I also want to extend my gratitude to the Ready Mix Concrete Foundation, which provided funding and support for my work. Additionally, the Transportation Scholars Program, Jones and Carter Inc., and the Chemical Lime Company have all financially supported my educational endeavors.

Finally, thanks to my mother and father for their encouragement and to my wife for all her patience and love.

NOMENCLATURE

w/c	water to cement
HDP	hollow dynamic pressurization
SDP	solid dynamic pressurization
RFT	radial flow through

TABLE OF CONTENTS

Page

Page

LIST OF FIGURES

Page

Page

LIST OF TABLES

Page

1 INTRODUCTION

1.1 PROBLEM STATEMENT

Though generally considered a very durable material, portland cement concrete has shown significant susceptibility to various forms of chemical and physical damage which reduce the service life of many concrete structures. Not surprisingly, the problem of concrete durability has a significant monetary impact on society. Various studies have tried to quantify the impact of these mechanisms with most estimates ranging in the billions of dollars per year in the United States alone [1] where much of the cost is borne by the taxpaying public. Corrosion of reinforcing steel is the most widespread form of concrete deterioration which is directly related to the ability of external chloride ions (usually in solution) to move into the pore network and react with the reinforcement [2].

Many if not all, of these degradation mechanisms are tied to moisture within the concrete. Alkali-aggregate reactivity [3], sulfate attack [4], corrosion of reinforcing steel [5], and freeze-thaw damage [2] are examples of real-world problems that are related to moisture intrusion into the pore network of the concrete. It has long been theorized that there is a fundamental link between concrete permeability and its durability [6] though real scientific data to support this claim is lacking. In many cases the actual mechanism of ion or moisture movement within the material is not saturated flow, but vapor

---

This thesis follows the style of Cement and Concrete Research.

diffusion or capillary sorption [7]. Nonetheless, the interplay of the various transport mechanisms is far from being fully understood, and saturated permeability provides a consistent and reproducible measurement of the penetrability of the concrete. In theory establishing the connection between saturated permeability and the various forms of concrete degradation would be a rather simple experiment, but due to the lack of a consistent and repeatable concrete permeability test the relationship between the various degradation mechanisms and permeability is not clearly defined.

As mentioned above, permeability, the relative resistance of a material to fluid transmission under pressure, seems to be a very good parameter for characterizing durability in concrete, though traditional methods of measuring this property leave much to be desired. Despite the importance of moisture intrusion into cementitious materials, and the potential utility for assessing concrete durability, to date no widely accepted technique for quantifying material permeability has been developed [7]. As the construction industry as a whole moves toward performance specifications the need arises for a reliable method of assessing the durability potential of portland cement concrete. An expeditious, accurate and consistent permeability test could potentially help fill this void. This type of test could be used for qualifying concrete mixtures by casting and testing trial cylinders. The test could also be used in the quality control/quality assurance by testing cylinders or cores respectively.

This research presents a pair of possible concrete permeability tests than could accommodate various materials with a wide range of material permeability values. Furthermore, the tests will be relatively quick to run and will show good repeatability and accuracy.

1.2 SCOPE

The permeability measurement techniques used in this research are generally not widely used and in the case of the Hollow Dynamic Pressurization (HDP) technique mostly unprecedented. For this reason, this research required a two part approach. The first part included the conceptual and theoretical development of the test methods while the second part included the experimental comparison of the methods to assess their accuracy, repeatability, and agreement. The general objectives of this research can be summarized as the successful development of an apparatus which can be used to test the permeability of various cementitious materials ranging from very permeable to almost impermeable.

1.3 THESIS OUTLINE

The second section of this document identifies the prior attempts to address the problems outlined in section 1.1. The third section outlines the development of the physical permeability testing apparatus and describes each apparatus in detail. The fourth section details the theory behind the radial flow through (RFT) test and the hollow dynamic pressurization (HDP) test. The fifth section discusses the specimen preparation and the general scheme for conducting the experimental part of the research. The sixth section

presents the results of the testing of both Vycor glass as well as cementitious materials. The seventh section presents a summary of, and the conclusions gained from, this research.

2 CURRENT STATE OF PERMEABILITY MEASUREMENTS

Permeability is generally described according to Darcy's Law

$$J = -\frac{k}{\eta_L}\nabla P \tag{1}$$

which relates the amount of fluid flow through a material, *J*, to the applied pressure gradient, ∇P, the viscosity of the fluid moving through the material, η_L, and the permeability, *k*. The classic problem with measuring the permeability of concrete is that the permeability is relatively low, and as such the amount of fluid flow is also relatively low. Since the fluid flow is typically measured, a low volume of fluid movement makes measurement sensitivity much more important. Practically the level of sensitivity needed is often difficult to obtain.

2.1 DIRECT PERMEABILITY MEASUREMENT

A typical permeability test would involve applying a differential pressure head to a sample and measuring the amount of fluid that passes through the sample in a specified period of time. Ye demonstrates a typical measurement technique involving several samples measured simultaneously [8]. Hearn and Mills propose a similar apparatus [9], though only one specimen is tested at a time. This measurement technique is considered direct since the measured quantity is the amount of fluid permeating through the material with respect to time. This type of method tests the permeability of a specimen and

assumes that the material is homogeneous across the entire specimen but cracks or other irregularities can have a significant impact on the measured permeability.

The chief drawback of current permeability measurement techniques is the large amount of time required to run a single test. Traditional methods of testing concrete permeability can take as long as several weeks to run and show high variability and limited repeatability [10]. Saturation of the specimens plays a role in the equilibration time for each direct permeability test. Specimens containing as little as 1% entrapped air (by volume) take 10 times longer to reach equilibrium flow than a saturated specimen [11]. Furthermore, the long test duration completely precludes permeability testing at early ages since the specimen being tested would age significantly during the test. To address the problem of slow flow rates, an increased pressures gradient is often employed to minimize test duration. With the increased pressure often comes a host of other problems such as specimen damage or leaking around seals [12].

2.2 NON DIRECT PERMEABILITY MEASUREMENT

Novel approaches based on poromechanics have recently been developed in an effort to more rapidly and accurately measure the permeability of cementitious materials. Poromechanical techniques involve measuring the time dependent deformation of a specimen related to fluid flow in the pore network induced by externally applied stress or temperature change. All of these tests have the advantage of being fast (the analysis is performed on non-steady state flow), though in some cases, the test requirements are impractical. Various examples are discussed by Scherer et al. [12] including beam

bending [13], thermopermeametry [14], and dynamic pressurization [15]. The beam bending technique involves a saturated, slender rod of material that is bent in a simple three point loading while the amount of force required to maintain the displacement is measured. As the rod is flexed, the material above the neutral axis experiences a compressive stress while the material below the neutral axis experiences a tensile stress. This stress gradient drives fluid from the top of the beam to the bottom and the time required to relax the induced stress indicates the permeability of the material. Thermopermeametry forces fluid movement by applying an increased temperature to one end of a saturated sample and measures the kinetics of thermal dilation. Both of these methods work reasonably well for model materials like Vycor glass or cement paste, but have significant limitations when real construction materials are used. The dynamic pressurization technique is of great interest because it seems to have the fewest practical limitations and therefore could potentially be used outside of research to aid the construction facilitation process.

The dynamic pressurization method involves the rapid hydrostatic pressurization of a cylindrical specimen within a pressure cell. The cylinder responds with a volumetric contraction that is dependent on the bulk modulus of the specimen and the pore fluid [15]. Then, as fluid flows into the pores of the specimen, the cylinder expands at a rate that is related to the rate of fluid flow in the pore network. By measuring the strain-time history, the permeability of the specimen can be obtained in a reasonable amount of time since the data collection occurs during the non-steady state flow condition.

The primary drawback of the SDP method is the requirement for complete saturation of the pore network prior to testing a sample [16]. Since gas bubbles are highly compressible, their presence in the pore network slows the expansion. Even though fluid is entering the specimen, the associated fluid influx goes to compressing the bubbles rather than increasing the pore fluid pressure. Finally, since the response is time dependent, this delay makes the results difficult if not impossible to interpret. Air volume fractions of 1% will double the equilibration time of the test, which significantly changes the measured permeability [15]. Obtaining complete saturation is possible for a lab prepared sample with a relatively high *w/c* (0.5 or greater) when proper procedures are observed from the moment of casting. Unfortunately, as the *w/c* drops, or if the proper procedures are neglected, saturation becomes much more difficult to obtain. Re-saturating a dried specimen, such as a field core, is equally difficult based on previous experience. A *w/c* of 0.4 represents the extreme practical limit of the SDP method and most realistic construction materials are somewhere near this value or even lower.

3 DEVELOPMENT OF A NEW PERMEABILITY TESTING APPARATUS

3.1 GENERAL APPARATUS REQUIREMENTS

As mentioned previously, the dynamic pressurization technique has a major limitation regarding the saturation of specimens. For this reason, one of the primary focuses of this research is to develop a method of saturating existing specimens for use with the dynamic pressurization method. To accomplish this task, a hollow specimen is considered so that a hydrostatic pressure can be applied to the outer radial surface of the specimen, forcing fluid into the pore network and forcing air through to the inside hollow core. This arrangement allows a relatively high hydrostatic pressure to be applied which allows for a large pressure gradient, while posing little danger of damaging the specimen. It is clear that this arrangement allows for a flow through permeability measurement to be made while saturating the specimen for dynamic pressurization. The apparatus will also need to be able to perform this type of flow through permeability measurement while also being able to perform dynamic pressurization method.

For the saturating specimens and for the dynamic pressurization technique, a significant hydrostatic pressure needs to be applied to a specimen. With this in mind, the primary component of the permeability testing apparatus is the pressure vessel which can withstand a significant internal pressure without leaking. Ideally the pressure vessel

would serve as a base on which various permeability tests could be run. As mentioned previously, measuring concrete permeability requires great sensitivity so an LVDT with high accuracy is employed. Also since many data points must be collected for both the dynamic pressurization method and for the flow through method, an electronic data collection system should be employed to minimize the time required with the apparatus. The apparatus should be able to test very permeable (young or high *w/c*) as well as very impermeable specimens (mature or low *w/c* or both).

The preceding requirements are very general and would apply to any concrete permeability testing apparatus. Because the dynamic pressurization technique is employed, certain other requirements are considered. An interesting requirement related to applying high pressure to a sample is the need for a means of reliving the pressure slowly to avoid high tensile stresses associated with a rapid depressurization of the pressure vessel.

3.2 RADIAL FLOW THROUGH APPARATUS

While saturating the specimen for dynamic pressurization, a flow through measurement of permeability can be made by applying the radial flow through (RFT) technique. The RFT test is relatively simple in concept and involves the application of a hydrostatic pressure to the outer face of a hollow cylindrical sample. This test apparatus is a hybrid between one used by Banthia [17] and one developed by El Dieb and Hooten [18]. As the fluid moves through the pore network of the sample there is a net increase in the fluid level inside the center hollow "tube." By monitoring this fluid level with an LVDT

over time, a flow rate can be determined and the intrinsic permeability, *k*, can be calculated according to

$$k = \frac{q\eta_L \ln[R_o / R_i]}{2P_{out}\pi h}, \quad (2)$$

where R_o and R_i are the outer and inner radii of the sample and h is the height or length of the sample. P_{out} is the pressure applied, q is the flow rate measured with the LVDT and η_L is the viscosity of the fluid used for testing. The intrinsic permeability, k, is a property only of the porous body through which the fluid flows. Intrinsic permeability has the dimensions of length squared, and can be converted to water permeability, k_w, according to

$$k_w = \frac{\rho g}{\eta_w} k, \quad (3)$$

where ρ is the density of water, g is the acceleration due to gravity and η_w is the viscosity of the water. At room temperature, k_w (m/s) is approximately equal to 10^7 k (m^2). Figure 1 illustrates the flow through apparatus.

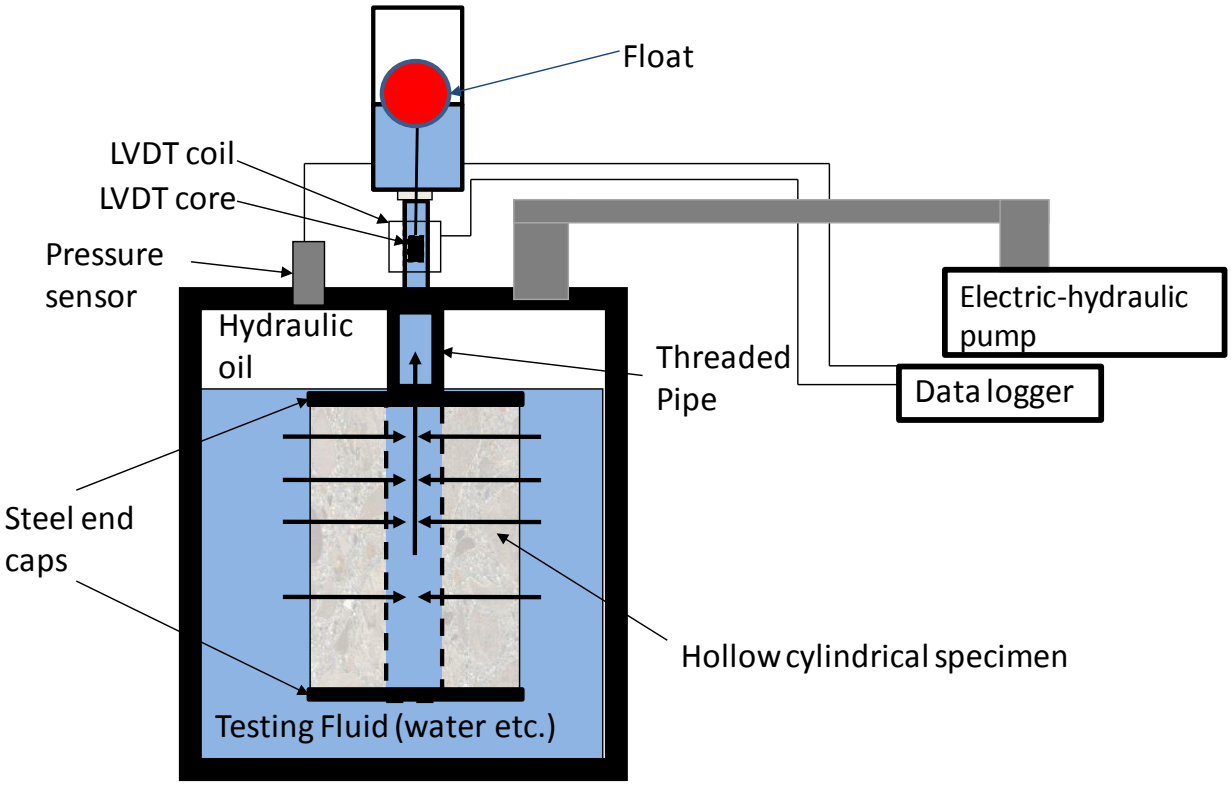

Figure 1: The radial flow through (RFT) apparatus that pressurizes the outer surface of a sample and monitors the fluid volume that flows through as a function of time.

The apparatus shown in Figure 1 allows various levels of pressure to be applied to the sample depending on its particular geometry, its relative permeability, and its strength. For a more impermeable or thicker specimen, the pressure on the outer face can be increased to increase the rate of fluid flow through the sample. Conversely, a very permeable (young) or thin walled specimen can also be tested by reducing the applied pressure.

3.3 HOLLOW DYNAMIC PRESSURIZATION APPARATUS

The hollow dynamic pressurization apparatus involves a pressure chamber, in which the specimen is pressurized, that can withstand an internal pressure of 13.5 MPa (2000 psi). As shown in Figure 2, the hollow specimen is attached to the top of the pressure chamber and is suspended in the fluid. The stainless steel LVDT connecting rod runs through the hollow center of the specimen up to the LVDT coil. This LVDT system (which is also used in the SDP) is completely non-contact, which allows the chamber to be completely sealed with all electrical connections outside the chamber.

The hydrostatic pressure was applied using an electric hydraulic pump which produced a relatively constant pressure that was regulated with a vented, inline pressure regulator. This setup allowed both pressurization and step depressurization, which is important to avoid high internal tensile stresses associated with a rapid release of the applied pressure [15]. The pressure was recorded with an electronic pressure sensor capable of 0.25% accuracy and was logged along with the displacement data using an electronic data logger.

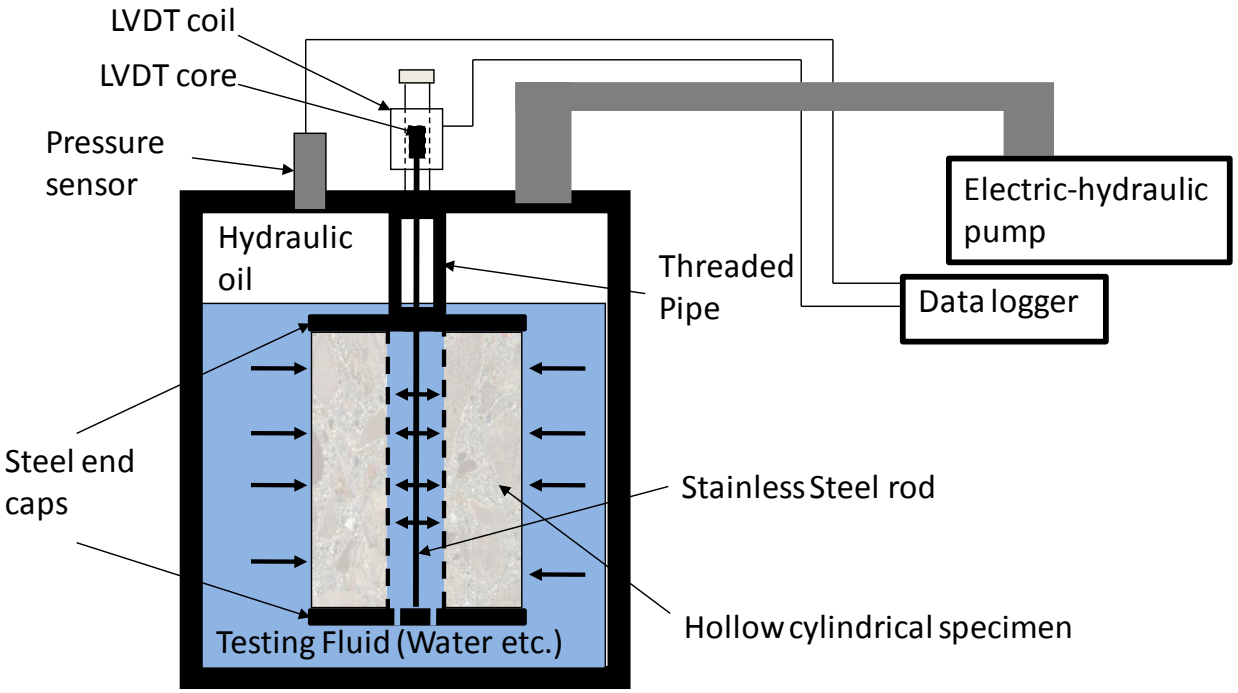

Figure 2: The hollow dynamic pressurization (HDP) apparatus consists of a pressure vessel and a non-contact LVDT system which measures the axial deformation of the specimen.

As mentioned above, the main advantage of the hollow specimen geometry is the ability to saturate a specimen by applying an external hydrostatic pressure. To facilitate this procedure, both the end plates and caps, shown in the figure on page 33, were drilled through and tapped with a 0.25 inch NPT pipe tap so that the specimen could be threaded onto a 0.25 inch pipe nipple which allowed the specimen to "hang" from the lid of the pressure chamber. The specimen was also plugged at the bottom end with a 0.25 inch NPT plug so that fluid only traveled through the sample and not through the ends. To saturate the specimen, a moderate hydrostatic pressure (70 kPa to 3.5 MPa) was applied to the outer surface of the specimen depending on the age and relative strength of the specimen. Since the specimen was sealed at both ends, the fluid would flow

through the material into the inner core, thus saturating the pore network. The amount of fluid which moved through the specimen was monitored with time and once an equilibrium flow rate was established, the specimen was considered saturated. This moderate pressure was then relieved slowly to minimize tensile stress related micro-cracking, and then the plug at the bottom of the specimen was removed and replaced with a perforated 0.25 inch NPT plug which was attached to the LVDT connecting rod. The saturated specimen was then ready for HDP testing.

3.4 SOLID DYNAMIC PRESSURIZATION APPARATUS

The SDP apparatus is very similar to the hollow dynamic pressurization apparatus, but for a few key differences. The solid specimens rest on the bottom of the pressure chamber with the stainless steel LVDT connecting rod extending from the top of the specimen up to the LVDT coil as shown in Figure 3. Since no end plates were used with the solid specimens, the LVDT connecting rod was attached to the top of the solid specimens directly. With the Vycor rods, a small nut was threaded on and then glued to the LVDT connecting rod and this nut was glued directly to the top surface of the Vycor rod. For the cement paste, a small hole, slightly larger in diameter than the LVDT connecting rod, was drilled into the top of the specimen, to a depth of approximately 5 mm, and was then filled with marine epoxy. The rod was then fitted into this small hole and the epoxy was allowed to cure. This particular arrangement is necessary since there is no hollow center in the specimen through which to run the steel LVDT connecting rod.

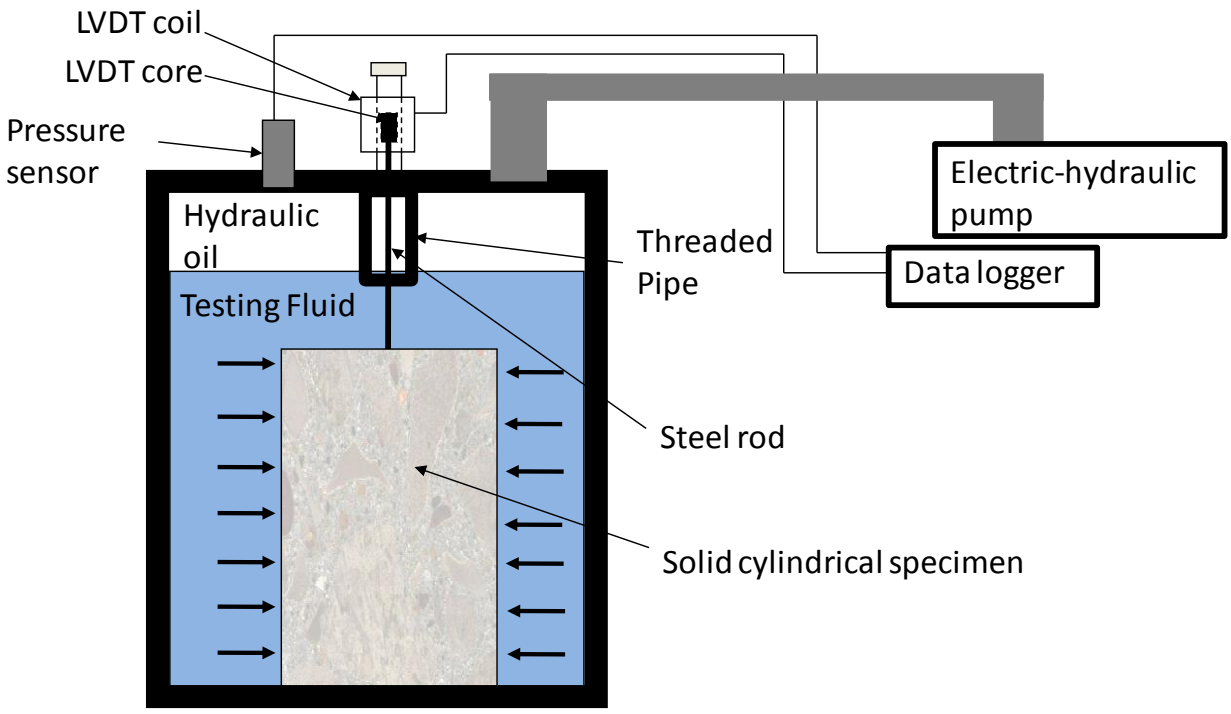

Figure 3: The solid dynamic pressurization (SDP) apparatus consists of a pressure vessel and a non-contact LVDT which measures the axial contraction of the specimen.

In order to measure the displacement of the specimen as it is compressed, the same non-contact LVDT system was employed with an electronic automated data logger. The magnetic core of the LVDT was mounted to a stainless steel threaded rod and the rod was attached to the specimen. In the case of the solid samples the rod was attached to the top plate of cement paste samples by means of a threaded connection and a stop nut, while the threaded stainless steel rod was glued directly to the top of the Vycor glass rod since no plates were used.

4 TEST THEORY

This research utilized three tests, one flow through test and two geometries of the dynamic pressurization technique. The theory behind the solid cylinder dynamic pressurization test was developed by Scherer [15]. In this research the hollow cylinder geometry was considered for dynamic pressurization and for flow through. In the subsequent sections the theory behind the radial flow through (RFT) test and the hollow cylinder dynamic pressurization (HDP) test are derived.

4.1 RADIAL FLOW THROUGH

Darcy's law may be expressed as

$$J = -\frac{k}{\eta_L}\nabla P \quad , \tag{4}$$

where J is the flux (dimensions of length/time), η_L is fluid viscosity (dimensions of length-time), k is the intrinsic permeability (dimensions of length squared), P is pore fluid pressure, and ∇ is the gradient, expressed as

$$\nabla = \hat{r}\frac{\partial}{\partial r} + \hat{\theta}\frac{\partial}{\partial \theta} + \hat{z}\frac{\partial}{\partial z}. \tag{5}$$

For the radial permeameter problem,

$$\nabla P = \frac{\partial P}{\partial r} \tag{6}$$

since the pressure distribution is irrotational and does not vary along the length. Therefore,

$$J = \frac{q}{A} = \frac{-k}{\eta_L}\frac{\partial P}{\partial r}, \tag{7}$$

where q is the flow rate (dimensions of volume/time), and A is the cross-sectional area of flow, which is $2\pi rh$ where r is the radial coordinate and h is the specimen height. Eq. (7) may then be expressed as

$$\frac{q}{2\pi rh} = \frac{-k}{\eta_L}\frac{\partial P}{\partial r}, \tag{8}$$

the solution of which is

$$P(r) = C - \frac{q\eta_L \ln[r]}{2k\pi h}, \tag{9}$$

where C is a constant. For a hollow cylinder with a pressure P_{out} applied to the outer surface, and with a negligible pressure on the inner surface,

$$C = \frac{q\eta_L \ln[R_o]}{2k\pi h}, \tag{10}$$

where a is the inner radius. The permeability solved as a function of flow rate due to P_{out} is

$$k = \frac{q\eta_L \ln[R_0 / R_i]}{2P_{out}\pi h}. \tag{11}$$

4.2 HOLLOW DYNAMIC PRESSURIZATION

The general solution for the axial strain in a hollow poroelastic cylinder has been derived by Kanj and Abouslemein [19, 20] and [21]. While this solution may be used to solve the problem in the Laplace transform domain, it requires numerical inversion into the time domain. In order to devise a simple approximate solution in the time domain, it is useful to approach the problem in the same manner that Scherer [15] solved for the axial strain in a solid poroelastic cylinder exposed to hydrostatic pressure. Viscoelastic relaxation of the materials was not considered since Scherer [15] demonstrated that such relaxation had a minimal effect on the outcome of the test.

The poroelastic constitutive equation for the axial plane strain (ε_z) is

$$\varepsilon_z(t) = \frac{1}{E_p}\left\{\sigma_z(r,t) - \upsilon_p\left[\sigma_r(r,t) + \sigma_\theta(r,t)\right]\right\} + \varepsilon_f(r,t) \quad , \tag{12}$$

where σ_z, σ_r, and σ_θ are the axial, radial, and tangential stresses, E_p is the Young's modulus of the porous body, υ_p is the Poisson's ratio of the porous body, and *r* and *t* are the radial coordinate and time, respectively. The free strain is given by

$$\varepsilon_f(r,t) = \frac{bP(r,t)}{3K_p} \quad , \tag{13}$$

where *P* is the pore pressure, K_p is the bulk modulus of the porous body, and

$$b = 1 - \frac{K_p}{K_s} \tag{14}$$

is the Biot coefficient. K_s is the bulk modulus of the solid material skeleton. Assuming the pore fluid transport obeys Darcy's Law, the continuity equation may be expressed as

$$\frac{\dot{P}(r,t)}{M} + b\dot{\varepsilon}(r,t) = \frac{k}{\eta_L}\nabla^2 P(r,t) \tag{15}$$

,

where *k* is the intrinsic permeability of the porous body (in dimensions of length squared), η_L is the pore fluid viscosity, ε is the volumetric strain, the overhead dots represent a partial time derivative, and

$$M = 1/\left(\frac{\phi}{K_L} + \frac{b-\phi}{K_s}\right) \tag{16}$$

is the Biot modulus. K_L is the bulk modulus of the pore fluid and ϕ is the volumetric pore fraction of the porous body.

In this problem, we are considering a porous hollow cylinder that is pressurized hydrostatically. However, no fluid flow is allowed through the axial faces such that only radial flow is considered. Therefore, eq. (15) becomes

$$\frac{\dot{P}(u,t)}{M} + b\dot{\varepsilon}(u,t) = \frac{k}{\eta_L (R_o - R_i)^2}\frac{1}{u}\frac{\partial}{\partial u}\left(u\frac{\partial P(u,t)}{\partial u}\right) \tag{17}$$

where $u = r/(R_o - R_i)$ is a dimensionless radial coordinate with *r* the radial coordinate, R_o the outer radius of the cylinder, and R_i the inner radius of the cylinder. As with a solid cylinder [15, 16], the volumetric strain of a hollow cylinder exposed to an applied hydrostatic pressure P_A is

$$\varepsilon(u,t) = 3\beta\varepsilon_f + 3(1-\beta)\langle\varepsilon_f(t)\rangle - \frac{P_A}{K_p} \tag{18}$$

where $\langle\varepsilon_f(t)\rangle$ is the volumetric average of the free strain such that

$$\langle\varepsilon_f(t)\rangle = \frac{2}{R_o^2 - R_i^2}\int_{R_i}^{R_o}\varepsilon_f(r,t)rdr = \frac{2(R_o - R_i)}{R_o + R_i}\times\int_{R_i/(R_o-R_i)}^{R_o/(R_o-R_i)}\varepsilon_f(uR_o - uR_i, t)udu\,. \tag{19}$$

The constant β is defined according to [15]

$$\beta = \frac{1+\nu_p}{3(1-\nu_p)}\,. \tag{20}$$

By combining eqs. (13), (17), and (19) a partial differential equation for the pore pressure is obtained in the same form as for a solid cylinder,

$$\frac{\partial P(u,\theta)}{\partial\theta} + \left(\frac{(1-\beta)b\lambda}{1-(1-\beta)b\lambda}\right)\frac{\partial\langle P(\theta)\rangle}{\partial\theta} - \left(\frac{\lambda}{1-(1-\beta)b\lambda}\right)\frac{\partial P_A(\theta)}{\partial\theta} = \frac{1}{u}\frac{\partial}{\partial u}\left(u\frac{\partial P(u,\theta)}{\partial u}\right), \tag{21}$$

where

$$\lambda = \frac{Mb}{K_p + Mb^2}\,. \tag{22}$$

The dimensionless time is $\theta = t/\tau_v$ where τ_v is a relaxation time expressed as

$$\tau_v = \frac{\eta_L (R_0 - R_i)^2}{k}\left(\frac{\beta b^2}{K_p} + \frac{1}{M}\right), \tag{23}$$

which controls the rate of pore pressure equilibration. In comparison to the relaxation time for the solid cylinder denoted in [15], the only difference in the expression for the relaxation time of the hollow cylinder is that the radius of the solid cylinder, *R*, is replaced by the term $(R_0 - R_i)$.

The goal of the following discussion is to illustrate a method for deriving an approximate analytical expression for τ_v as a function of $\varepsilon_z(t)$ in the time domain. The solution of eq. (21) is readily obtained in the Laplace transform domain. The result is the transformed pressure as a function of *u* and *s* (the reduced time transform variable). Consider a step pressurization as a function of time, i.e.

$$P(t) = H(t)P_A, \tag{24}$$

where $H(t)$ is the Heaviside function and P_A is the magnitude of the applied pressure. In this case, the axial strain immediately after the pressurization is

$$\varepsilon_z(t^{0+}) = -(1 - b\lambda)\frac{P_A}{3K_p}, \tag{25}$$

which is the same as for a solid cylinder. The final strain after pressurization is

$$\varepsilon_z(t \to \infty) = \frac{-P_A}{3K_s}, \tag{26}$$

which is also the same as for a solid cylinder. The time-dependent axial strain may therefore be expressed as

$$\varepsilon_z(\theta) = \varepsilon_z(\theta \to \infty) + \left\{\varepsilon_z(\theta^{0+}) - \varepsilon_z(\theta \to \infty)\right\}\Omega(\theta), \tag{27}$$

where $\Omega(\theta)$ is the compliance function. The Laplace transform of eq. (27) is simply

$$\bar{\varepsilon}_z(s) = s\bar{\varepsilon}(s \to 0) + \left\{s\bar{\varepsilon}(s \to \infty) - s\bar{\varepsilon}(s \to 0)\right\}\bar{\Omega}(s) \tag{28}$$

where the overbars denote the Laplace transformed quantities, *s* is the transform variable, and the initial and final value theorems of Laplace transforms are used.

The stresses in the hollow cylinder, $\sigma_r(r,t)$, $\sigma_\theta(r,t)$, and $\sigma_z(r,t)$, can be determined using the thermoelastic solution of a long, hollow cylinder [22] since thermal strains caused by variations in temperature are analogous to the free strains (eq. (13)) caused by changes in pore pressure. By combining the transformed stresses with the transform of eq. (12) and $\bar{P}(u, s, R_o / R_i)$ found by solving eq. (21) in the Laplace Transform domain, $\bar{\varepsilon}_z(s)$ was be determined as a function of *P*. Then, by substituting $\bar{\varepsilon}_z(s)$ into eq. (28), $\bar{\Omega}(s)$ was determined. The answer was inverted numerically into the reduced time domain with the Stehfest Algorithm [23, 25] to obtain $\Omega(\theta)$. The relaxation functions for a hollow cylinder and for a solid cylinder [15] are plotted in Figure 4.

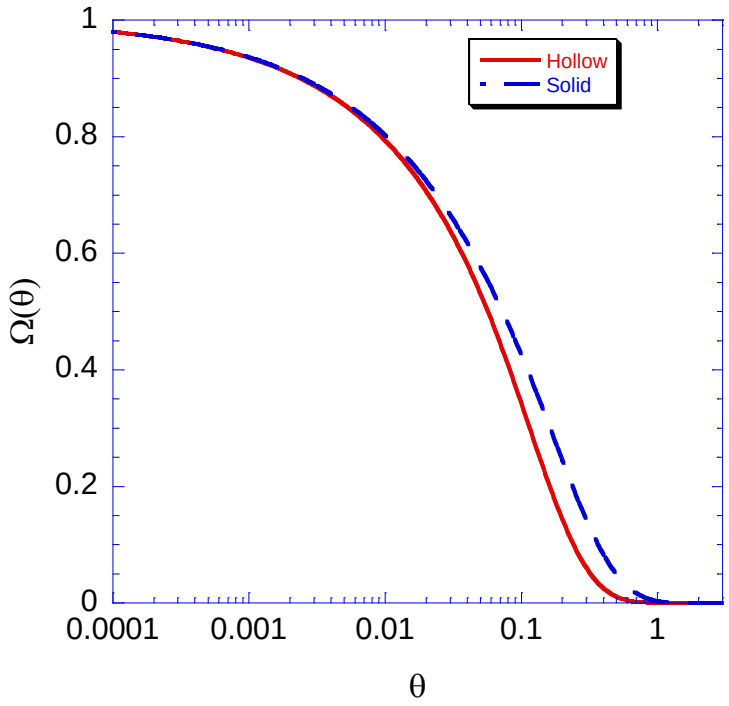

Figure 4. Comparison of relaxation functions for solid and hollow cylinders. Note that the early behavior (θ < 0.01) is comparable for both functions. In this case R_o/R_i is equal to 3.937 which corresponds to a 10.16 cm (4 inch) diameter cylinder with a 2.54 cm (1 inch) diameter hole.

The important feature to recognize in Figure 4 is that at short times ($\theta < 0.01$), the solid and hollow cylinder functions are virtually identical. The implication is that the short-time response of the hollow cylinder is able to be represented by the same function as the solid cylinder, shown by Scherer [15] to be

$$\Omega(\theta) \approx 1 - \frac{4}{\sqrt{\pi}}\left[1-(1-\beta)b\lambda\right]\sqrt{\theta} \quad . \tag{29}$$

As a result, the relaxation function over the full time span can be approximated by a function of the form

$$\Omega(\theta) \approx \exp\left\{\frac{4}{\sqrt{\pi}}\left[1-(1-\beta)b\lambda\right]\left(\frac{\theta^m-\sqrt{\theta}}{1-\theta^n}\right)\right\} \tag{30}$$

where *m* and *n* are fit parameters. For the hollow cylinder these fit parameters *m* and *n* are dependent on the geometry of the specimen being tested, particularly the ratio of the outer and inner radii (R_o/R_i). The equations for determining *m* and *n* are

$$m = 5.6152\left(\frac{R_o}{R_i}\right)^{-0.19623} \tag{31}$$

and

$$n = 0.40086 + 0.0056243 \times Ln\left(\frac{R_o}{R_i}\right)^{1.8506}, \tag{32}$$

where the numerical coefficients are determined by curve fitting the *m* and *n* results of several different radius ratios as shown in Figure 5 and Figure 6.

For the solid cylinder, equation (28) can also be used since the initial and final strains are identical to those of the hollow cylinder. Equation (30) is also identical except that for the solid cylinder the value of m=2.2 and the value of n=0.55 according to [15, 25]. Equation (23) changes to account for the lack of a hole in the center of the specimen to become

$$\tau_v = \frac{\eta_L R^2}{k}\left(\frac{\beta b^2}{K_p}+\frac{1}{M}\right), \tag{33}$$

where *R* is simply the radius of the cylinder.

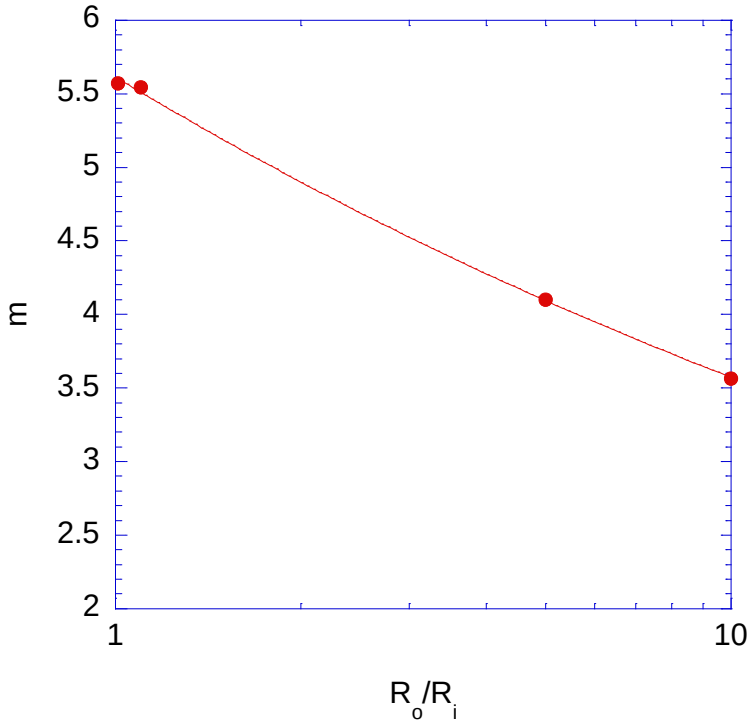

Figure 5: The fit parameter *m* is determined by curve fitting several different radius ratios.

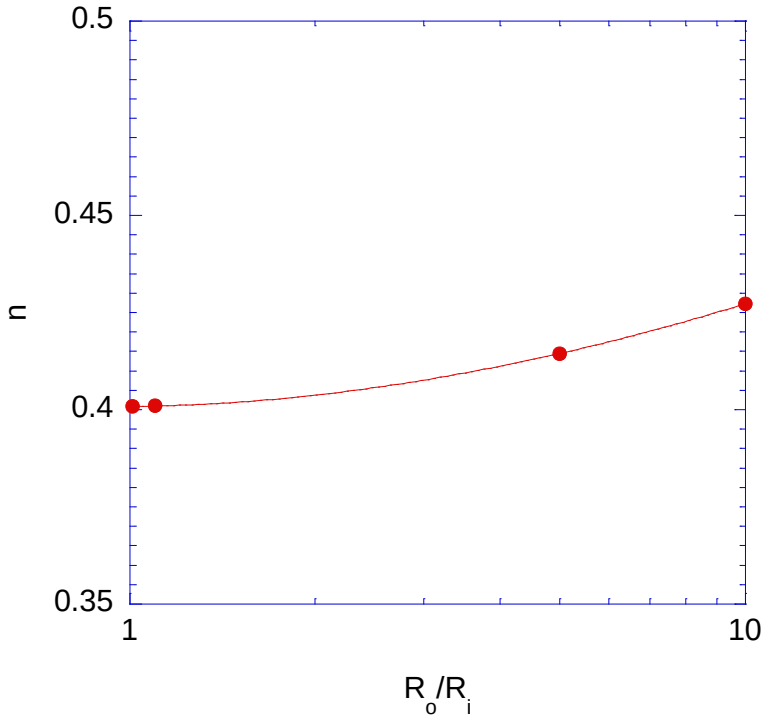

Figure 6: The fit parameter *n* is determined by fitting the results of various radius ratios.

Figure 7 shows the numerically inverted data for $\Omega(\theta)$ fit by eq. (30). Using fit parameters of $m = 4.4924$ and $n = 0.4235$ which correspond to a radius ratio of 4, yielded an R^2 value of 0.99983.

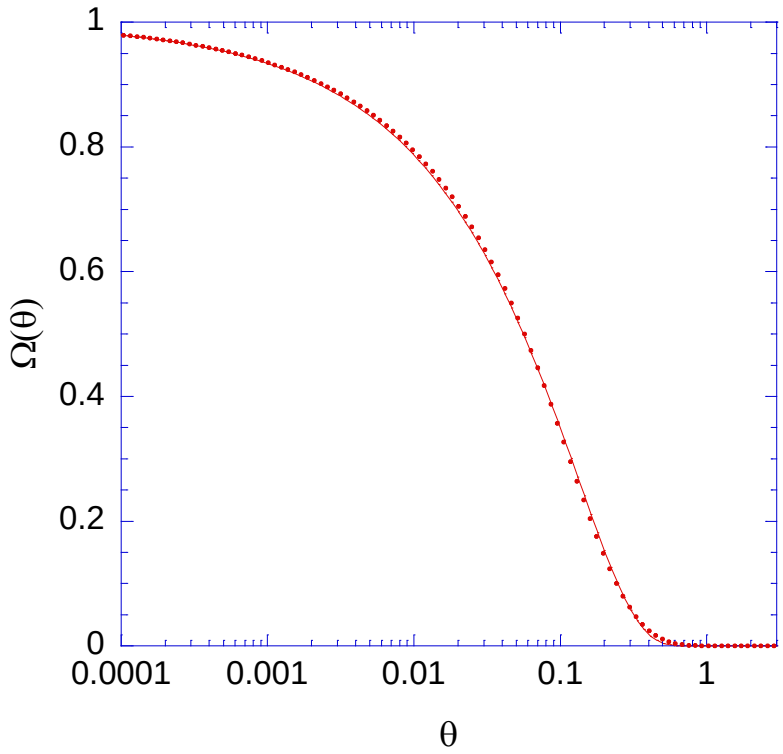

Figure 7. Approximation of the relaxation function Ω(θ) using eq. (30). The discrete points are numerically inverted data for Ω(θ) while the solid line is the approximate function. The function is evaluated using properties typical of concrete: β = 1/2, b = 2/3, λ = 1/4.

In order to obtain the permeability value of a given specimen, the strain versus time data must be obtained through testing, and then fit using eq. (27). Eq. (30) must first be substituted into (27), and the appropriate m and n values obtained from (31) and (32) must be used to determine the value of τ_v from (27). Next, the values of η_L, R_o, and R_i can be entered directly into (23). β can be calculated according to (20) using 0.2 as an approximate value for v_p. K_p and b can be determined from the strain time data and (25). Finally, M can be calculated using (16) by assigning a value to K_L (typically a textbook value – e.g. $K_L = 2.2\ GPa$ for water) and by calculating K_s from the strain versus time

data according to (26). The intrinsic permeability k may be determined directly by substituting values of β, τ_v, K_p, M, b, η_L, R_o, and R_i into (23).

5 EXPERIMENTAL TECHNIQUES

5.1 SPECIMEN MATERIALS AND PREPARATION

In this study, Vycor glass and cement paste samples were tested for permeability. The Vycor glass was type 7930 and was acquired in hollow tubes and solid rods. The tubes and rods were 21 cm (8.25 in) long. The rods tested had a 6.35 mm (0.25 in) diameter and the tubes had an inner diameter of 1.9 cm (0.75 in) and an outer diameter of 2.1 cm (0.827 in). The rods and tubes were vacuum saturated in glycerol, a solution of glycerol and water, or pure distilled water prior to testing depending on the type of testing to be performed. The hollow cement paste samples were cast in 6.72 x 15.24 cm (3 x 6 in) cylinder molds while the solid specimens were cast in 3.7 cm (1.45 in) tubes. The hollow specimens additionally had a 3.7 cm (1.45 in) diameter hole cast down the center through the length of the specimen. The cement used was a common Type I/II and was mixed at *w/c* of 0.5 and 0.6.

The cement paste was mixed according to ASTM C305-99. To achieve the hollow cylinder geometry, a thin walled polyethylene tube was glued into the center of the cylinder mold and a hole was cut in the center of the lid to accommodate this tube. Both the lid itself and the hole in the lid were sealed with silicone to prevent any moisture from leaving the cylinder during initial curing. The specimens were de-molded at approximately 12 hours and were immediately placed in a saturated lime water solution

to prevent any leaching of the internal calcium hydroxide. Additionally, the specimens in the lime water were placed under vacuum to promote saturation.

The concrete cylinders were prepared using the mix design shown in Table 1. This mix represents a typical bulk concreting mix that might be encountered in construction of a driveway or sidewalk. The maximum nominal size of the coarse aggregate was 9.5 mm (3/8 in). This relatively small coarse aggregate was chosen to ensure that a single aggregate particle did not transverse the entire flow distance of the sample. Generally, aggregates should be less than or equal to 1/3 of the flow distance within the cylinder [18]. For a 7.62 cm (3 in) diameter specimen with a 1.27 cm (1/2 in) hole down the center, 9.5 mm (3/8 in) aggregate is the largest that can be used and still satisfy this rule of thumb.

Table 1: The concrete mix design used in the testing is representative of a typical driveway or sidewalk mix.

Concrete Mix Design				
Cement Type I/II	334	kg/m^3	564	lbs/yd^3
Water	200	kg/m^3	338	lbs/yd^3
Coarse Aggregate (9.5mm max)	1232	kg/m^3	2079	lbs/yd^3
Fine Aggregate	610	kg/m^3	1030	lbs/yd^3

The concrete specimens were also cast with a 1.27 cm (1/2 in) diameter polythene tube down the center of the cylinder in a standard 7.62 cm by 15.24 cm (3 in by 6 in) cylinder

mold. Lids were used during the initial curing and the samples were de-molded and placed in lime water after approximately 12 hours.

The specimens were trimmed on a diamond blade wet saw to ensure that their ends were uniform and parallel to one another. Steel plates were glued onto the ends of the hollow cement paste specimens with a two-part marine epoxy to prevent any fluid from moving through the axial faces of the specimen and to facilitate mounting inside the testing apparatus. The Vycor glass tubes would have been similarly sealed, but the thin wall thickness required caps which attached both to the ends as well as a small portion of the side of the tube. These caps were also secured with the marine epoxy. The sealing of the specimens is shown schematically in Figure 8. The solid rods were not sealed, but due to their extremely slender nature very little fluid would flow through the ends compared to the amount through the sides. As discussed in [15] and [25] the relaxation time is affected by flow through the ends of a cylinder, though this effect is related to the square of the length to width ratio. Since these solid specimens are extremely slender (height to width ratio greater than 32 for the Vycor and 8 for the cement paste) this effect will be extremely small and is neglected in this analysis.

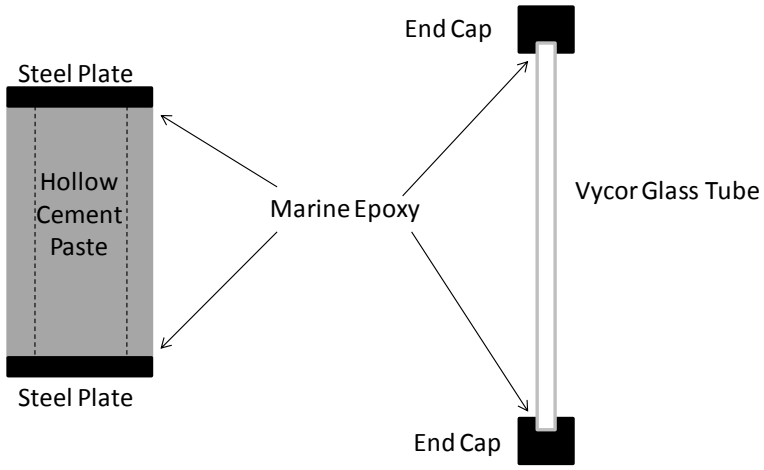

Figure 8: The hollow Vycor and cement paste specimens are sealed at each end with special caps, secured by a two part marine epoxy.

5.2 POROSITY DETERMINATION

One of the parameters necessary for determining *k* for both the SDP and HDP tests is the specimen porosity. Vichit-Vadakan and Scherer [26] show that porosity of cementitious materials determined by oven drying agrees with porosity measured by 2-propanol exchange and is much quicker. In this study, the oven drying technique was used for determining porosity. For the cement paste samples, this method involved obtaining a small, representative disc of the material and saturating it under vacuum. The saturated surface dry weight and the dimensions of the sample were obtained using a digital balance capable of 0.001 gram accuracy and a digital caliper with 0.001 cm accuracy. The sample was then placed in the oven at 110 degrees Celsius. After drying overnight, the dry weight was obtained and the porosity was determined according to

$$\phi = \frac{M_{SSD} - M_{OD}}{V_{SSD} \times \rho_{Water}}, \tag{34}$$

where M_{SSD} is the mass in the saturated surface dry state, M_{OD} is the mass in the oven dry state, V_{SSD} is the measured volume in the saturated surface dry state, and ρ_{Water} is the density of water.

For the Vycor glass, the dimensions of a solid rod were accurately measured using the same digital caliper to determine its volume. The rod was then vacuum saturated and weighed in the saturated surface dry condition. Finally, the rod was oven dried at 110 degrees Celsius and weighed again. The porosity of the Vycor was also calculated using equation (34).

The initial porosity of the cement paste was determined from the mix design, and then at subsequent ages with the oven drying test to establish a best fit curve for each material. This curve was used to accurately estimate the porosity of a given specimen at a particular age. The porosity of the Vycor glass was not time dependent and was not tested at different ages. The cement paste porosity versus age plot is shown in Figure 9 with an exponential fit. The porosity of the Vycor glass is also shown in Figure 9 for comparison purposes.

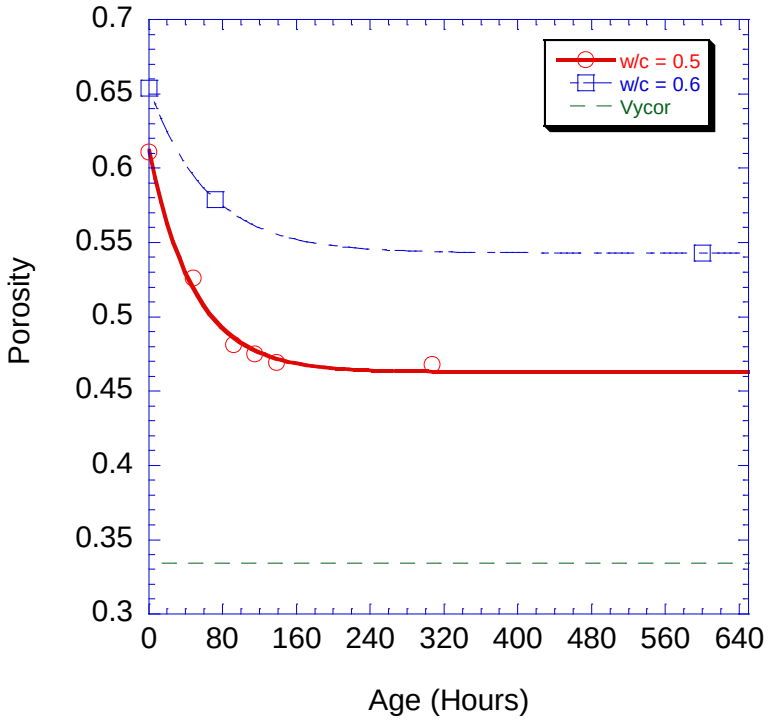

Figure 9: The porosity of the cement paste specimens as a function of age.

5.3 FLUID VISCOSITY DETERMINATION

One of the primary advantages of the dynamic pressurization technique is the increased speed of each test. This advantage actually became a hindrance when the Vycor glass was tested in water. The HDP test with the Vycor tube in water ran completely in approximately 0.1 seconds (determined by calculation), so data collection was impossible. As shown in equation (23) the relaxation time is directly related to the fluid viscosity. By changing the viscosity of the testing fluid, the relaxation time of the test could be adjusted to a more reasonable length of time. Glycerol was chosen as a complimentary fluid to water for several reasons. First, glycerol is roughly 1,000 times

more viscous than water; this slowed the HDP test more than enough for reasonable data collection to proceed. Additionally, the glycerol molecules are similar in size to water molecules. This similarity is important because of the small average pore size in the Vycor. Finally, glycerol and water are readily soluble in one another, which facilitates custom viscosity blends.

In order to obtain the necessary inputs for the permeability calculations, a few values, which are not obtained from either the SDP or HDP tests, must be determined. First, the dynamic viscosity of the particular pore fluid used must be determined. The viscosity of water is very well known [27], and it does not change very much with changes in temperature. However, glycerol varies substantially with a small change in temperature so the viscosity at laboratory temperature (~23° C) was determined using a Brookfield rotational viscometer. The results of the viscosity testing are shown in Table 2.

Table 2: Since the Vycor tubes have a thin wall thickness, fluids with higher viscosities than water were used to slow the Hollow Dynamic Pressurization test.

Fluid	Viscosity (Pa-s)
Distilled Water	0.00102
65wt% Glycerol	0.0128
90wt% Glycerol	0.1823
Glycerol	1.067

5.4 FLUID BULK MODULUS DETERMINATION

In addition to the viscosity, the bulk modulus, K_L, changes with each fluid blend. Though not as influential in the final permeability determination as the viscosity, K_L

must be accurately estimated in order to obtain sensible permeability results with the dynamic pressurization techniques. In the case of pure water and pure glycerol this determination was a simple matter of using a reference value obtained from a source such as [27]. For the water/glycerol blends, the rule of mixtures,

$$K_{L-Blend} = f_1(K_{L-1}) + f_2(K_{L-2}), \tag{35}$$

was employed to estimate the bulk modulus of the blend where $K_{L\text{-}Blend}$ is the bulk modulus of the fluid blend, f_1 is the volume fraction of liquid 1, $K_{L\text{-}1}$ is the bulk modulus of liquid 1, $K_{L\text{-}2}$ is the bulk modulus of liquid 2 and f_2 is the volume fraction of liquid 2. The bulk moduli of the various liquids used in both the HDP and the SDP test are shown in Table 3.

Table 3: The bulk modulus values for the testing fluid are used in calculating the permeability for each specimen with the dynamic pressurization methods.

Fluid	K_L(Pa)
Distilled Water	2.2×10^9
65wt% Glycerol	3.57×10^9
90wt% Glycerol	4.23×10^9
Glycerol	4.52×10^9

5.5 TESTING PROGRAM

The general scheme in this experimental sequence was to first establish the HDP test as accurate and repeatable by testing the Vycor glass. The permeability values obtained from the HDP test were compared to those obtained with the SDP and RFT tests. This

allowed the comparison of the new HDP test to another poromechanical test and to a direct flow through test. Once the validation had been established, cement paste specimens were tested using the same HDP versus SDP and HDP versus RFT comparison scheme. Finally a single concrete specimen was tested, with the HDP test, to determine the applicability of the HDP technique to actual concrete.

6 RESULTS AND DISCUSSION

6.1 VYCOR

To validate the HDP method, Vycor glass specimens were tested using the HDP, SDP and RFT techniques. The results from the RFT and the SDP were each compared to the results obtained from the HDP test to determine the equivalency of the results.

The final input parameter required for calculating permeability for both the SDP and HDP techniques is a strain-time history, which can be fit to determine the relaxation time, τ_v, and ultimately the permeability of the material. Figure 10 shows a typical strain-time history for the HDP test, shown on both the time and log-time axes. These results are for a hollow Vycor tube tested in pure glycerol. The plots show that equilibrium is reached in approximately nine hours, which is roughly equivalent to the fit parameter τ_v.

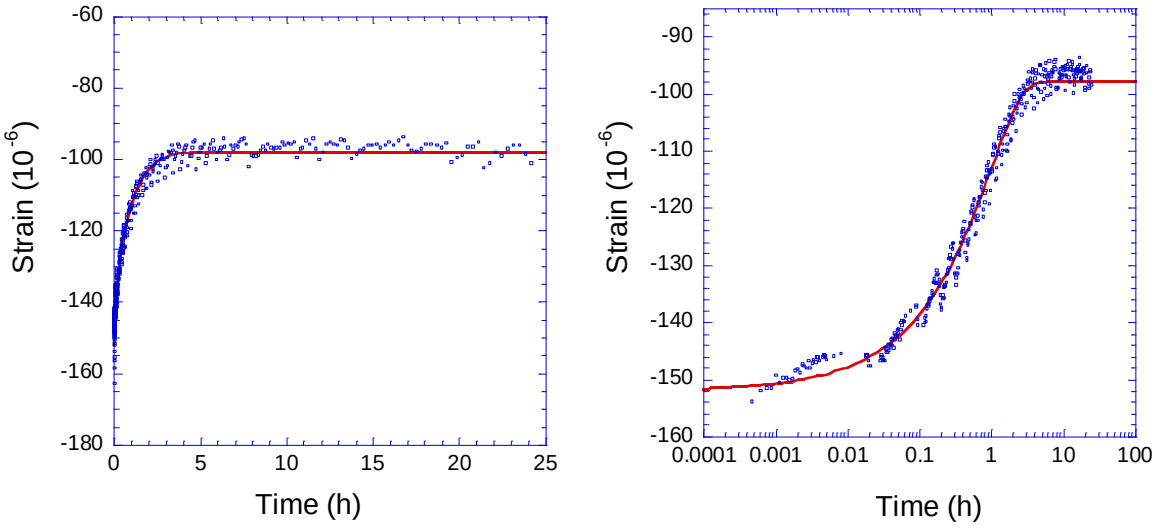

Figure 10: Typical hollow dynamic pressurization strain data shown on time and log-time axes. The log-time axis more clearly shows when the specimen has fully relaxed.

6.1.1 Hollow Dynamic Pressurization Versus Radial Flow Through

In order to facilitate the most direct comparison possible between the RFT and the HDP, two intermediate fluid blends were created with viscosities that fell in between that of water and pure glycerol. The viscosities of the blends were intentionally optimized to allow the HDP test to run quickly. Water was used only for the flow through and the 100% glycerol was only used for the HDP. Multiple repetitions of each test were conducted to establish a valid statistical comparison with these combinations. The combined results are shown in Table 4 with the associated means and standard deviations.

Table 4: The tabulated results of the Vycor permeability testing show good agreement between the various test permutations of fluid and test method.

Hollow Dynamic Pressurization Results Permeability (nm^2)				Hollow Flow Through Results Permeability (nm^2)	
Trial	Glycerol	65wt% Glycerol	90wt% Glycerol	Water	65wt% Glycerol
1	0.021	0.018	0.023	0.016	0.012
2	0.024	0.019	0.030	0.028	0.014
3	0.020	0.015	0.026	0.025	0.019
4	0.032	0.018	0.021	0.013	0.014
5	0.014	0.015	0.021	0.017	0.016
6	0.028	0.017	0.021	0.018	0.020
7	0.034	0.019	0.023	0.022	0.015
8	0.019	0.023	0.020	0.023	0.016
9		0.018	0.017	0.024	
10		0.019	0.015	0.021	
11			0.016	0.023	
12				0.036	
13				0.024	
Mean	0.02409	0.01808	0.02113	0.02239	0.01559
Standard Deviation	0.00685	0.00231	0.00439	0.00582	0.00267
Coeficient of Variation	28.46%	12.77%	20.79%	26.01%	17.11%
Combined COV	24.46%			29.58%	

The maximum difference in the measured permeability values reported in Table 4 (between the flow through test using 65% glycerol and the HDP test using glycerol) is a mere 35%. When the exact same fluid was used in the flow through and HDP tests (both used 65% glycerol), the percent difference in mean permeabilities between the techniques was only 23%. The HDP test shows excellent repeatability with these means falling very close to one another.

With the HDP and the RFT technique, the greatest coefficient of variation was 28%, and the greatest combined coefficient of variation was 30% which are both near the lower end of the range of typical variability of permeability measurements [8, 28, 29]. Additionally, the results shown in Table 4 agree reasonably well with the Vycor permeability results obtained by Vichit-Vidakan and Scherer [30] both in mean and in standard deviation.

When evaluating the agreement in means of two data sets the Student's T-Test is frequently employed. For this test a characteristic 't' statistic is calculated according to

$$t = \frac{\mu_1 - \mu_2 - \Delta}{\sqrt{\frac{s_1^2}{m} + \frac{s_2^2}{n}}} \tag{36}$$

where μ_1 is the mean of the first data set, μ_2 is the mean of the second data set, Δ is the null value, s_1 is the standard deviation of the first data set, s_2 is the standard deviation of the second set, m is the number of data points in the first data set, and n is the number of data points in the second set [31]. This 't' value is then compared to a reference value based on the confidence level and the number of data points in the combined data set. Typically, results are tested at the 95% confidence level, which means that the determination is predicted to be correct 95% of the time. By using the reference value corresponding to the 95% confidence level and the appropriate number of data points, the null value Δ can be determined. Once the Δ value is obtained the percent difference can be determined according to,

$$\%\, percent\ difference = \frac{\Delta}{(\mu_1 + \mu_2)/2} \times 100 \tag{37}$$

With the data presented in Table 4 it can be shown that the percent difference in the permeability values from the HDP test and the RFT test will be 5.4% or less 95% of the time; this difference is much smaller than the typical coefficient of variation reported in literature [8, 28, 29] for permeability of cementitious materials obtained with a single test method.

From a practical perspective, the percent difference between the Vycor glass permeability measured using the flow through technique and the HDP technique is statistically insignificant. Therefore, the HDP test has been successfully validated and has been shown to yield the same permeability as a flow-through test for Vycor glass.

6.1.2 Hollow Dynamic Pressurization Versus Solid Dynamic Pressurization

The results from the testing of hollow and solid Vycor specimens for permeability show good correlation between the HDP and the SDP techniques. The difference between the average permeability determined from the HDP and the SDP is 13%. The permeability values for the Vycor specimens are presented in Table 5.

Table 5: The measured Vycor permeability and associated statistical quantities measured with various fluids.

	Hollow DP Results			Solid DP Results	
	Permeability (nm^2)			Permeability (nm^2)	
Trial	Glycerol	65wt%	90wt%	Glycerol	65wt%
1	0.021	0.018	0.023	0.038	0.008
2	0.024	0.019	0.030	0.011	0.013
3	0.020	0.015	0.026	0.013	0.012
4	0.032	0.018	0.021	0.024	0.009
5	0.014	0.015	0.021	0.024	0.008
6	0.028	0.017	0.021	0.031	0.009
7	0.034	0.019	0.023	0.019	0.014
8	0.019	0.023	0.020	0.035	0.016
9		0.018	0.017		0.018
10		0.019	0.015		0.018
11			0.016		
Average	0.024086	0.018081	0.021126	0.0244	0.0122776
Standard Deviation	0.006854	0.00231	0.004392	0.00982	0.0040541
Coeficient of Variation	28.46%	12.77%	20.79%	40.26%	33.02%
Combinded Coeficient of Variation	24.46%			52.75%	

Typical concrete permeability tests show high variability between repetitions. Reported coefficients of variation between 20% and 130% [8, 28, 29] are typical of this type of testing. With the hollow and the SDP techniques, the greatest coefficient of variation was 40%, and the greatest combined coefficient of variation was 53%, which are both toward the lower end of this range. Additionally, the results shown in Table 5 agree reasonably well with the Vycor permeability results obtained by Vichit-Vidakan and Scherer [30] both in mean and in standard deviation.

With the data presented in Table 5 it can be shown that the percent difference in the permeability values from the HDP test and the SDP test will be 17% or less 95% of the time; this difference is much smaller than the typical coefficient of variation reported in literature [29] for permeability of cementitious materials obtained with a single test method.

From a practical perspective, the percent difference between the Vycor glass permeability measured using the SDP technique and the HDP technique is statistically insignificant. Therefore, the HDP test has been successfully validated and has been shown to yield the same permeability as the SDP test for Vycor glass.

6.2 CEMENTITIOUS MATERIALS

In order to obtain a statistically significant amount of data in a reasonable length of time with the RFT test, specimens with a *w/c* of 0.6 were chosen for their relatively high permeability. Choosing specimens with high permeability helps the RFT test to run more quickly while reducing the risk of leaking since the fluid will be more likely to flow through the specimen than through any sealed connection. For the SDP to HDP comparison, a *w/c* of 0.5 was chosen because the specimens are simpler to cast and there is no real need for increased speed with the dynamic pressurization techniques.

6.2.1 Hollow Dynamic Pressurization Versus Radial Flow Through

The difference between a low permeability material and a high permeability material is worth noting. The difference between a 0.5 *w/c* paste and a 0.6 *w/c* paste is reported as a full order of magnitude (i.e. 0.001 nm^2 as compared to 0.01 nm^2) by Grasley et al. [26]; this difference in measured permeability is a change of 900%. Based on the results shown in Table 6, the difference between the mean values of the two methods is 32%. This level of sensitivity is clearly sufficient to discern two different construction materials.

Using equations (36), (37), and the data presented in Table 6, the percent difference between the results obtained with the HDP test and the RFT test will be 38% or less 95% of the time. This value is higher than that obtained with the Vycor glass principally because of the material variability in the cement paste.

Table 6: The permeability results from the 0.6 *w/c* paste show good correlation between the HDP and the radial flow through techniques.

Trial	**Hollow Dynamic Pressurization** Permeability (nm^2)	**Radial Flow Through** Permeability (nm^2)
1	0.414	0.339
2	0.370	0.289
3	0.364	0.260
4	0.496	0.279
5	0.400	0.277
6	0.426	0.316
7	0.502	0.300
8	0.375	0.298
9	0.500	0.253
Mean	0.42751	0.29005
Standard Deviation	0.05760	0.02682
Coeficient of Variation	13.47%	9.25%

Additionally, it should be noted that the 32% difference is between two totally different test methods. The ranges reported by Banthia and Mindess in [29], and for most other studies, were representative of a single test method. The small differences between the HDP and the RFT results could be due to material differences between the two samples used for the two tests or an inherent, systematic difference in the two test methods.

Material differences between the two samples were kept to a minimum since the samples were cast from the same mix, and were cured identically. Additionally the inherent nature of cement paste is very homogeneous and lends itself to good consistency. With

all of this in mind, the difference between the two means is quite small and material variability is likely the source of the difference. Future research could involve testing several different specimens for both RFT and HDP to investigate the effect of material variability.

One possible systematic difference between the HDP test and the RFT test involves the viscoelastic nature of the specimens tested. Cement paste (and Vycor glass) specimens relax stresses through viscoelastic deformation, with respect to time, which could have a skewing effect on the HDP data. This effect is clearly small, but could play a part in the small difference in the average values obtained from the two test methods. Any viscoelastic effect would be minimized when testing concrete versus cement paste due to the elastic nature of typical aggregates.

The coefficient of variation gives a good idea of the relative precision of a test method. In the case of the flow through and HDP methods, a coefficient of variation around ten percent indicates very good precision for both methods with the HDP method showing slightly better.

Finally, a single concrete specimen was tested with the HDP method to assess the feasibility of testing a more realistic construction material; the measured permeability was 0.006 nm^2. This value is very reasonable, though more testing would be needed to assess its accuracy.

6.2.2 Hollow Dynamic Pressurization Versus Solid Dynamic Pressurization

In order to generate the most direct comparison possible, the HDP and the SDP methods were performed on hollow and solid cement paste specimens beginning approximately 90 hours after the specimens were cast. Specifically, a hollow specimen was tested in one pressure vessel and a solid specimen in a companion pressure vessel, with the test beginning at effectively the same moment. At these early ages many test repetitions could be obtained in a reasonably short period of time. By simultaneously testing these samples, the effect of any age differences between specimens was avoided since the solid sample was the same age as the hollow sample and vice versa. Since the hollow and solid specimens were cast from the same mix, and were tested at an identical age, the permeability results from the two tests can be readily compared at a given age to evaluate the new HDP method.

For comparison purposes, permeability data from the literature was also included to compliment the data collected in this study. Cement paste with a *w/c* of 0.6 was tested by Vichat-Vidakan and Scherer [26] using the beam bending technique and these results are plotted along with those gathered in this study using the HDP and SDP techniques in Figure 11.

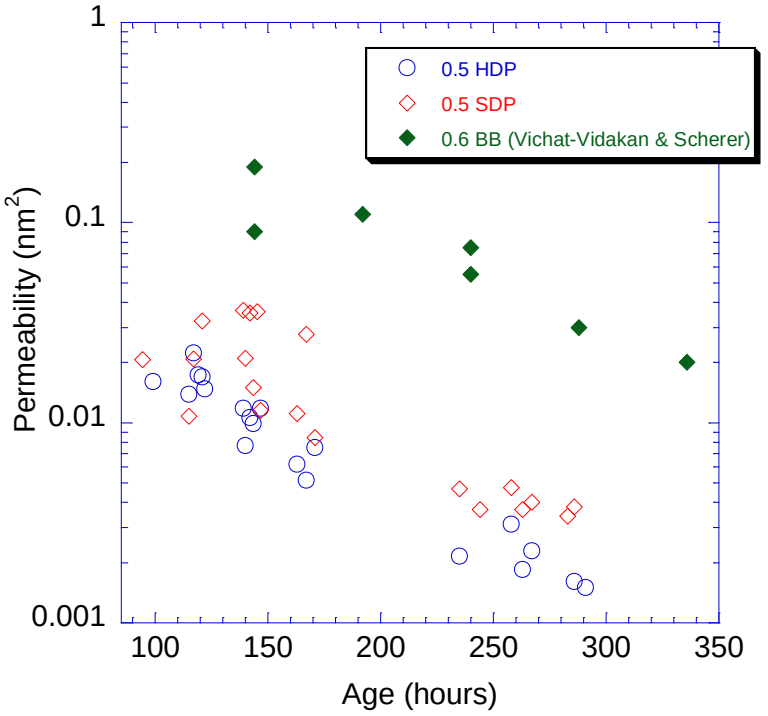

Figure 11: The results of the hollow dynamic pressurization test and the solid dynamic pressurization tests shown as a function of age. For comparison purposes the results from some other studies are included.

The results presented in Figure 11 show good agreement between the SDP and HDP methods over the range of time that the data was collected. The differences between the two methods could be attributable to some curing differences stemming from the geometry of the specimens. As mentioned previously, the results from the HDP and SDP tests on the 0.5 *w/c* paste are clearly much different than the results of the beam bending test on the 0.6 *w/c* paste. Also the variability of the HDP and SDP tests appears to be similar based on the scatter in the data points when compared to the beam bending data.

7 SUMMARY

Since saturated permeability of a material provides insight into the interconnectivity of the pore network of that material and since no widely accepted concrete permeability test exists, the Hollow Dynamic Pressurization (HDP) test is presented as an accurate and repeatable method for measuring the permeability of cementitious materials. The hollow specimen geometry allows for the saturation of the pore network of the specimen by applying a hydrostatic pressure to the outer radial surface of the unsaturated specimen which forces fluid into the pore network and forces air bubbles out. Since saturation is a rigorous requirement of the dynamic pressurization technique, the ability to saturate an existing specimen represents a major advantage over the solid dynamic pressurization (SDP) technique. The HDP test is more rapid than traditional flow through techniques and shows excellent repeatability both with Vycor glass and with cement paste. To evaluate this new method, the HDP test was compared to the SDP test and to the radial flow through (RFT) technique.

By comparing the results obtained from the HDP, SDP, and RFT tests, the HDP test has been validated since the values were essentially identical to those obtained with the other test methods. The coefficient of variation obtained with the HDP test is much lower than for other permeability tests reported in the literature [8, 28, 29]. The particular permeability values obtained agreed reasonably well with values obtained in literature for similar materials. With all of the above in mind, the new HDP test shows promise as an acceptable permeability test for cementitious materials.

REFERENCES

[1] Vitaliano, D.F., Infrastructure costs of road salting. Resources, Conservation and Recycling, 7 (1-3) (1992) 171-180.

[2] Mehta, K., High-performance concrete durability affected by many factors, Concrete Construction, 37 (5) (1992) 367-370.

[3] Gillott, J.E., Review of expansive alkali-aggregate reactions in concrete, Journal of Materials in Civil Engineering, 7 (4) (1995) 278-282.

[4] Haynes, H., R. O'Neill, and P.K. Mehta, Concrete deterioration from physical attack by salts, Concrete International, 18 (1) (1996) 63-69.

[5] Neville, A., Chloride attack of reinforced concrete: An overview, Materials and Structures/Materiaux et Constructions, 28 (176) (1995) 63-70.

[6] Mehta, P.K., Durability of concrete - the zigzag course of progress, Indian Concrete Journal, 80 (8) (2006) 9-16.

[7] Neville, A., Suggestions of research areas likely to improve concrete, Concrete International, 18 (5) (1996) 44-49.

[8] Ye, G., P. Lura, and K. Van Breugel, Modelling of water permeability in cementitious materials, Materials and Structures/Materiaux et Constructions, 39 (293) (2006) 877-885.

[9] Hearn, N. and R.H. Mills, Simple permeameter for water or gas flow, Cement and Concrete Research, 21 (2-3) (1991) 257-261.

[10] Hooton, R.D. Permeability and pore structure of cement pastes containing flyash, slag, and silica fume (1986). Denver, CO, ASTM, Philadelphia, PA.

[11] Scherer, G.W., Poromechanics analysis of a flow-through permeameter with entrapped air, Cement and Concrete Research, 38 (3) (2008) 368-378.

[12] Scherer, G.W., J.J. Valenza, II, and G. Simmons, New methods to measure liquid permeability in porous materials. Cement and Concrete Research, 37 (3) (2007) 386-397.

[13] Scherer, G.W., Measuring permeability of rigid materials by a beam-bending method: I, theory, Journal of the American Ceramic Society, 83 (9) (2000) 2231-2239.

[14] Scherer, G.W., Thermal expansion kinetics: Method to measure permeability of cementitious materials. I. Theory, Journal of the American Ceramic Society, 83 (11) (2000) 2753-2761.

[15] Scherer, G.W., Dynamic pressurization method for measuring permeability and modulus: I. Theory, Materials and Structures/Materiaux et Constructions, 39 (294) (2006) 1041-1057.

[16] Gross, J. and G.W. Scherer, Dynamic pressurization: Novel method for measuring fluid permeability, Journal of Non-Crystalline Solids, 325(1-3) (2003) 34-47.

[17] Bhargava, A. and N. Banthia, Measurement of concrete permeability under stress, Experimental Techniques, 30 (5) (2006) 28-31.

[18] El-Dieb, A.S. and R.D. Hooton, High pressure triaxial cell with improved measurement sensitivity for saturated water permeability of high performance concrete, Cement and Concrete Research, 24 (5) (1994) 854-862.

[19] Abousleiman, Y.N. and M.Y. Kanj, The generalized lame problem-part ii: Applications in poromechanics, Journal of Applied Mechanics, Transactions of the ASME, 71 (2) (2004) 180-189.

[20] Kanj, M.Y. and Y.N. Abousleiman, The generalized lame problem - part i: Coupled poromechanical solutions. Journal of Applied Mechanics, Transactions ASME, 71 (2) (2004) 168-179.

[21] Sawaguchi, H. and M. Kurashige, Constant strain-rate compression test of a fluid-saturated poroelastic sample with positive or negative Poisson's ratio, Acta Mechanica, 179 (3-4) (2005) 145-56.

[22] Sherief, H.H., A.E.M. Elmisiery, and M.A. Elhagary, Generalized thermoelastic problem for an infinitely long hollow cylinder for short times, Journal of Thermal Stresses, 27 (10) (2004) 885-902.

[23] Stehfest, H., Numerical inversion of Laplace transforms, Communications of the ACM, 13 (1) (1970) 47-49.

[24] Wolfram Research, Numerical inversion performed using the package NumericalInversion, © Mallet, A. 2000, University of Mauritius. in Wolfram Research, Inc,: Champaign, IL.

[25] Grasley, Z.C., Scherer, G.W., Lange, D.A., and Valenza, J.J., Dynamic pressurization method for measuring permeability and modulus: II. Cementitious materials, Materials and Structures/Materiaux et Constructions, 40 (7) (2007) 711-721.

[26] Vichit-Vadakan, W., G.W. Scherer, and M. Grutzeek, Measuring permeability of rigid materials by a beam-bending method: III, cement paste, Journal of the American Ceramic Society, 85 (6) (2002) 1537-1544.

[27] Munson, B.R., Young, Donald F., and OIkiishi, Theodore H., Fundamentals of fluid mechanics, 4th ed, John Wiley and Sons Inc, Hoboken, NJ. 2002

[28] Hooton, R.D., Permeability and pore structure of cement pastes containing fly ash, slag, and silica fume, Denver, CO: ASTM, Philadelphia, PA, (1986)

[29] Banthia, N. and S. Mindess, Water permeability of cement paste, Cement and Concrete Research, 19 (5) (1989) 727-736.

[30] Vichit-Vadakan, W. and G.W. Scherer, Measuring permeability of rigid materials by a beam-bending method: II. Porous glass, Journal of the American Ceramic Society, 83 (9) (2000) 2240-2245.

[31] Devore, J.L., Probability and statisitics. 6 ed, Brooks/Cole-Thompson Learning, Belmont, CA, 2004

APPENDIX A. VYCOR PLOTS

VYCOR FLOW THROUGH PLOTS

65% Glycerol

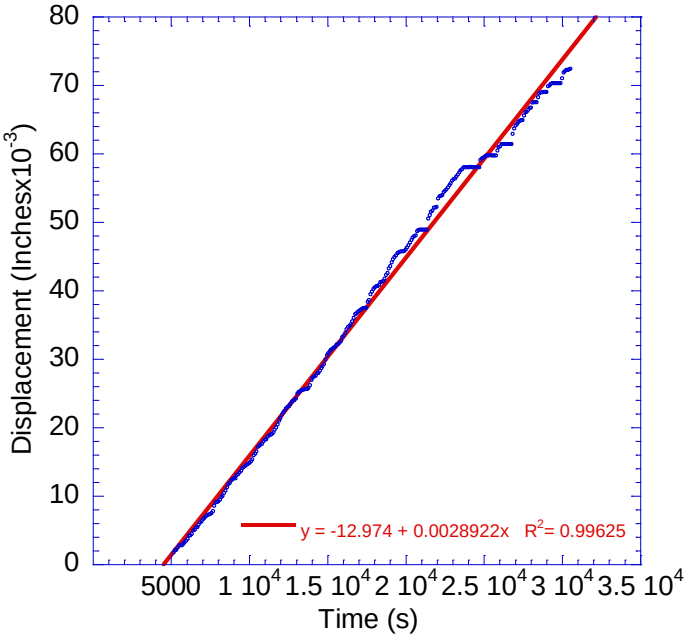

Figure A- 1: Measured displacement versus time response of a Vycor tube sample when tested in 65 weight percent glycerol.

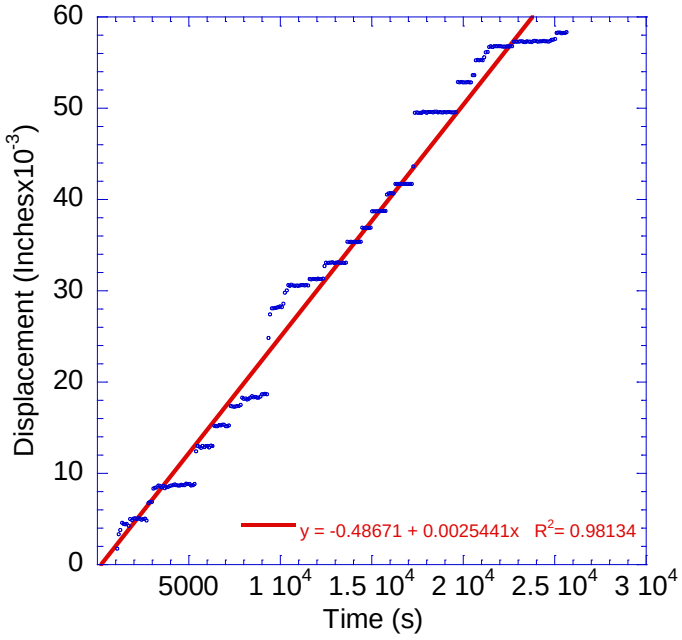

Figure A- 2: Measured displacement versus time response of a Vycor tube sample when tested in 65 weight percent glycerol.

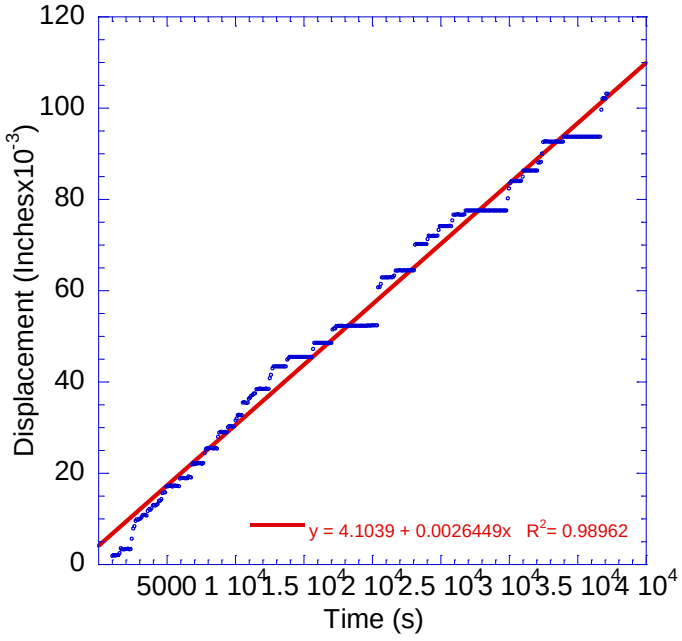

Figure A- 3: Measured displacement versus time response of a Vycor tube sample when tested in 65 weight percent glycerol. The stair-step nature of the data is due to minor sticking of the float within the test apparatus.

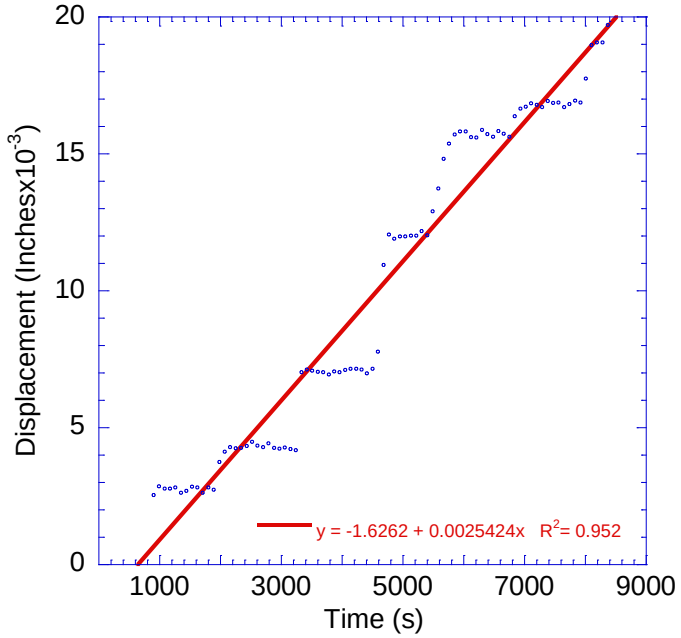

Figure A- 4: Measured displacement versus time response of a Vycor tube sample when tested in 65 weight percent glycerol. The stair-step nature of the data is due to minor sticking of the float within the test apparatus.

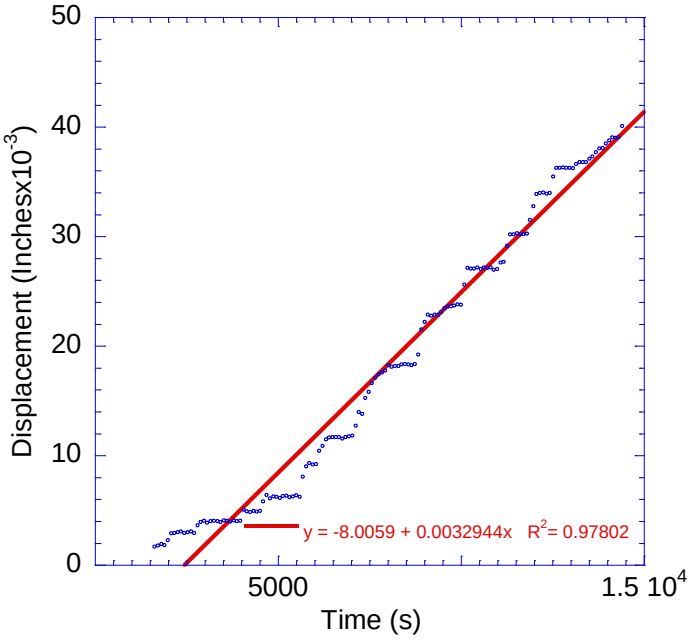

Figure A- 5: Measured displacement versus time response of a Vycor tube sample when tested in 65 weight percent glycerol. The stair-step nature of the data is due to minor sticking of the float within the test apparatus.

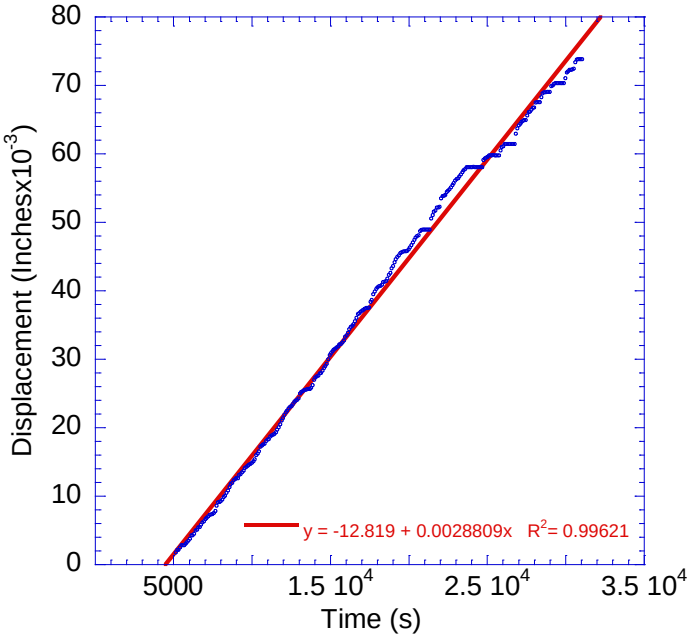

Figure A- 6: Measured displacement versus time response of a Vycor tube sample when tested in 65 weight percent glycerol. The stair-step nature of the data is due to minor sticking of the float within the test apparatus.

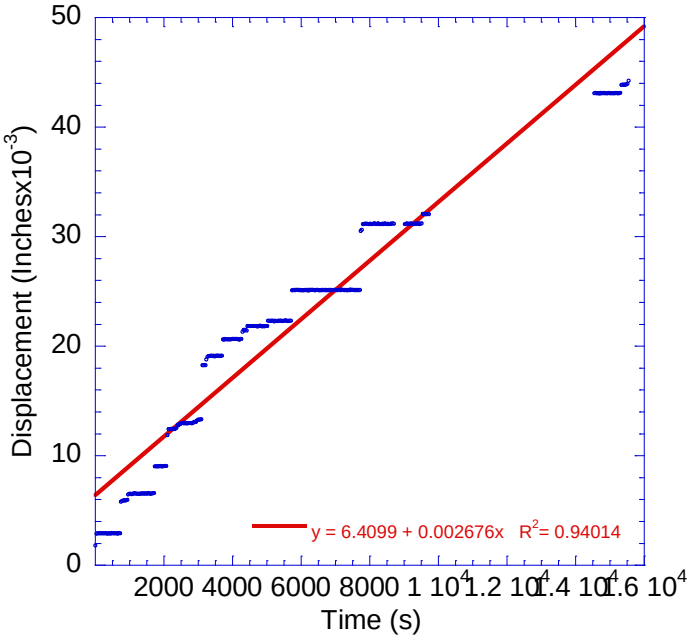

Figure A- 7: Measured displacement versus time response of a Vycor tube sample when tested in 65 weight percent glycerol. The stair-step nature of the data is due to minor sticking of the float within the test apparatus.

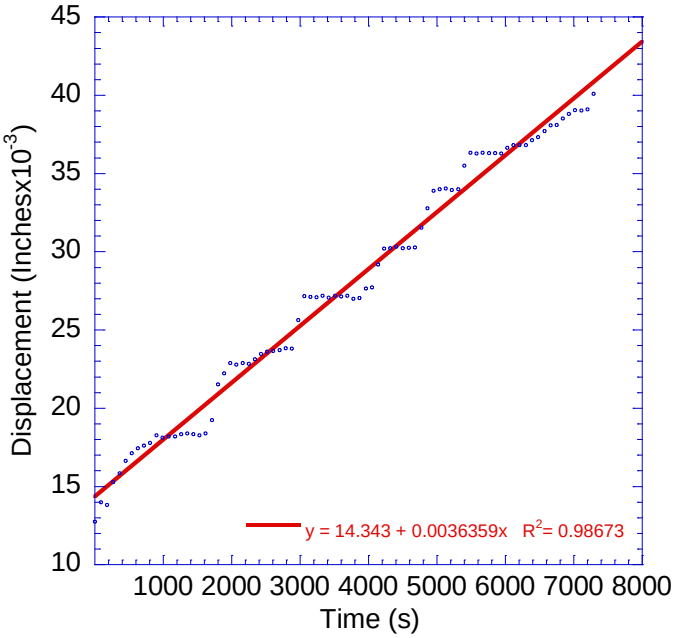

Figure A- 8: Measured displacement versus time response of a Vycor tube sample when tested in 65 weight percent glycerol. The stair-step nature of the data is due to minor sticking of the float within the test apparatus.

Water

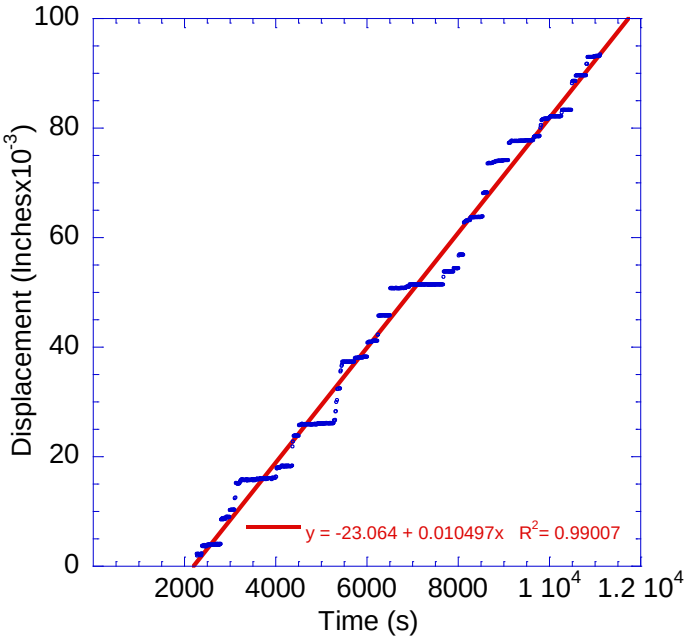

Figure A- 9: Measured displacement versus time response of a Vycor tube sample when tested in water with an applied hydrostatic pressure of 414 kpa (60 psi).

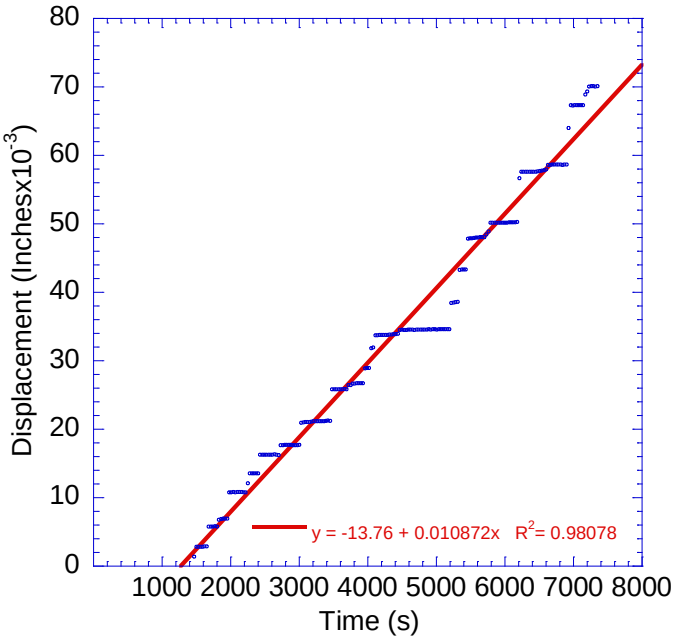

Figure A- 10: Measured displacement versus time response of a Vycor tube sample when tested in water with an applied hydrostatic pressure of 552 kpa (80 psi).

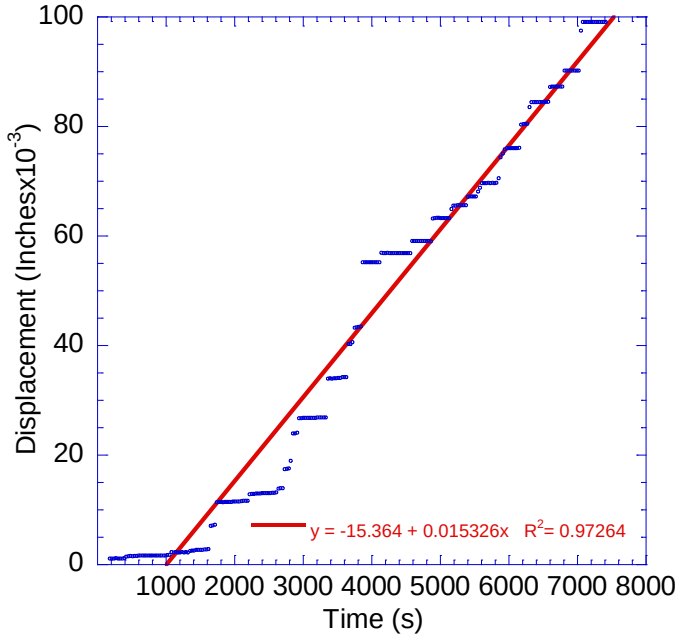

Figure A- 11: Measured displacement versus time response of a Vycor tube sample when tested in water with an applied hydrostatic pressure of 552 kpa (80 psi).

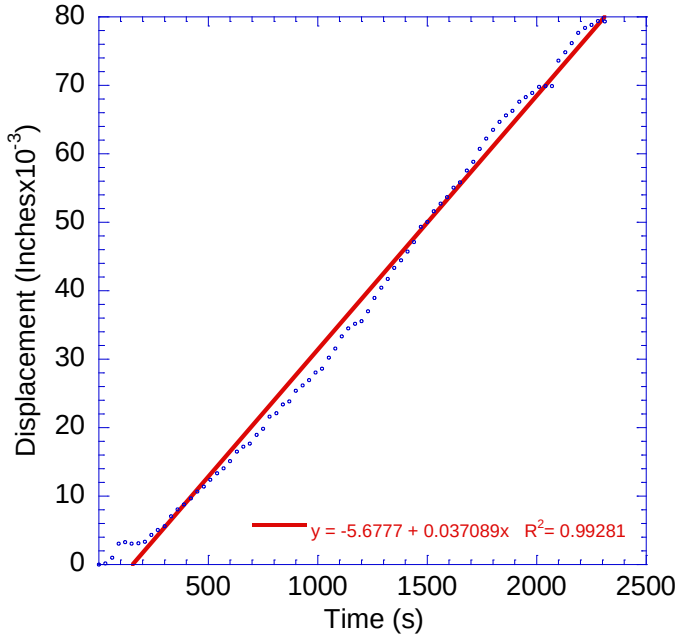

Figure A- 12: Measured displacement versus time response of a Vycor tube sample when tested in water with an applied hydrostatic pressure of 1.38 Mpa (200 psi).

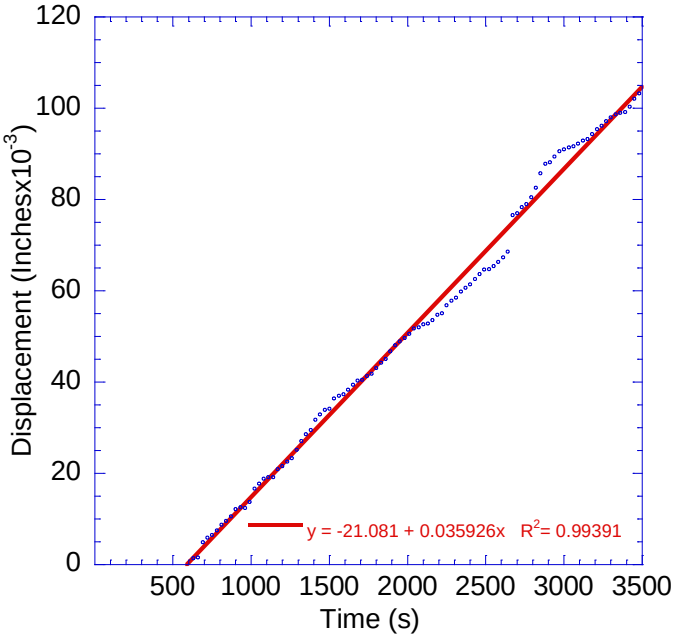

Figure A- 13: Measured displacement versus time response of a Vycor tube sample when tested in water with an applied hydrostatic pressure of 1.38 Mpa (200 psi).

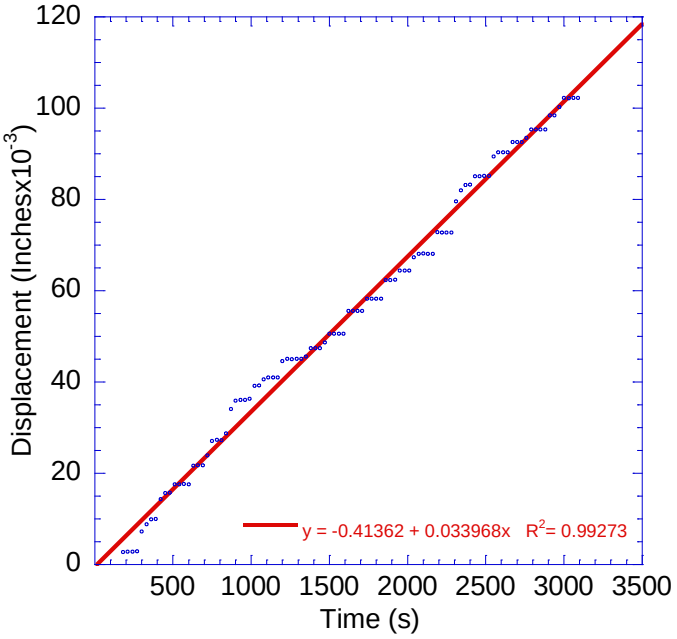

Figure A- 14: Measured displacement versus time response of a Vycor tube sample when tested in water with an applied hydrostatic pressure of 1.38 Mpa (200 psi).

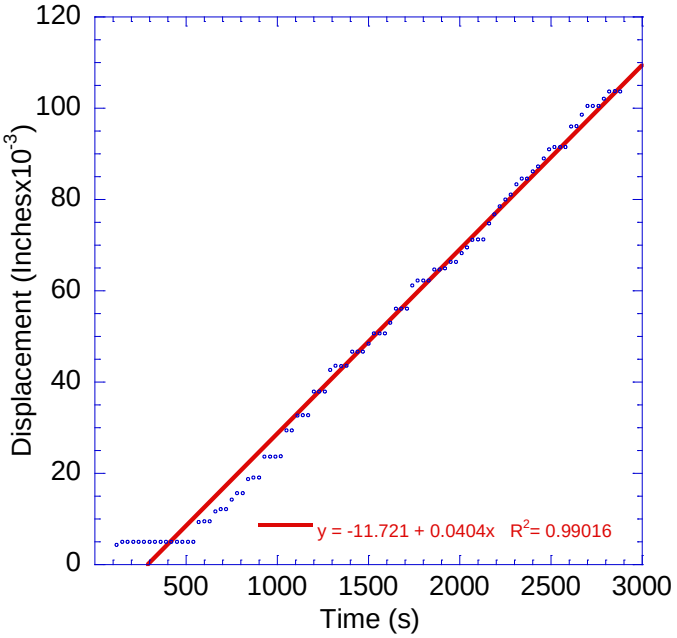

Figure A- 15: Measured displacement versus time response of a Vycor tube sample when tested in water with an applied hydrostatic pressure of 1.38 Mpa (200 psi).

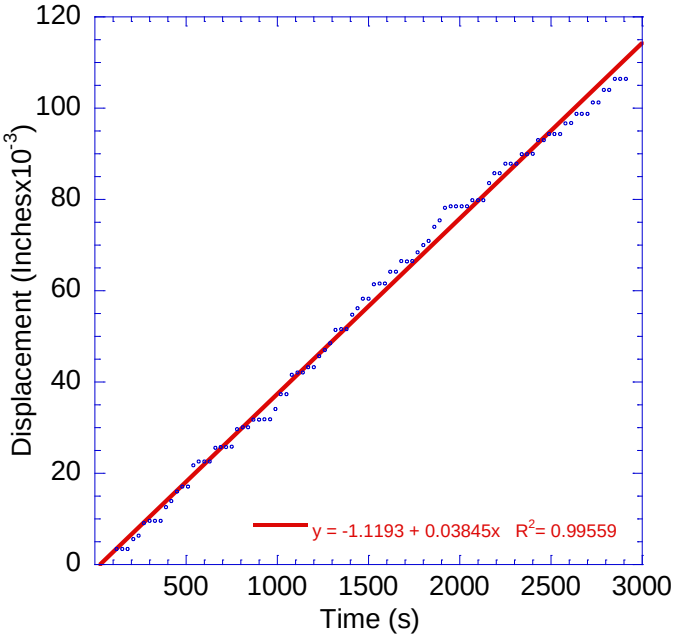

Figure A- 16: Measured displacement versus time response of a Vycor tube sample when tested in water with an applied hydrostatic pressure of 1.38 Mpa (200 psi).

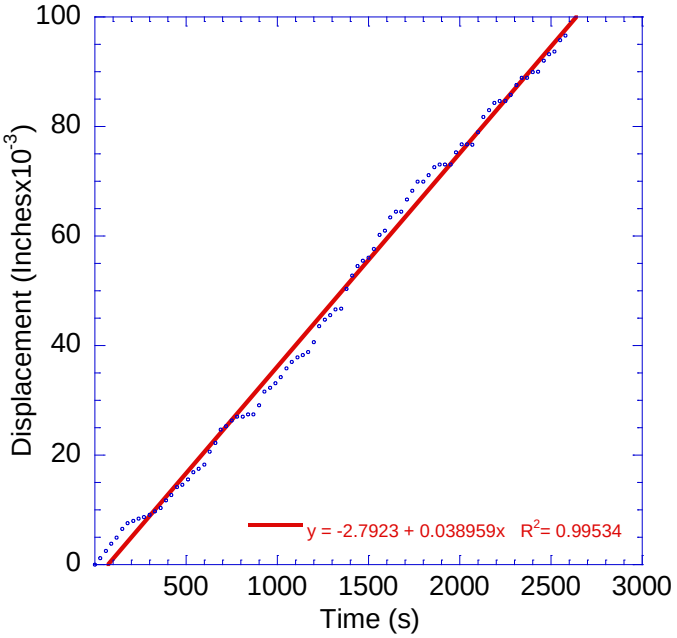

Figure A- 17: Measured displacement versus time response of a Vycor tube sample when tested in water with an applied hydrostatic pressure of 1.38 Mpa (200 psi).

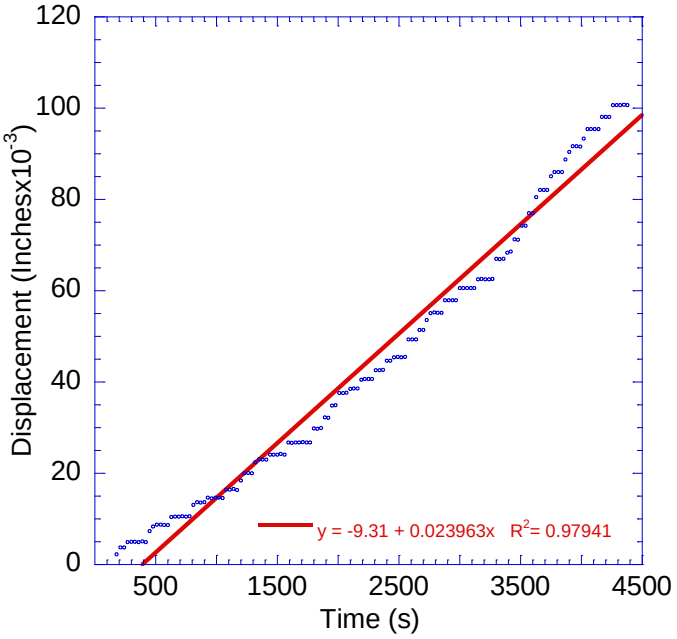

Figure A- 18: Measured displacement versus time response of a Vycor tube sample when tested in water with an applied hydrostatic pressure of 1.38 Mpa (200 psi).

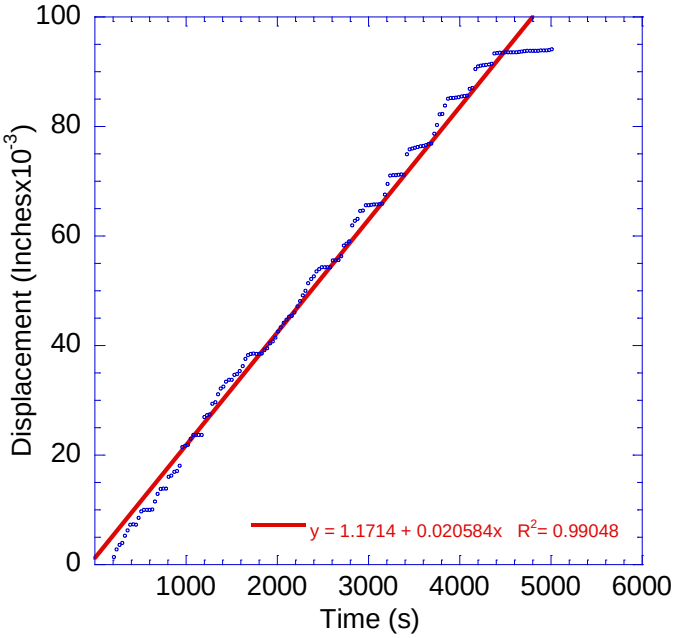

Figure A- 19: Measured displacement versus time response of a Vycor tube sample when tested in water with an applied hydrostatic pressure of 1.38 Mpa (200 psi).

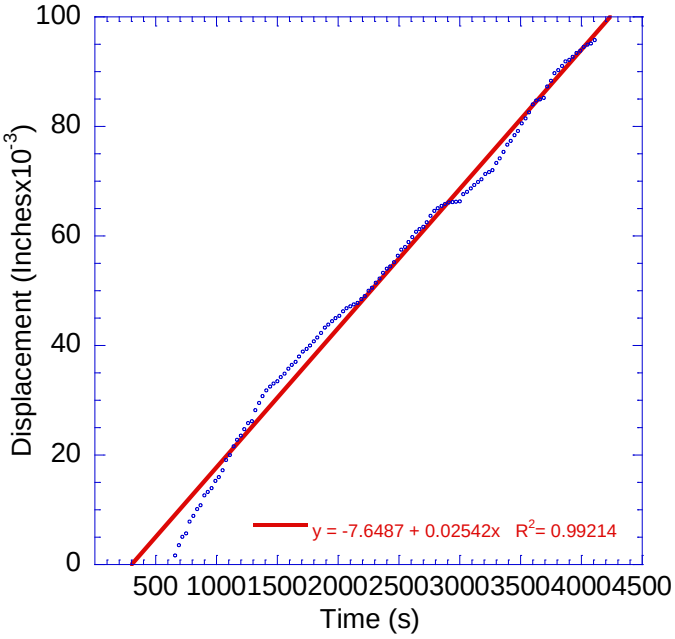

Figure A- 20: Measured displacement versus time response of a Vycor tube sample when tested in water with an applied hydrostatic pressure of 1.38 Mpa (200 psi).

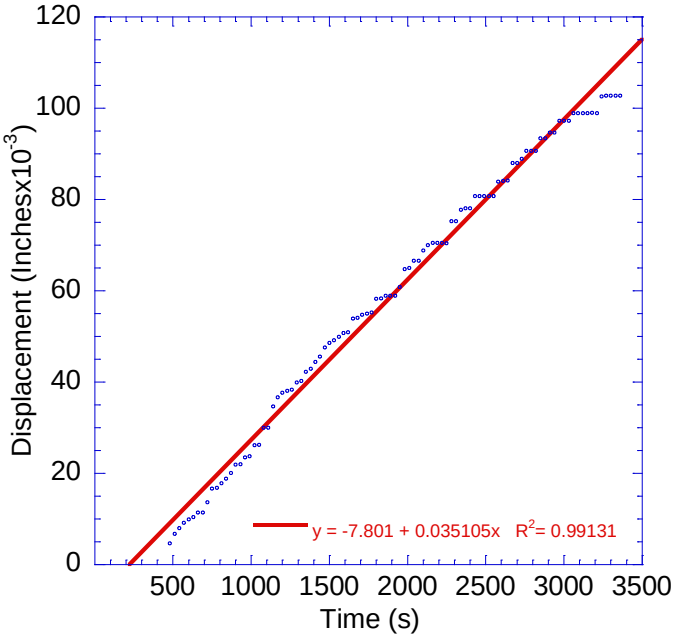

Figure A- 21: Measured displacement versus time response of a Vycor tube sample when tested in water with an applied hydrostatic pressure of 1.38 Mpa (200 psi).

Vycor Hollow Dynamic Pressurization Plots

100% Glycerol

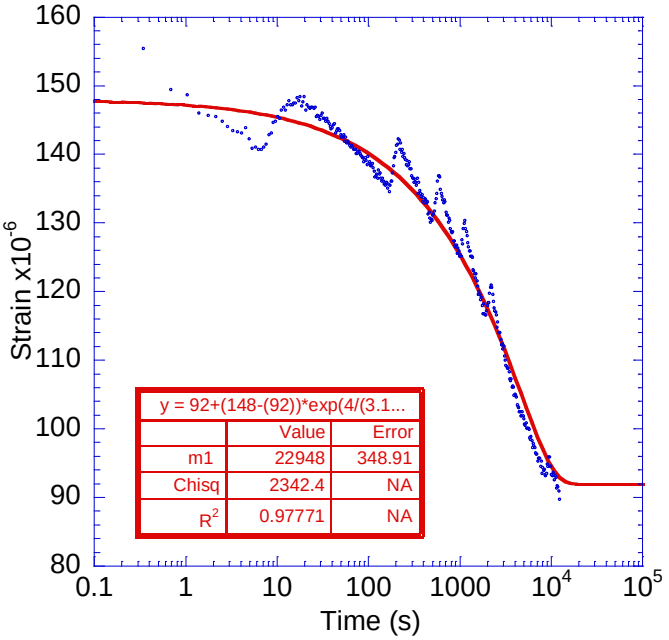

Figure A- 22: The strain versus time response of a Vycor tube tested in 100% glycerol. The spikes in the early time range are attributed to the hydraulic pump cycling on and off trying to supply a steady pressure. Compressive strain is positive.

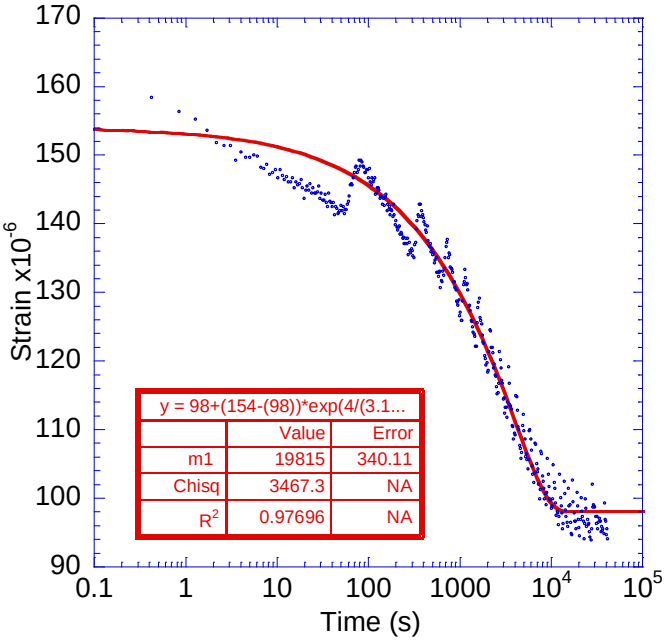

Figure A- 23: The strain versus time response of a Vycor tube tested in 100% glycerol. The spikes in the early time range are attributed to the hydraulic pump cycling on and off trying to supply a steady pressure. Compressive strain is positive.

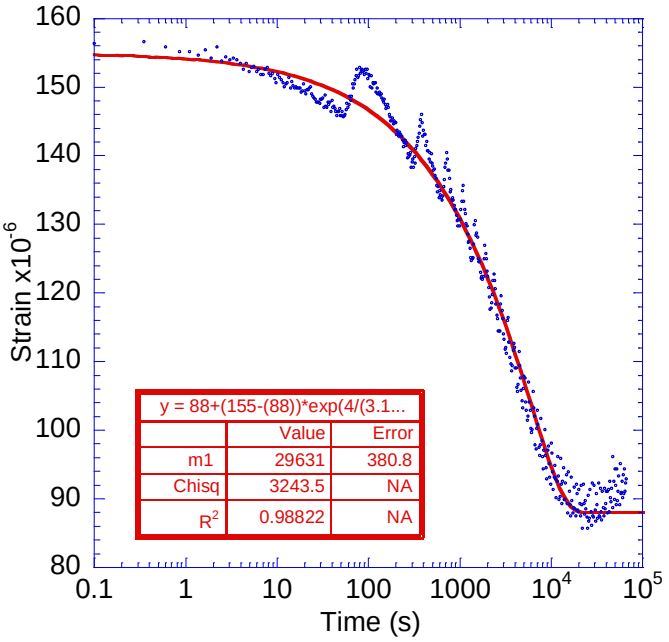

Figure A- 24: The strain versus time response of a Vycor tube tested in 100% glycerol. The spikes in the early time range are attributed to the hydraulic pump cycling on and off trying to supply a steady pressure. Compressive strain is positive.

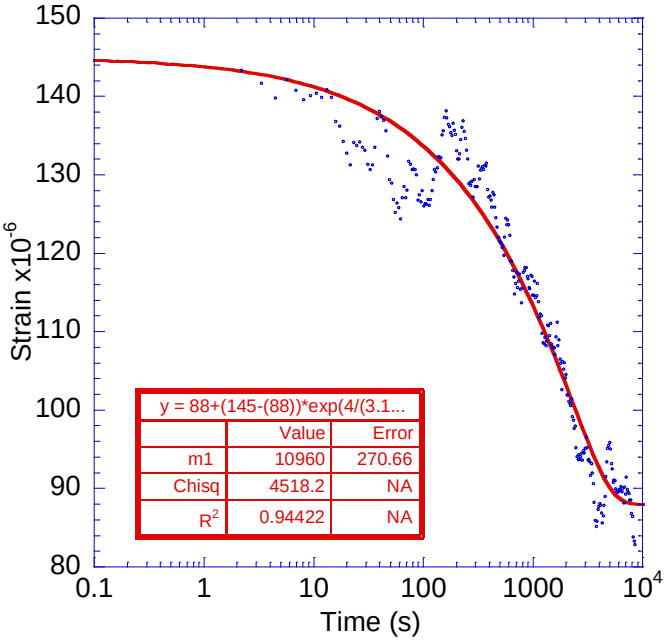

Figure A- 25: The strain versus time response of a Vycor tube tested in 100% glycerol. The spikes in the early time range are attributed to the hydraulic pump cycling on and off trying to supply a steady pressure. Compressive strain is positive.

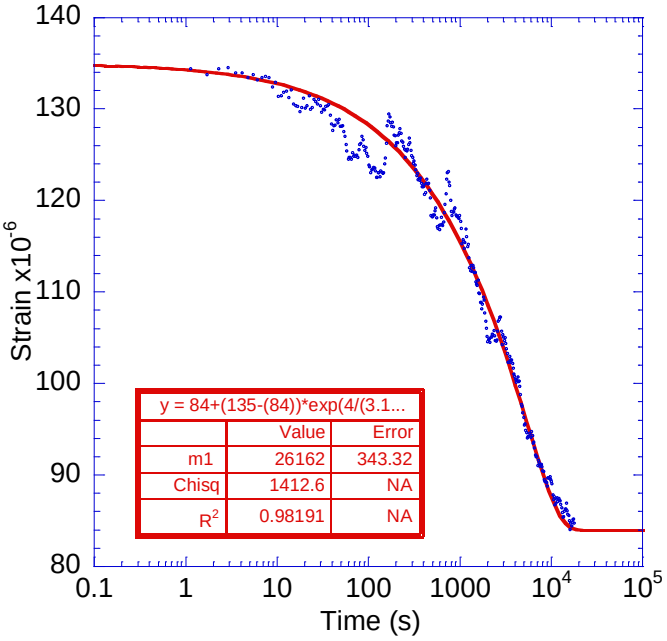

Figure A- 26: The strain versus time response of a Vycor tube tested in 100% glycerol. The spikes in the early time range are attributed to the hydraulic pump cycling on and off trying to supply a steady pressure. Compressive strain is positive.

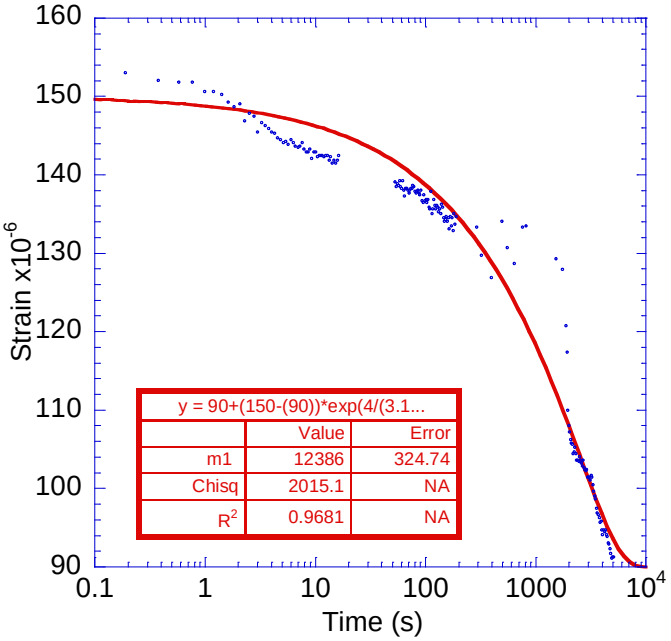

Figure A- 27: The strain versus time response of a Vycor tube tested in 100% glycerol. Compressive strain is positive.

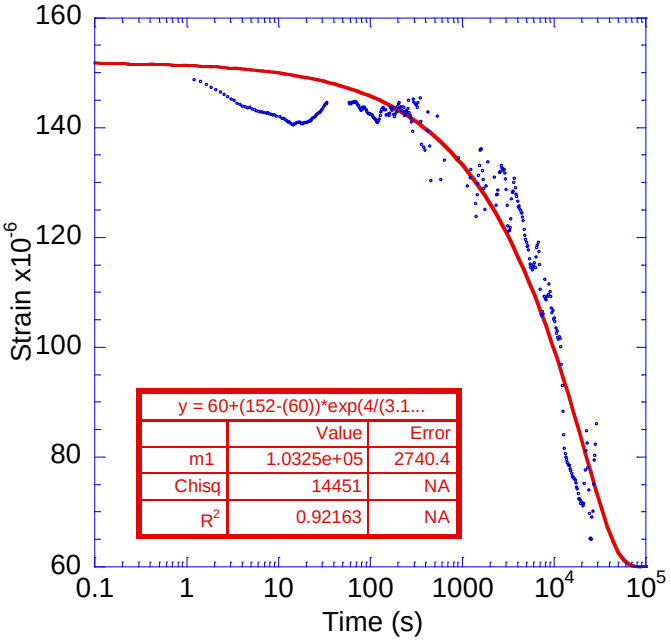

Figure A- 28: The strain versus time response of a Vycor tube tested in 100% glycerol. The spikes in the early time range are attributed to the hydraulic pump cycling on and off trying to supply a steady pressure. Compressive strain is positive.

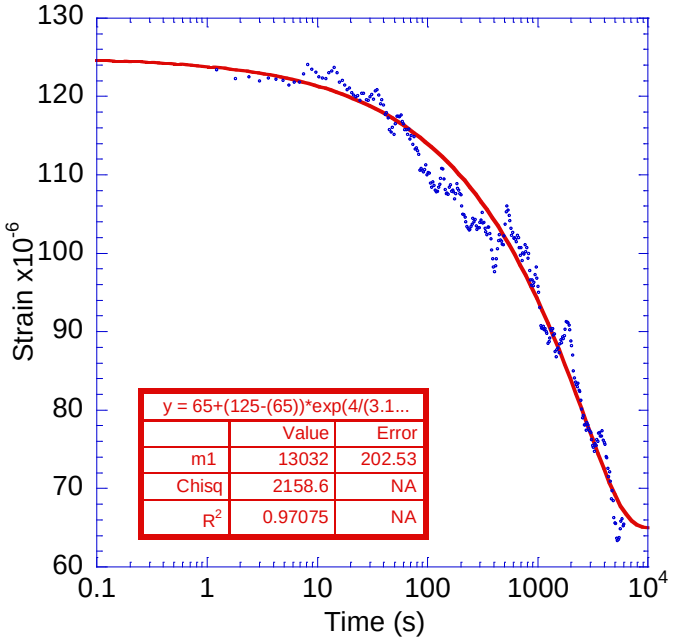

Figure A- 29: The strain versus time response of a Vycor tube tested in 100% glycerol. The spikes in the early time range are attributed to the hydraulic pump cycling on and off trying to supply a steady pressure. Compressive strain is positive.

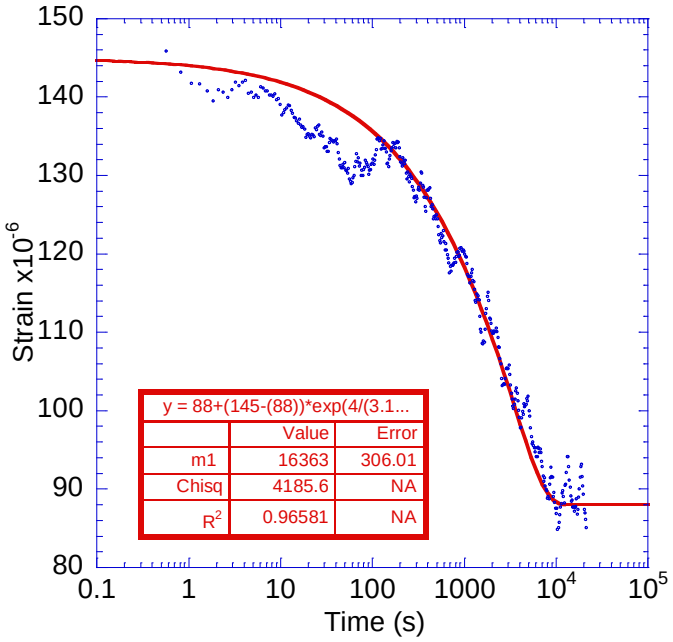

Figure A- 30: The strain versus time response of a Vycor tube tested in 100% glycerol. The spikes in the early time range are attributed to the hydraulic pump cycling on and off trying to supply a steady pressure. Compressive strain is positive.

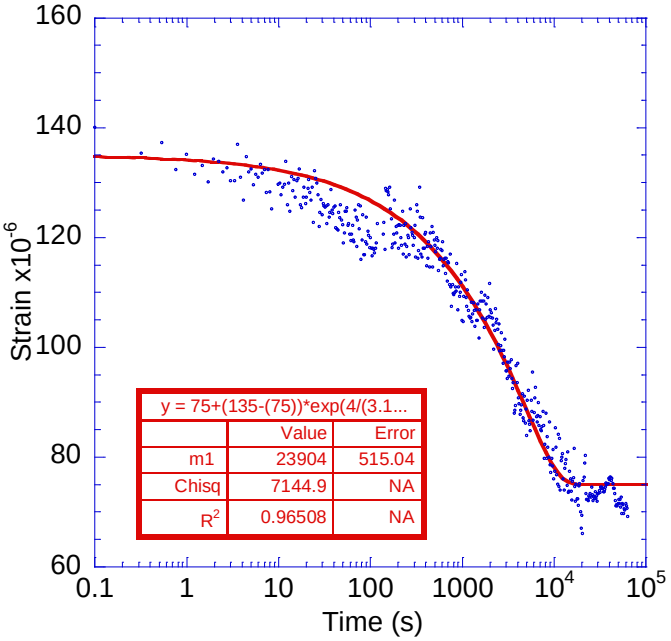

Figure A- 31: The strain versus time response of a Vycor tube tested in 100% glycerol. Compressive strain is positive.

90% Glycerol

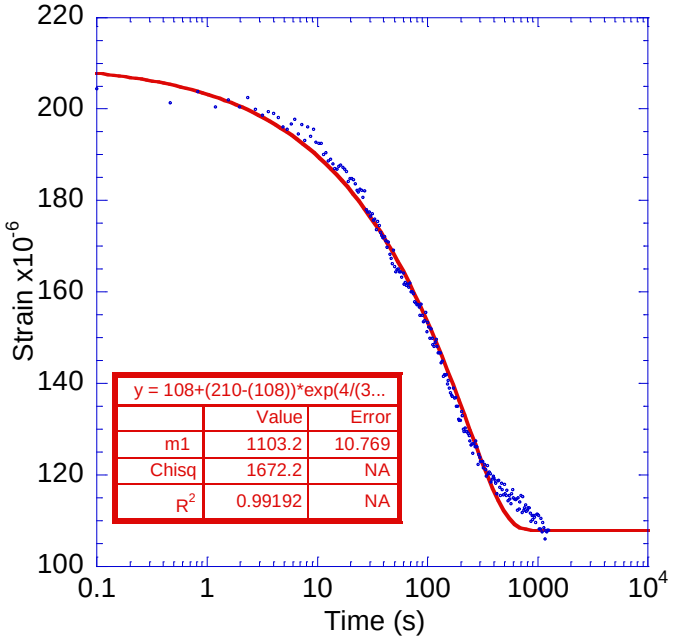

Figure A- 32: The strain versus time response of a Vycor tube tested in 90 weight percent glycerol. Compressive strain is positive.

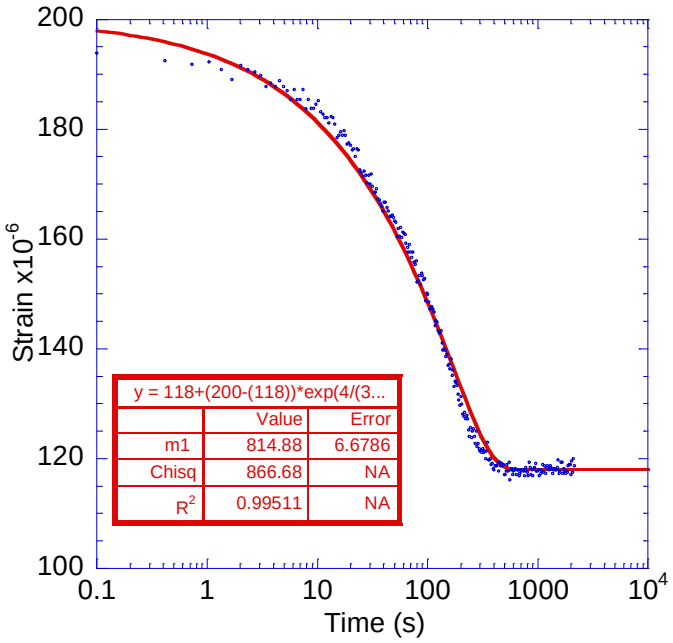

Figure A- 33: The strain versus time response of a Vycor tube tested in 90 weight percent glycerol. Compressive strain is positive.

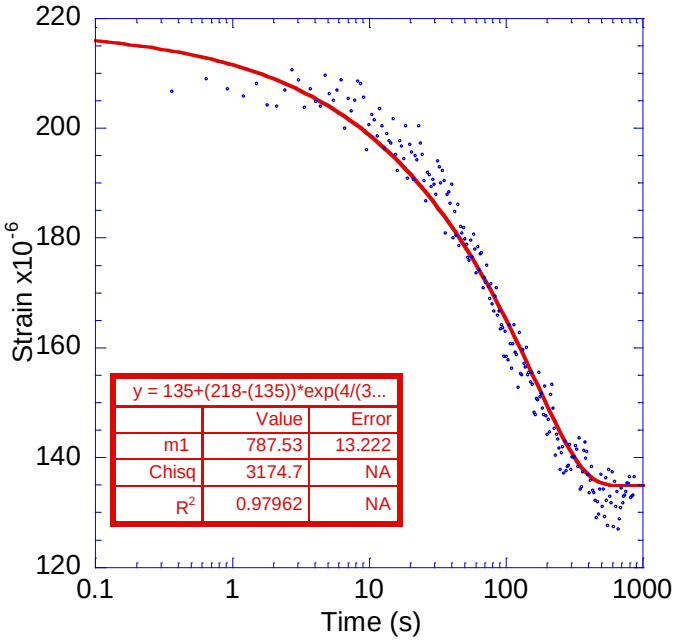

Figure A- 34: The strain versus time response of a Vycor tube tested in 90 weight percent glycerol. Compressive strain is positive.

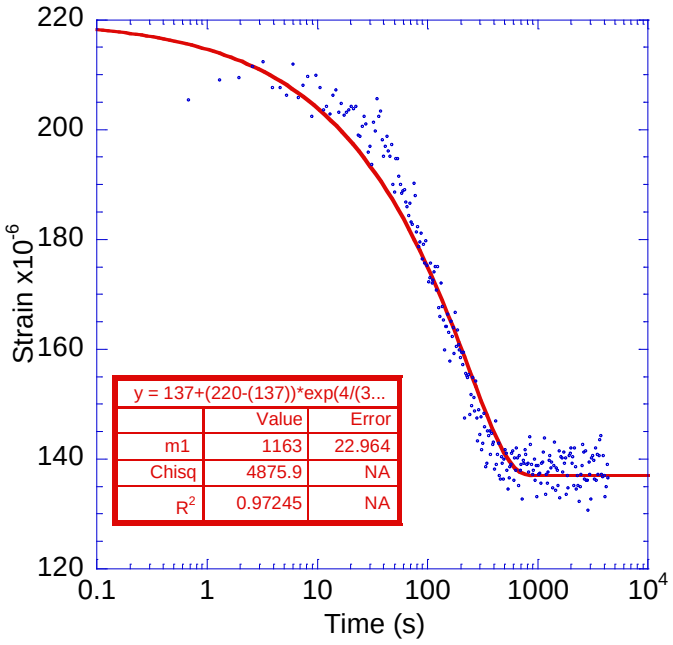

Figure A- 35: The strain versus time response of a Vycor tube tested in 90 weight percent glycerol. Compressive strain is positive.

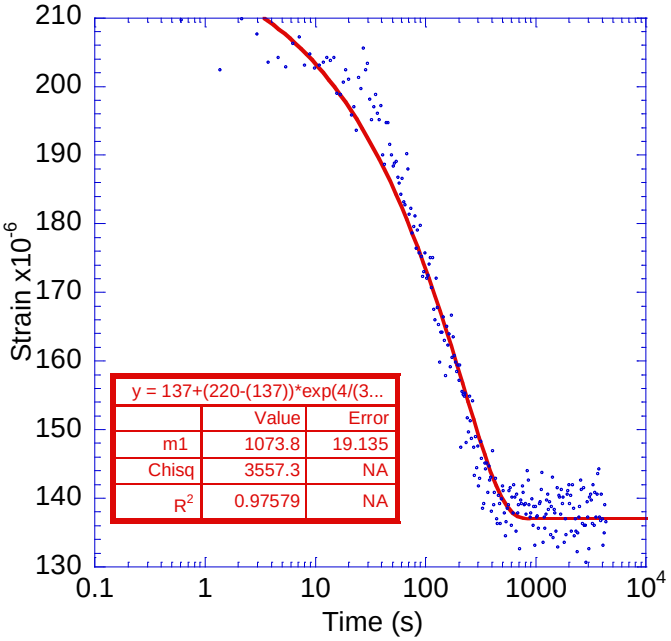

Figure A- 36: The strain versus time response of a Vycor tube tested in 90 weight percent glycerol. Compressive strain is positive.

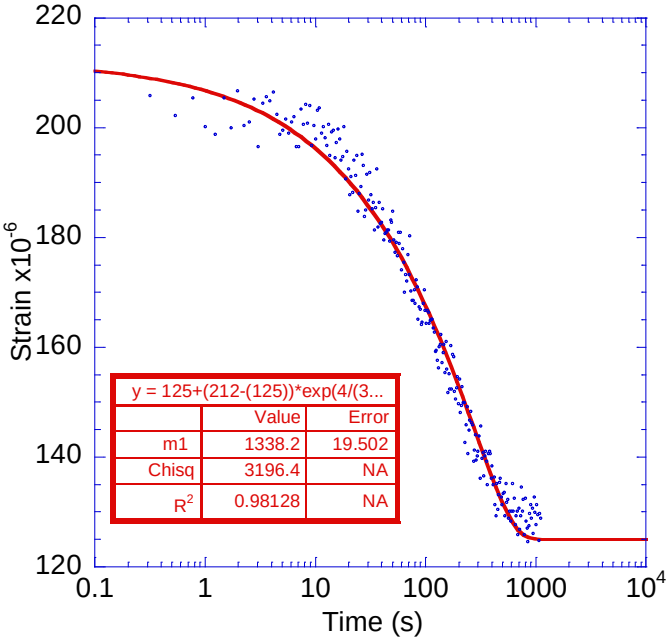

Figure A- 37: The strain versus time response of a Vycor tube tested in 90 weight percent glycerol. Compressive strain is positive.

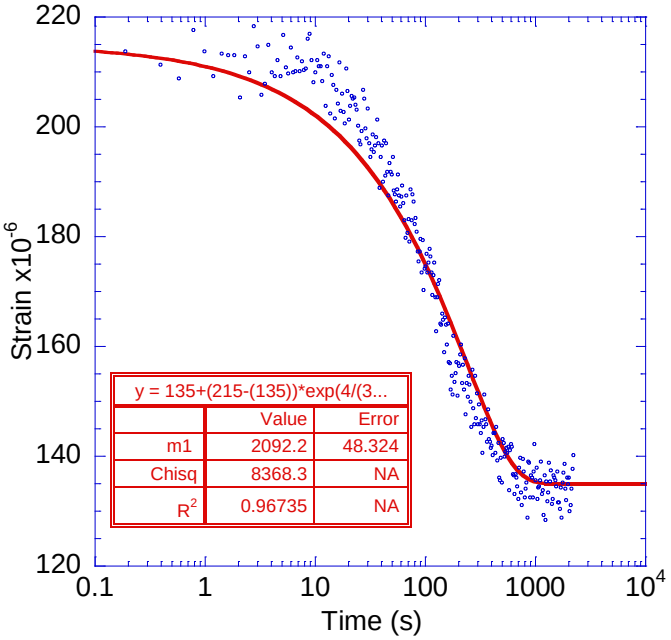

Figure A- 38: The strain versus time response of a Vycor tube tested in 90 weight percent glycerol. Compressive strain is positive.

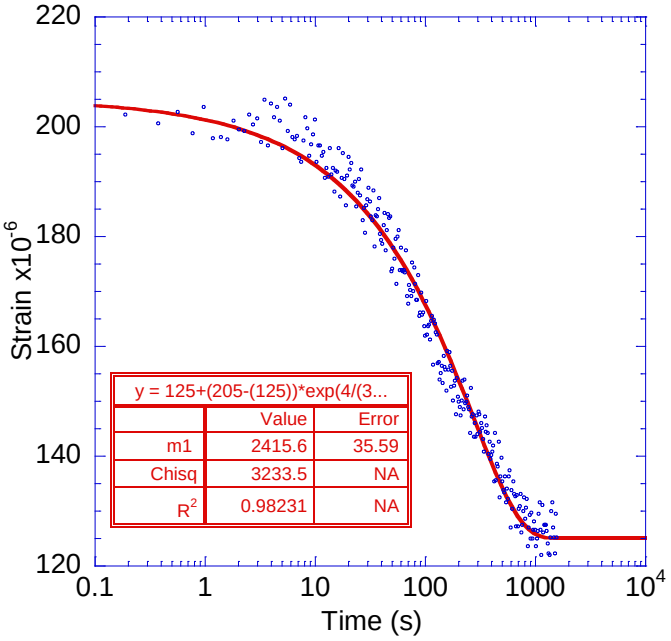

Figure A- 39: The strain versus time response of a Vycor tube tested in 90 weight percent glycerol. Compressive strain is positive.

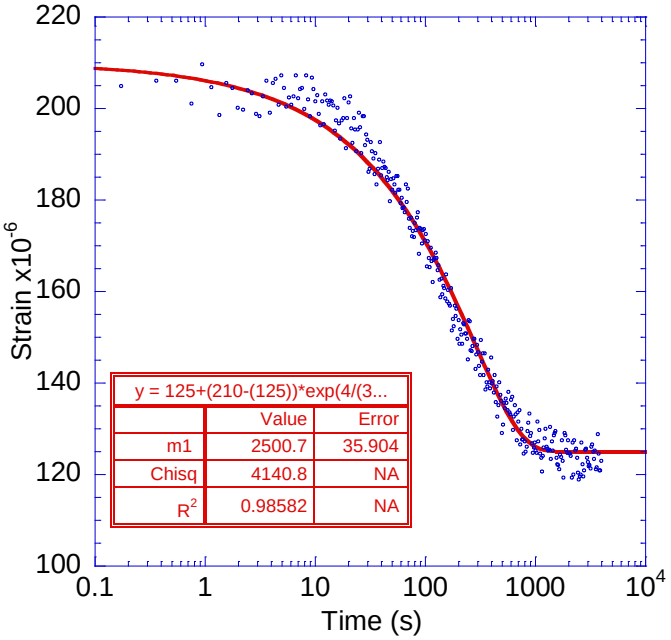

Figure A- 40: The strain versus time response of a Vycor tube tested in 90 weight percent glycerol. Compressive strain is positive.

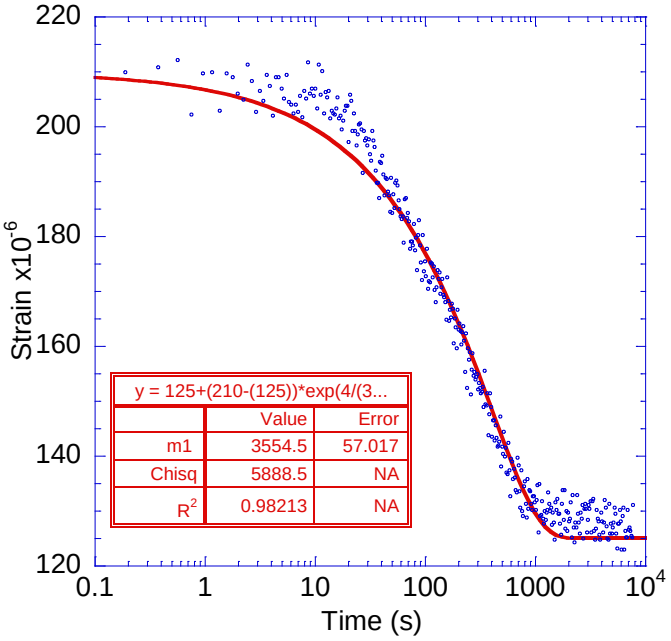

Figure A- 41: The strain versus time response of a Vycor tube tested in 90 weight percent glycerol. Compressive strain is positive.

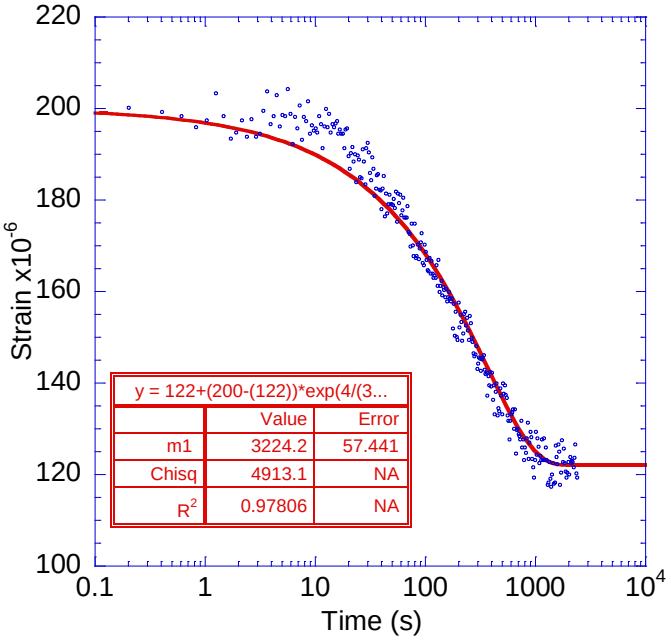

Figure A- 42: The strain versus time response of a Vycor tube tested in 90 weight percent glycerol. Compressive strain is positive.

65% Glycerol

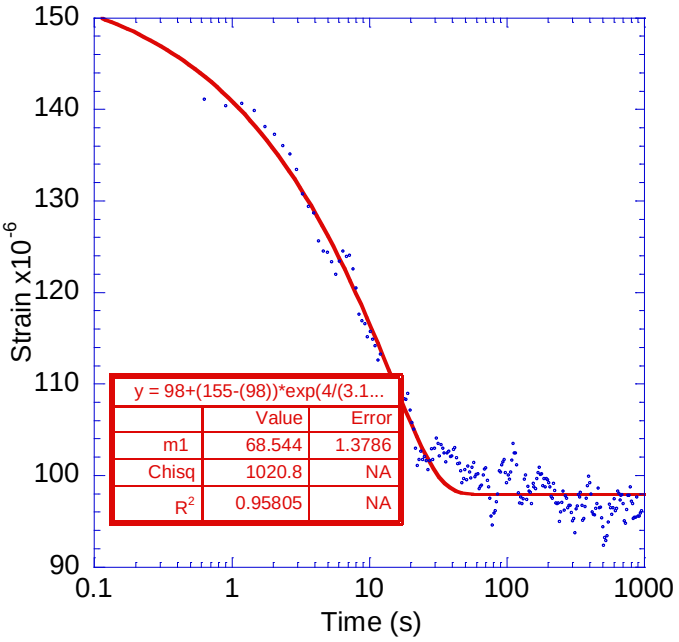

Figure A- 43:The strain versus time response for a Vycor tube tested in 65 weight percent glycerol. Note how quickly these data are collected. Compressive strain is positive.

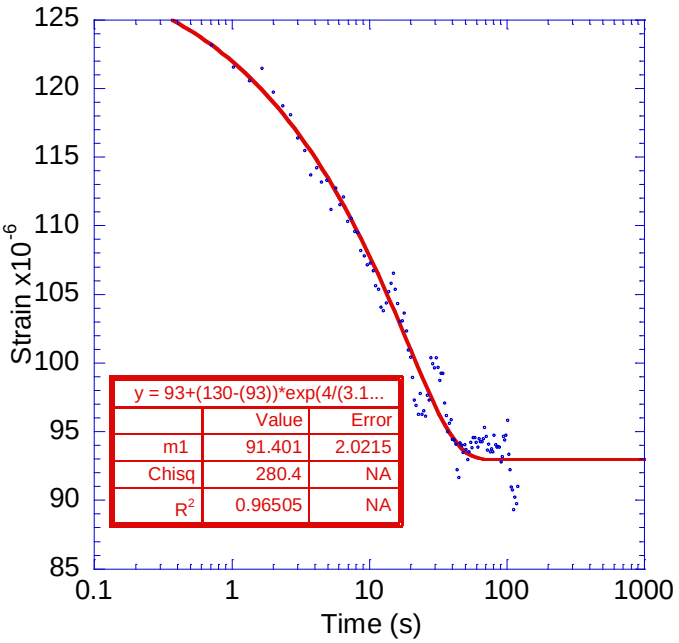

Figure A- 44: The strain versus time response for a Vycor tube tested in 65 weight percent glycerol. Note how quickly these data are collected. Compressive strain is positive.

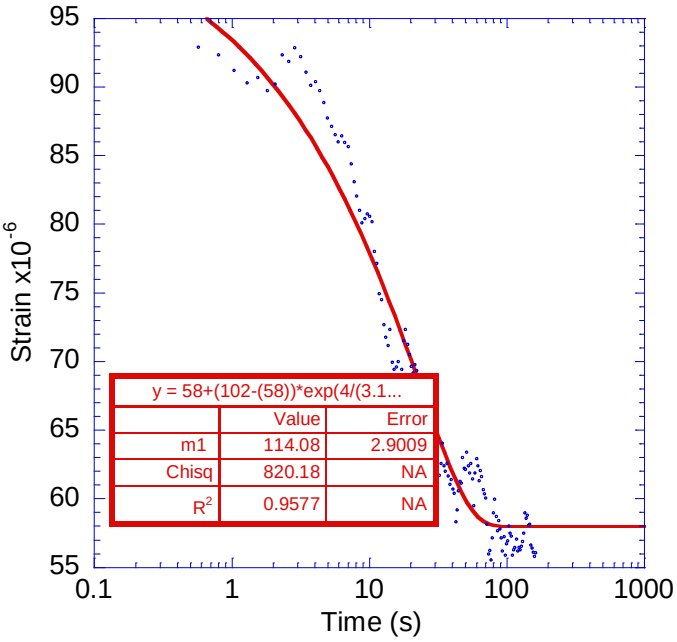

Figure A- 45: The strain versus time response for a Vycor tube tested in 65 weight percent glycerol. Note how quickly these data are collected. Compressive strain is positive.

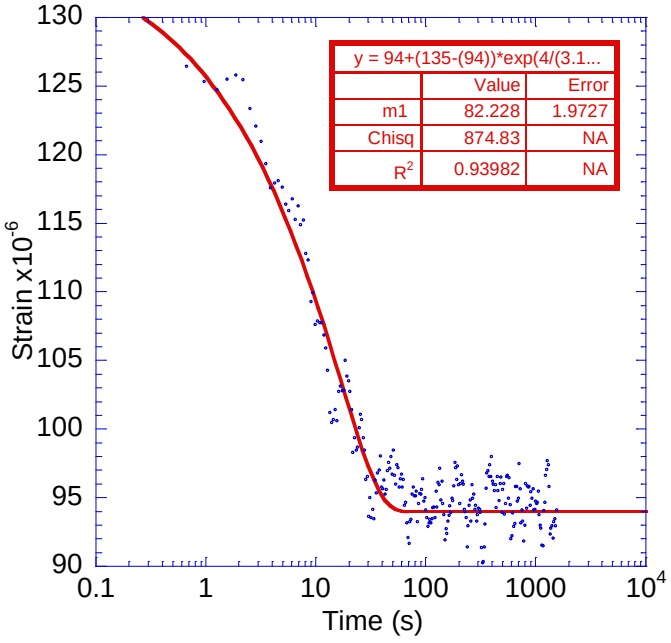

Figure A- 46: The strain versus time response for a Vycor tube tested in 65 weight percent glycerol. Note how quickly these data are collected. Compressive strain is positive.

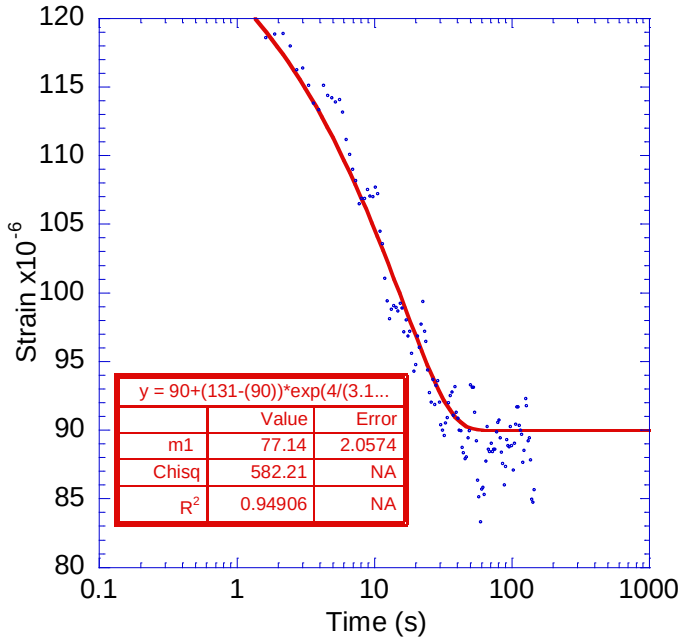

Figure A- 47: The strain versus time response for a Vycor tube tested in 65 weight percent glycerol. Note how quickly these data are collected. Compressive strain is positive.

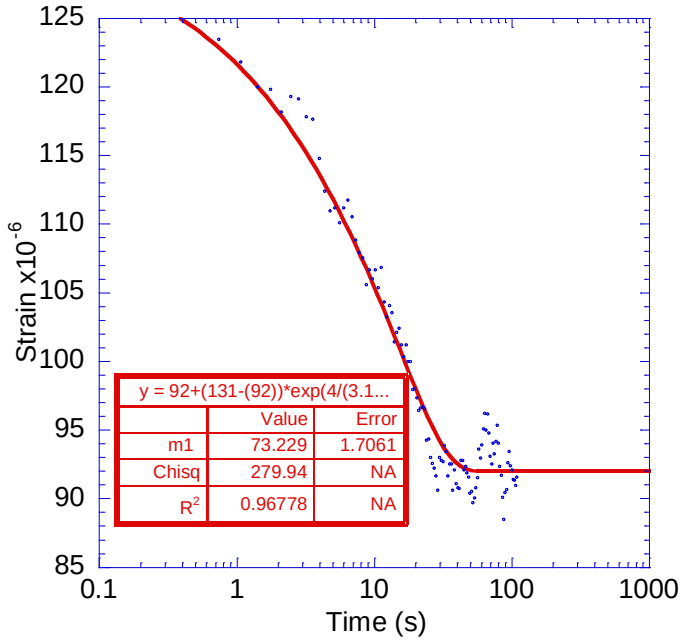

Figure A- 48: The strain versus time response for a Vycor tube tested in 65 weight percent glycerol. Note how quickly these data are collected. Compressive strain is positive.

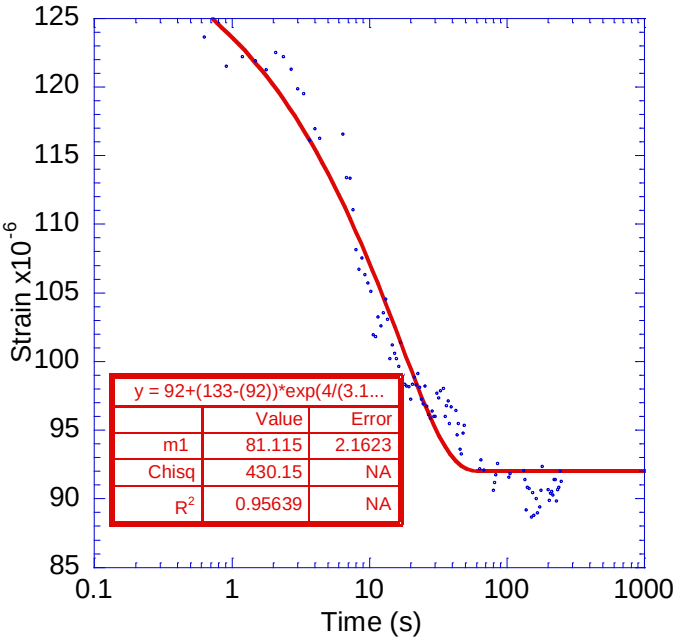

Figure A- 49: The strain versus time response for a Vycor tube tested in 65 weight percent glycerol. Note how quickly these data are collected. Compressive strain is positive.

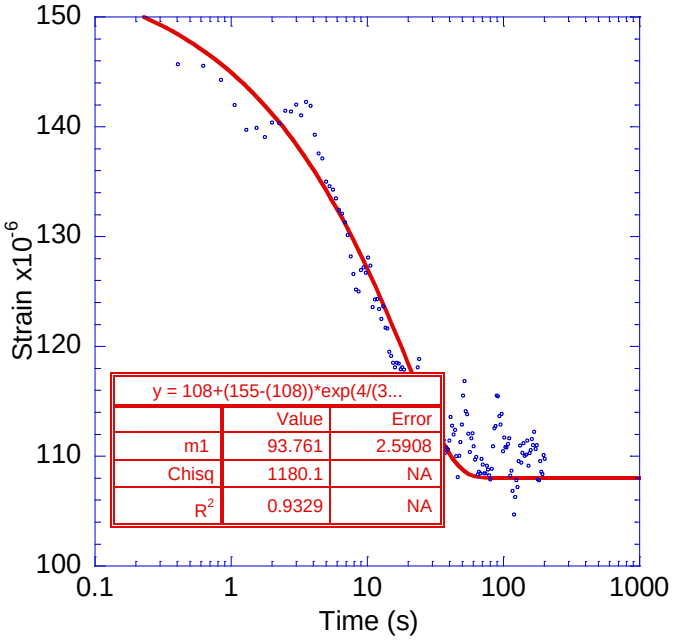

Figure A- 50: The strain versus time response for a Vycor tube tested in 65 weight percent glycerol. Note how quickly these data are collected. Compressive strain is positive.

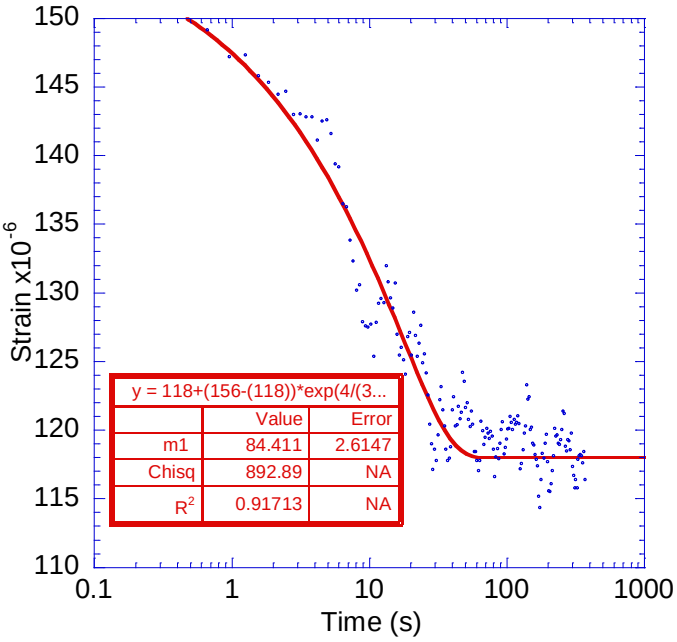

Figure A- 51: The strain versus time response for a Vycor tube tested in 65 weight percent glycerol. Note how quickly these data are collected. Compressive strain is positive.

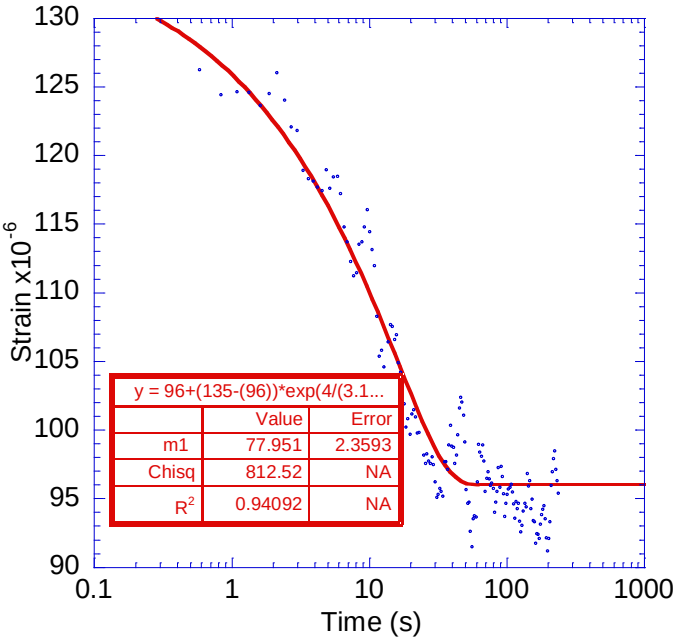

Figure A- 52: The strain versus time response for a Vycor tube tested in 65 weight percent glycerol. Note how quickly these data are collected. Compressive strain is positive.

Vycor Solid Dynamic Pressurization Plots

100% Glycerol

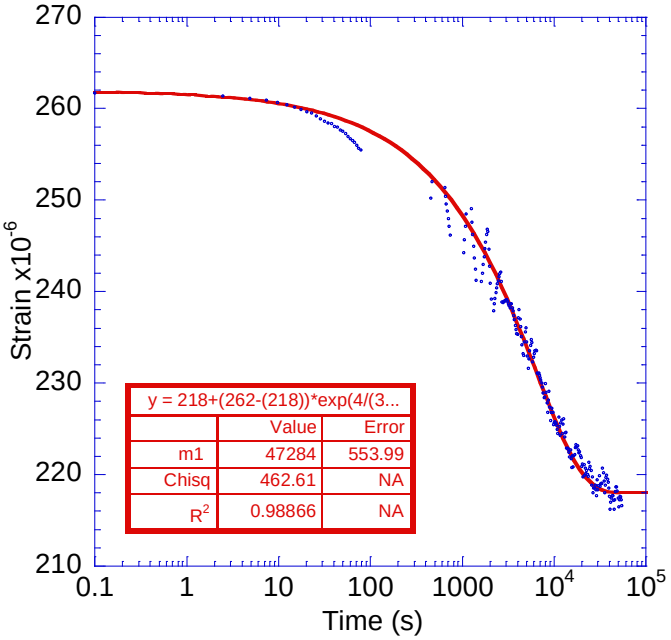

Figure A- 53: The strain versus time response for a Vycor rod tested in pure glycerol. Compressive strain is positive.

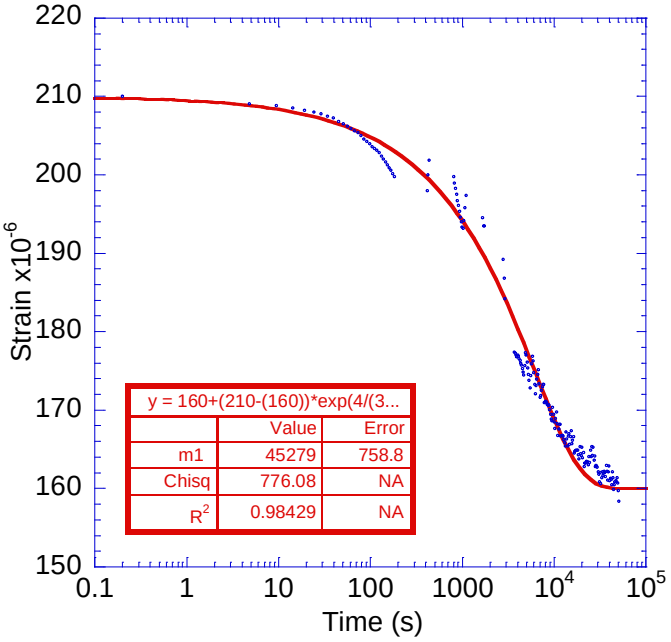

Figure A- 54: The strain versus time response for a Vycor rod tested in pure glycerol. Compressive strain is positive.

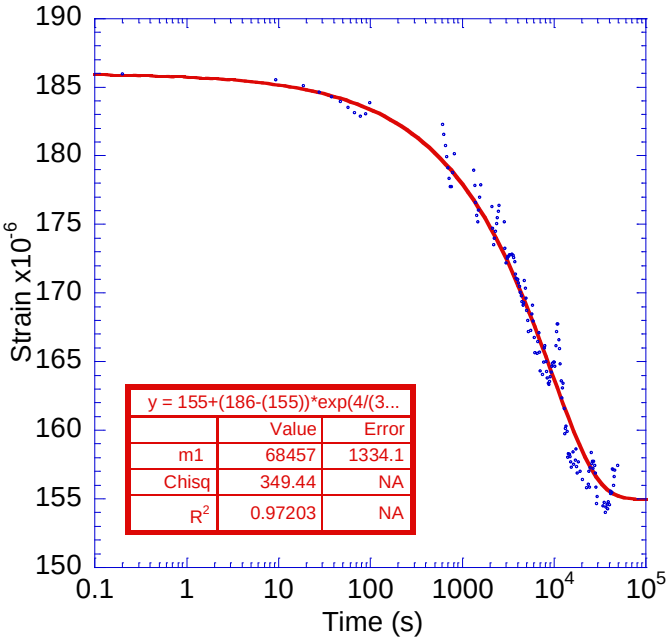

Figure A- 55: The strain versus time response for a Vycor rod tested in pure glycerol. Compressive strain is positive.

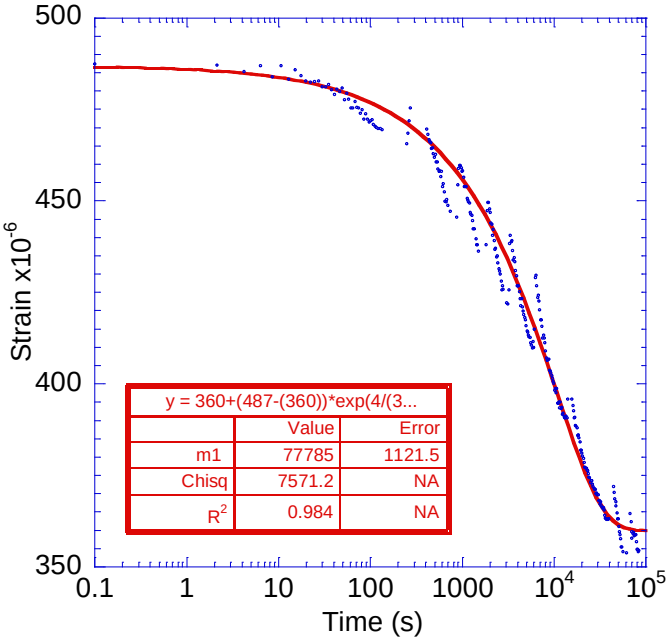

Figure A- 56: The strain versus time response for a Vycor rod tested in pure glycerol. Compressive strain is positive.

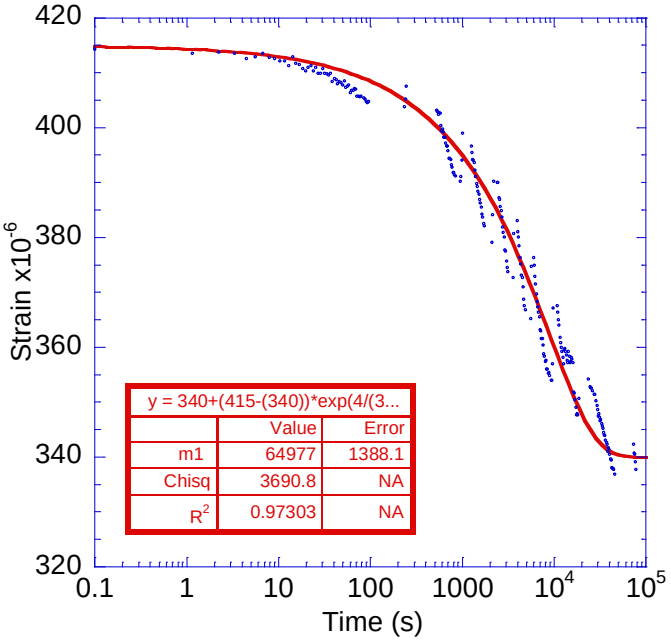

Figure A- 57: The strain versus time response for a Vycor rod tested in pure glycerol. Compressive strain is positive.

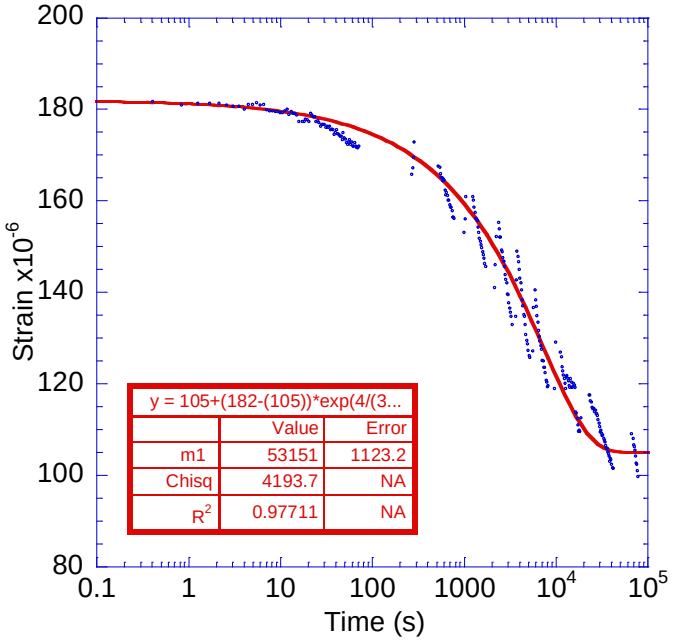

Figure A- 58: The strain versus time response for a Vycor rod tested in pure glycerol. Compressive strain is positive.

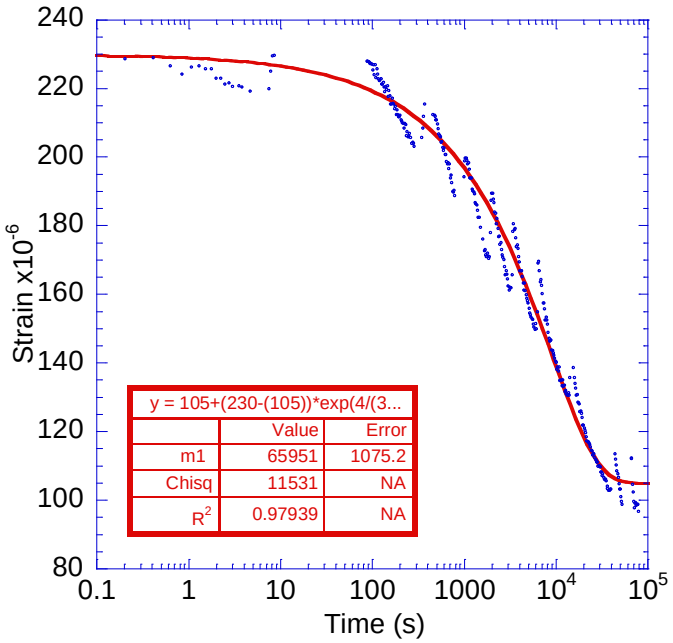

Figure A- 59: The strain versus time response for a Vycor rod tested in pure glycerol. Compressive strain is positive.

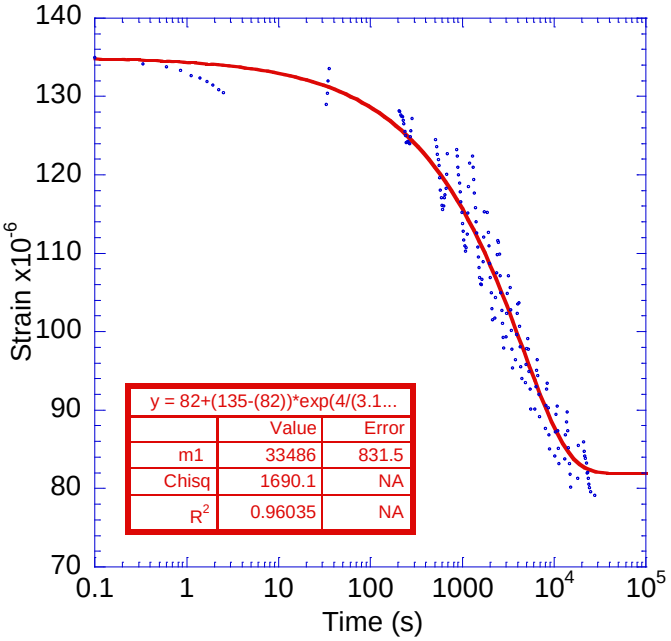

Figure A- 60: The strain versus time response for a Vycor rod tested in pure glycerol. Compressive strain is positive.

65% Glycerol

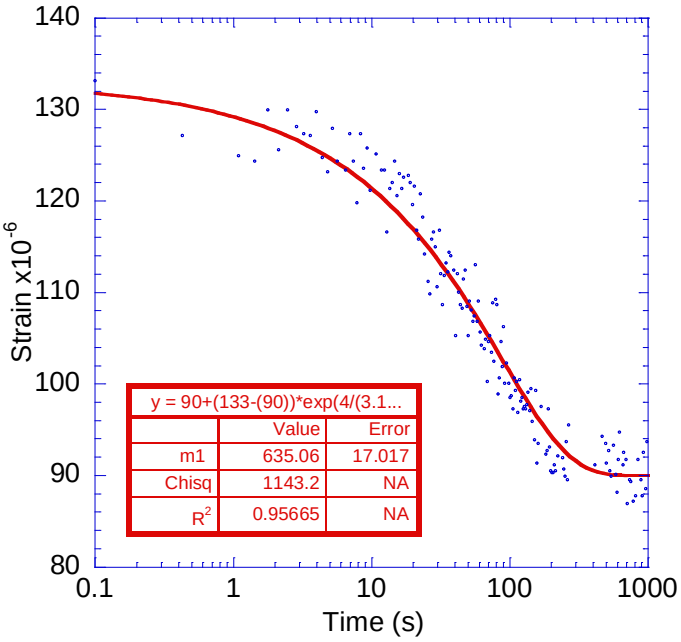

Figure A- 61: The strain versus time response for a Vycor rod tested in 65% glycerol. Compressive strain is positive.

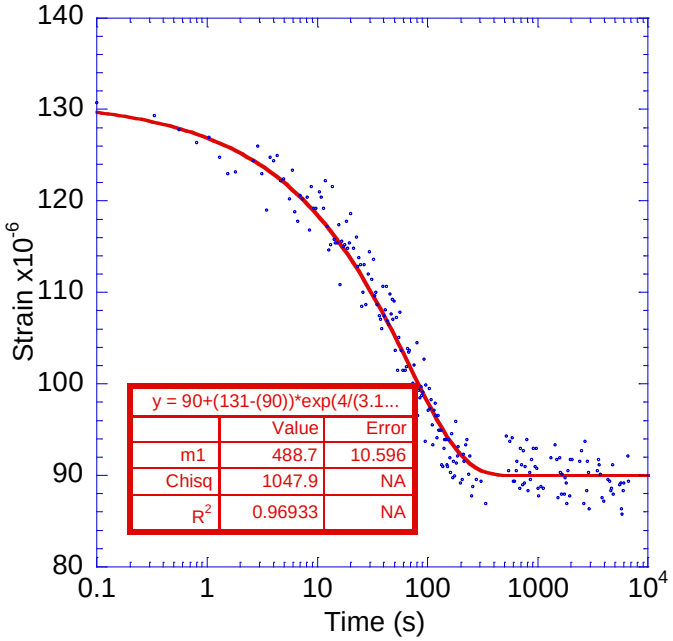

Figure A- 62: The strain versus time response for a Vycor rod tested in 65% glycerol. Compressive strain is positive.

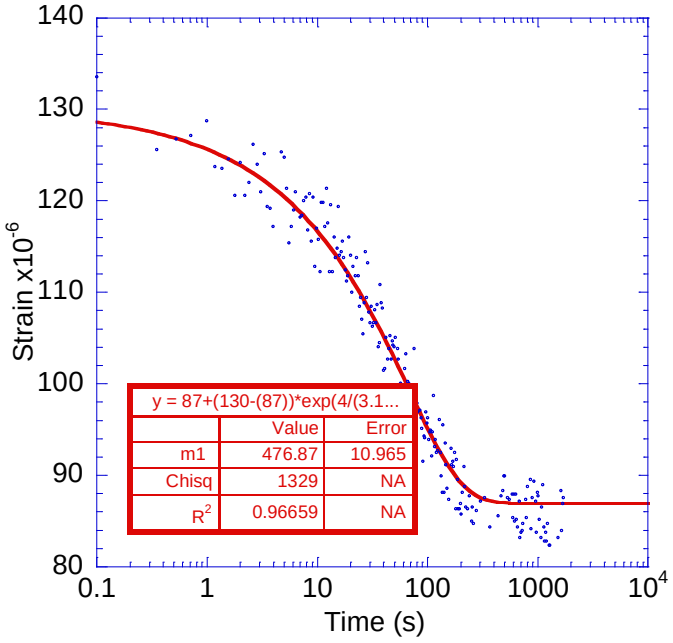

Figure A- 63: The strain versus time response for a Vycor rod tested in 65% glycerol. Compressive strain is positive.

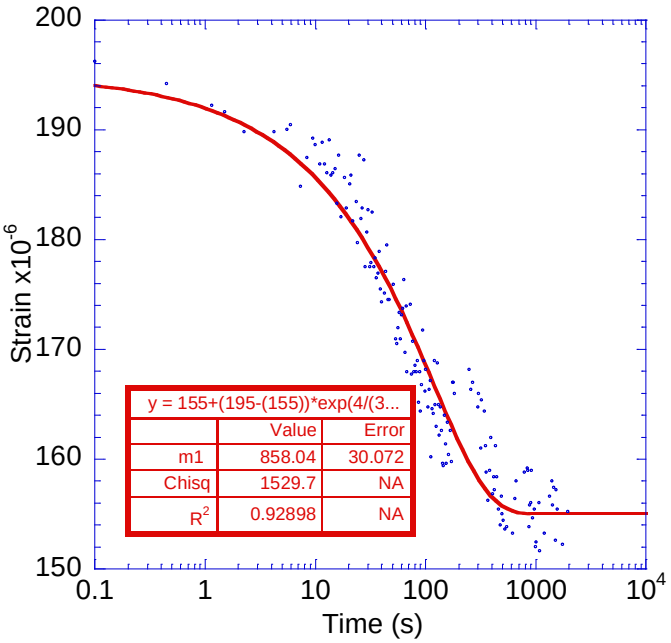

Figure A- 64: The strain versus time response for a Vycor rod tested in 65% glycerol. Compressive strain is positive.

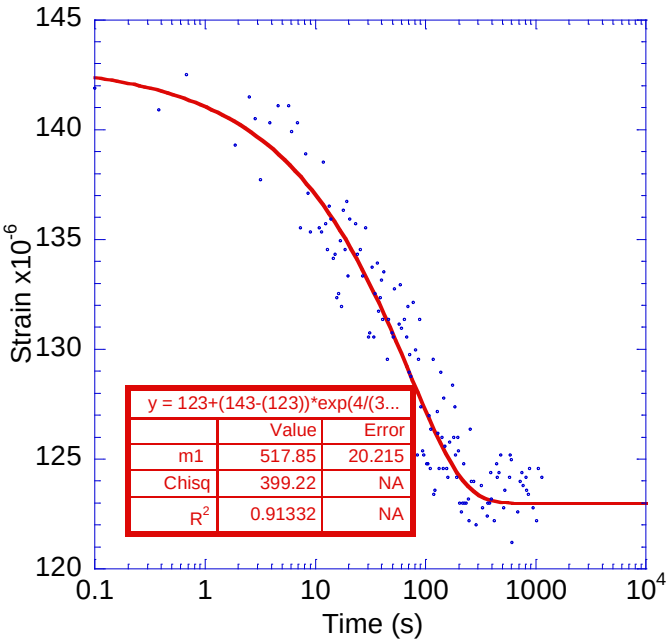

Figure A- 65: The strain versus time response for a Vycor rod tested in 65% glycerol. Compressive strain is positive.

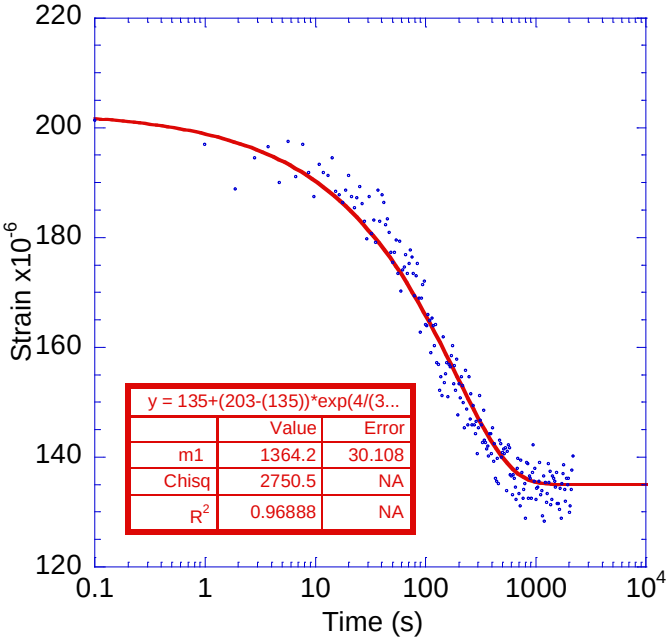

Figure A- 66: The strain versus time response for a Vycor rod tested in 65% glycerol. Compressive strain is positive.

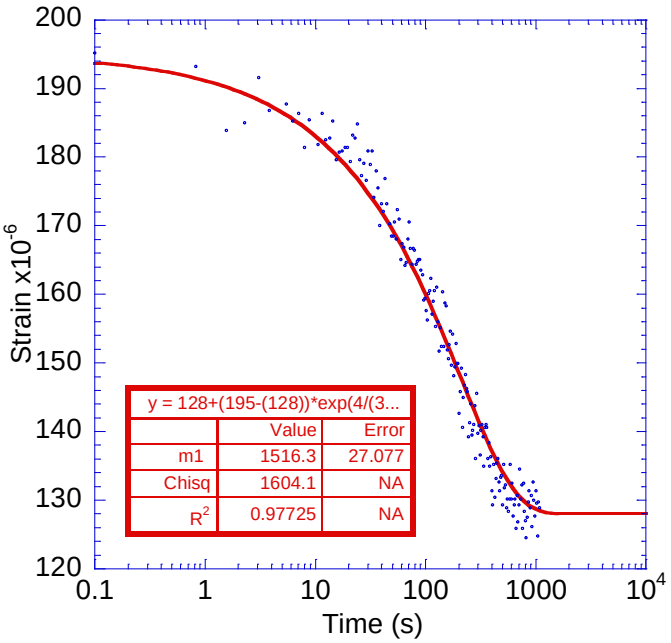

Figure A- 67: The strain versus time response for a Vycor rod tested in 65% glycerol. Compressive strain is positive.

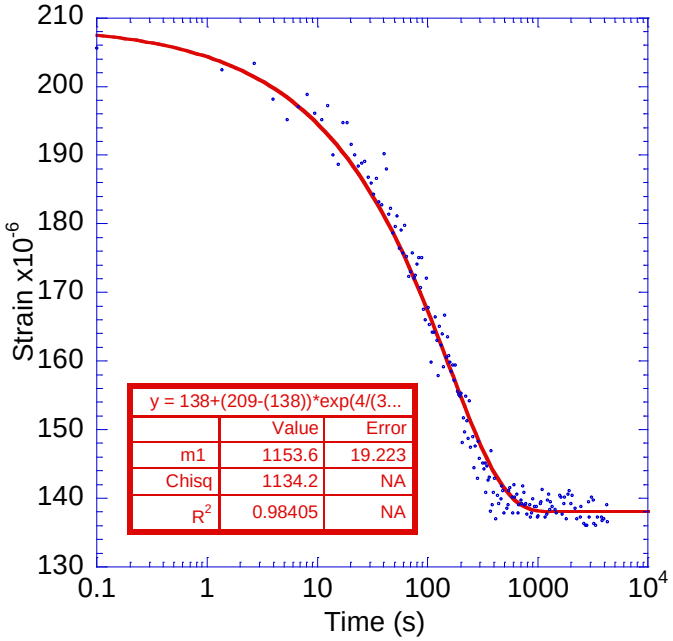

Figure A- 68: The strain versus time response for a Vycor rod tested in 65% glycerol. Compressive strain is positive.

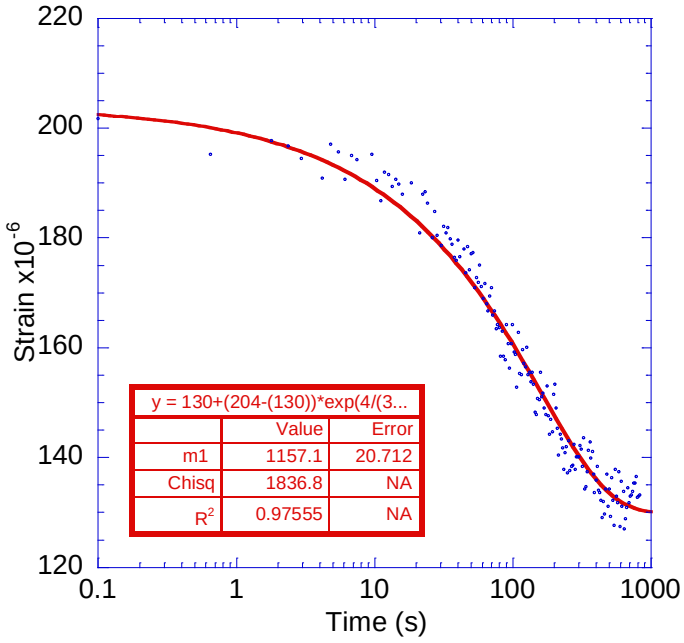

Figure A- 69: The strain versus time response for a Vycor rod tested in 65% glycerol. Compressive strain is positive.

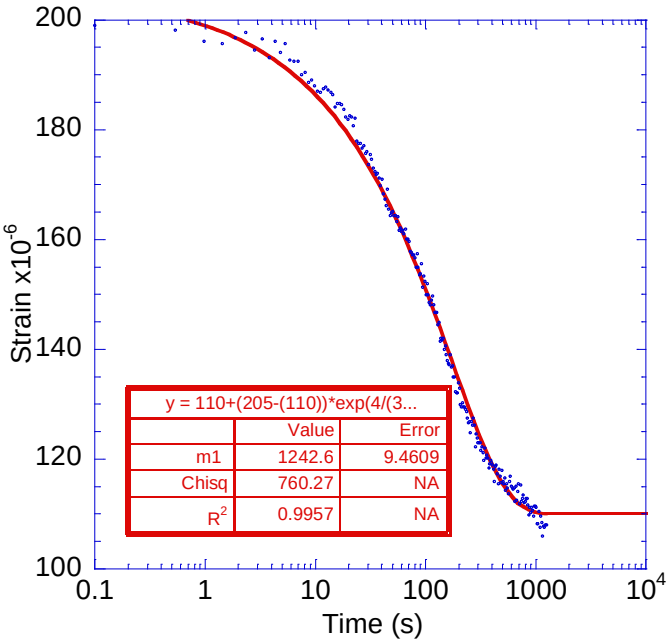

Figure A- 70: The strain versus time response for a Vycor rod tested in 65% glycerol. Compressive strain is positive.

APPENDIX B. CEMENTITIOUS MATERIALS PLOTS

Cement Paste Flow Through Plots

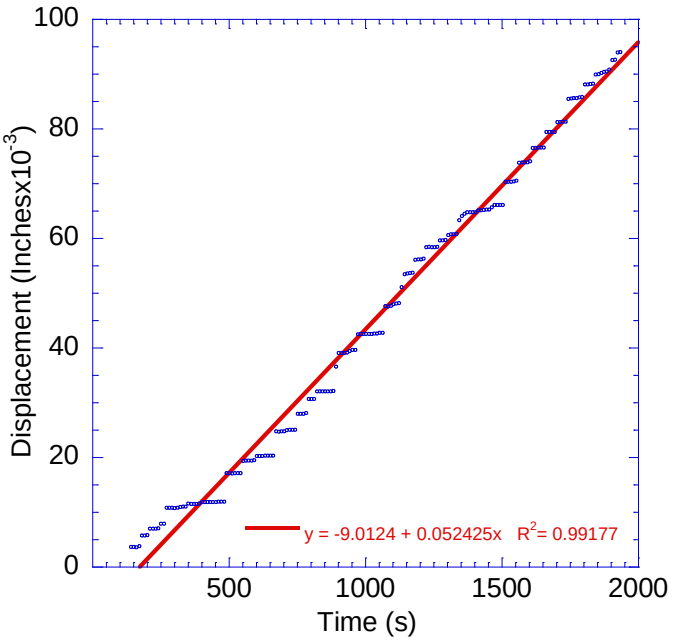

Figure B- 1: The displacement versus time results for a 0.6 water to cement ratio specimen at an age of 32 days and an applied pressure of 1.72 Mpa (250 psi). The testing fluid was water.

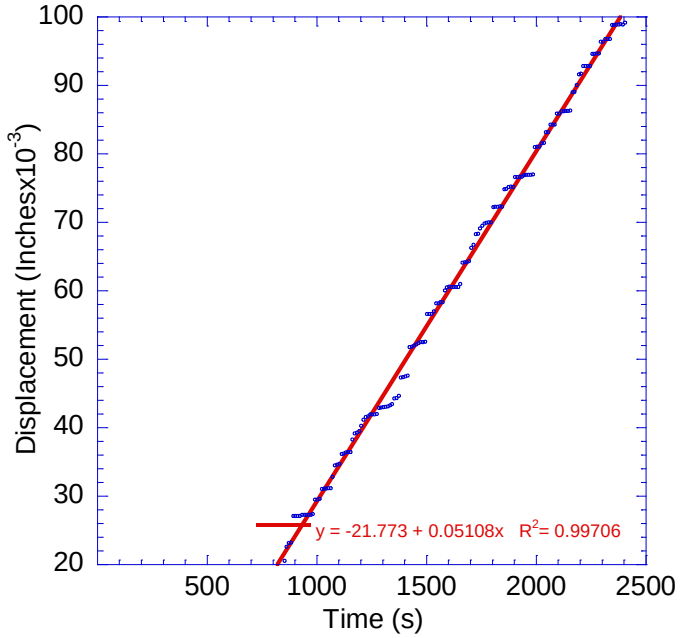

Figure B- 2: The displacement versus time results for a 0.6 water to cement ratio specimen at an age of 32 days and an applied pressure of 1.72 Mpa (250 psi). The testing fluid was water.

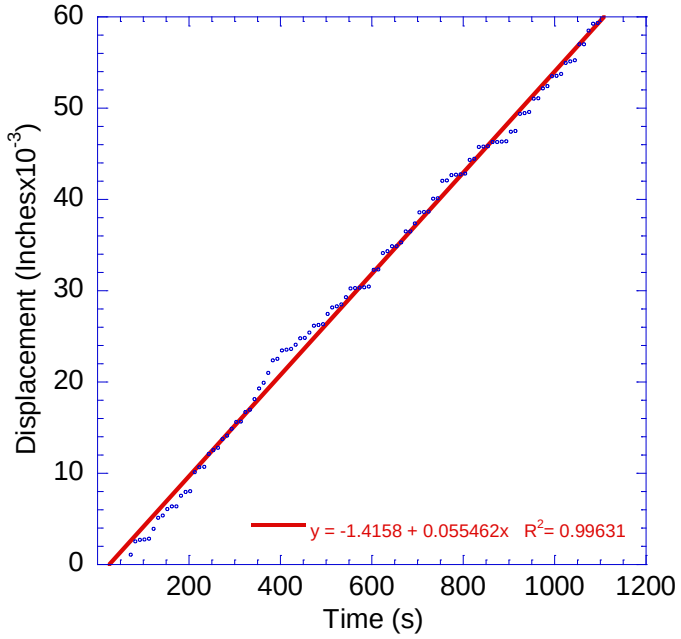

Figure B- 3: The displacement versus time results for a 0.6 water to cement ratio specimen at an age of 32 days and an applied pressure of 1.72 Mpa (250 psi). The testing fluid was water.

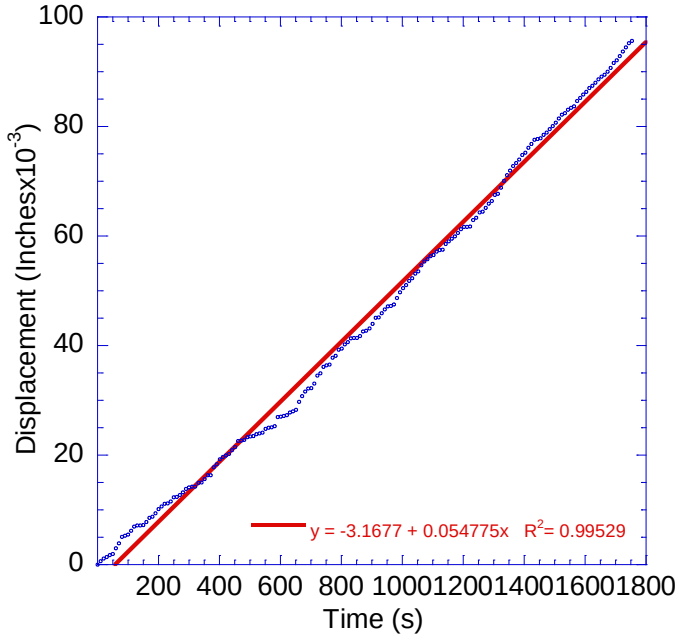

Figure B- 4: The displacement versus time results for a 0.6 water to cement ratio specimen at an age of 32 days and an applied pressure of 1.72 Mpa (250 psi). The testing fluid was water.

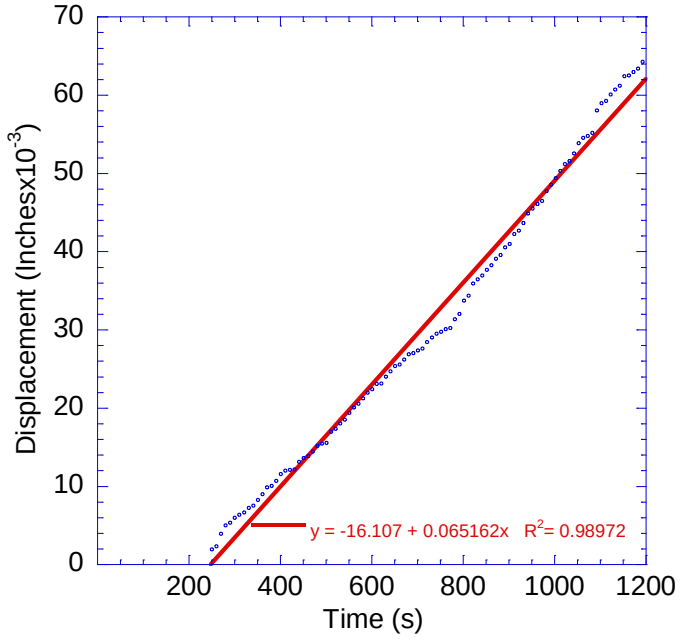

Figure B- 5: The displacement versus time results for a 0.6 water to cement ratio specimen at an age of 32 days and an applied pressure of 1.72 Mpa (250 psi). The testing fluid was water.

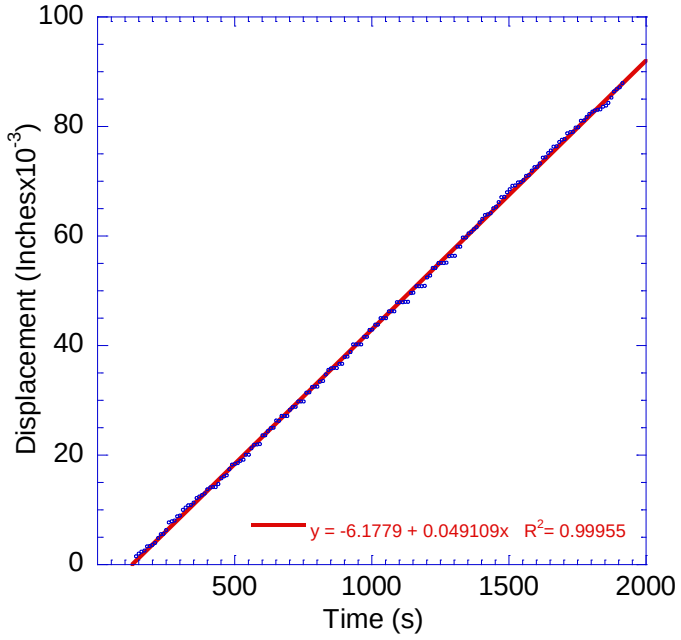

Figure B- 6: The displacement versus time results for a 0.6 water to cement ratio specimen at an age of 32 days and an applied pressure of 1.72 Mpa (250 psi). The testing fluid was water.

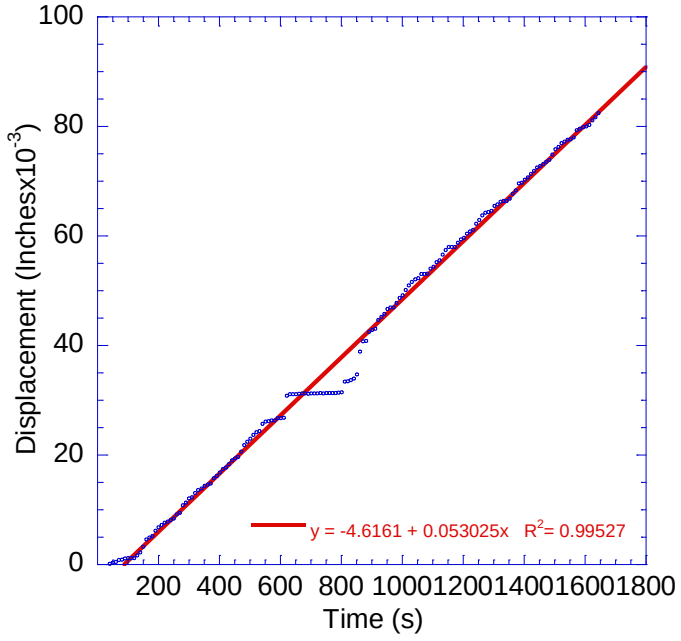

Figure B- 7: The displacement versus time results for a 0.6 water to cement ratio specimen at an age of 32 days and an applied pressure of 1.72 Mpa (250 psi). The testing fluid was water.

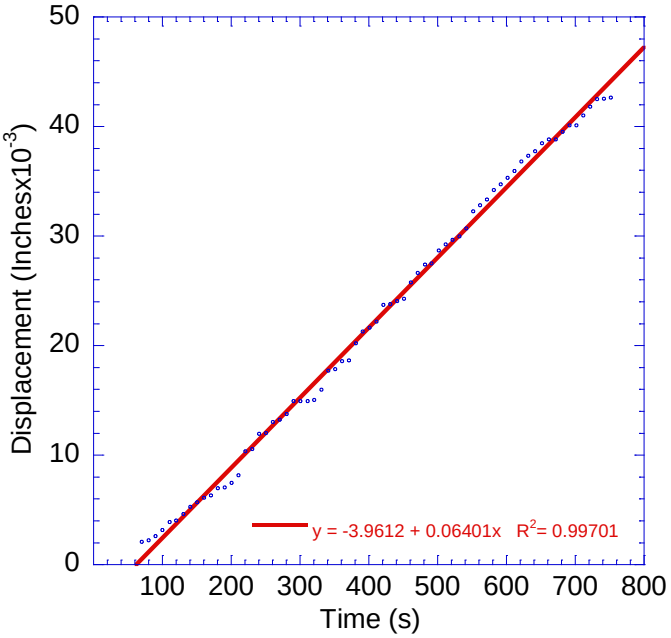

Figure B- 8: The displacement versus time results for a 0.6 water to cement ratio specimen at an age of 32 days and an applied pressure of 1.72 Mpa (250 psi). The testing fluid was water.

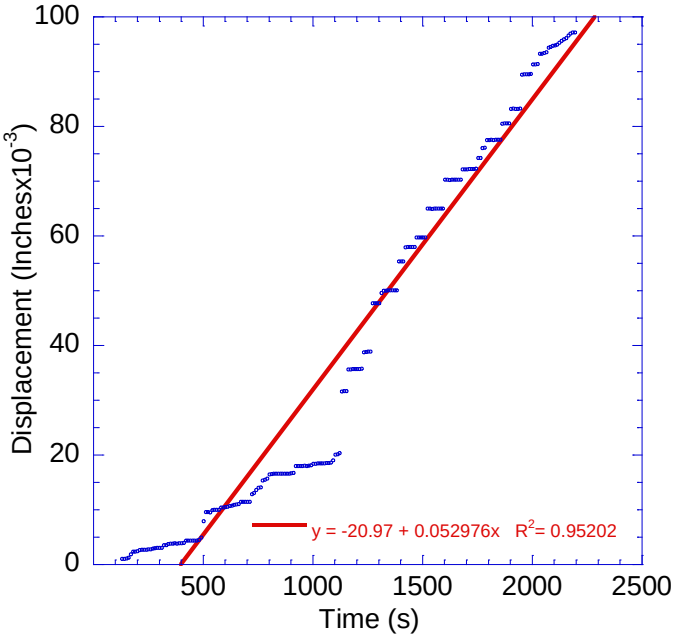

Figure B- 9: The displacement versus time results for a 0.6 water to cement ratio specimen at an age of 32 days and an applied pressure of 1.72 Mpa (250 psi). The testing fluid was water.

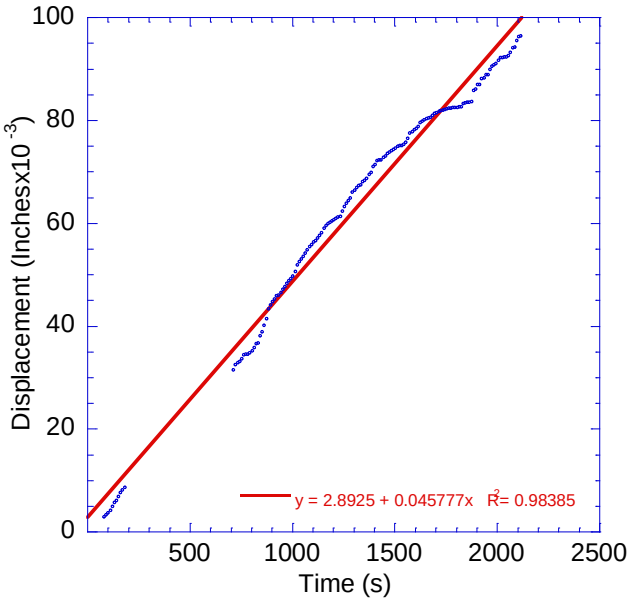

Figure B- 10: The displacement versus time results for a 0.6 water to cement ratio specimen at an age of 32 days and an applied pressure of 1.72 Mpa (250 psi). The testing fluid was water.

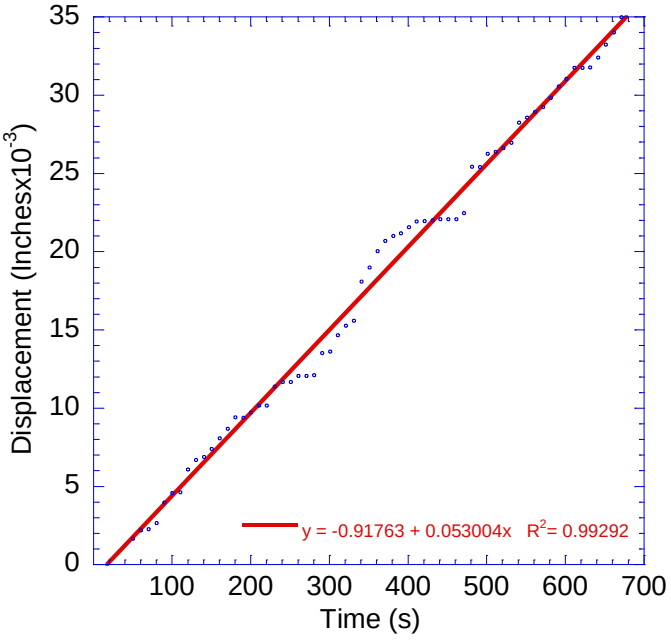

Figure B- 11: The displacement versus time results for a 0.6 water to cement ratio specimen at an age of 32 days and an applied pressure of 1.72 Mpa (250 psi). The testing fluid was water.

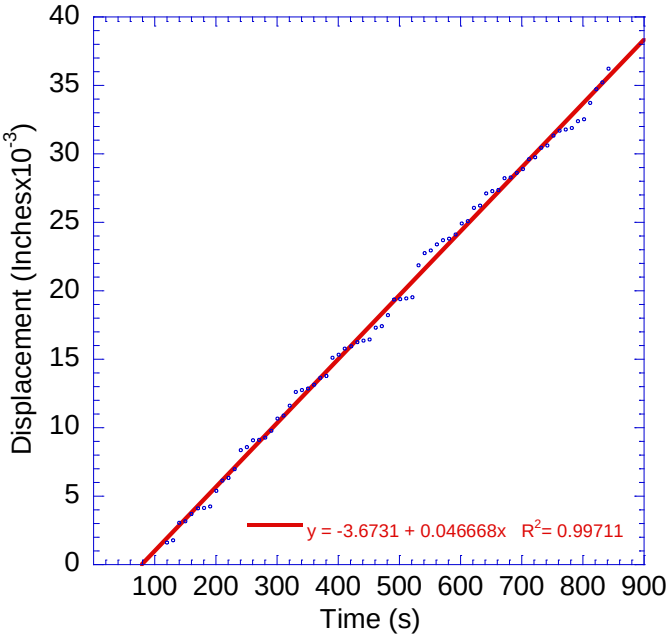

Figure B- 12: The displacement versus time results for a 0.6 water to cement ratio specimen at an age of 32 days and an applied pressure of 1.72 Mpa (250 psi). The testing fluid was water.

Cement Paste Hollow Dynamic Pressurization Plots

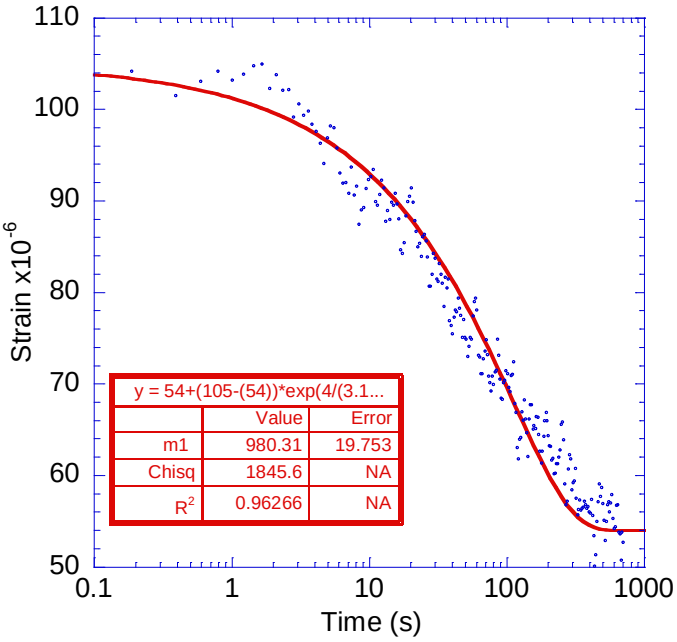

Figure B- 13: The strain versus time results for a 0.6 water to cement ratio specimen at an age of 33 days. The specimen was tested in water. Compressive strain is positive.

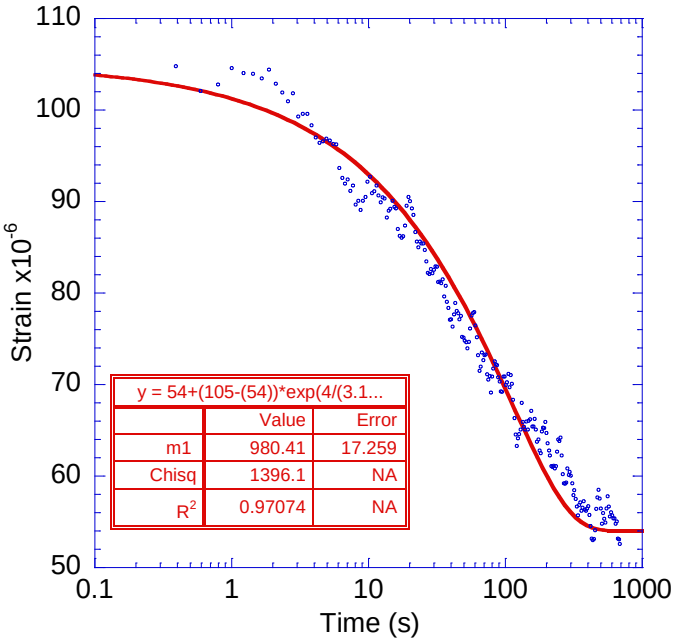

Figure B- 14: The strain versus time results for a 0.6 water to cement ratio specimen at an age of 33 days. The specimen was tested in water. Compressive strain is positive.

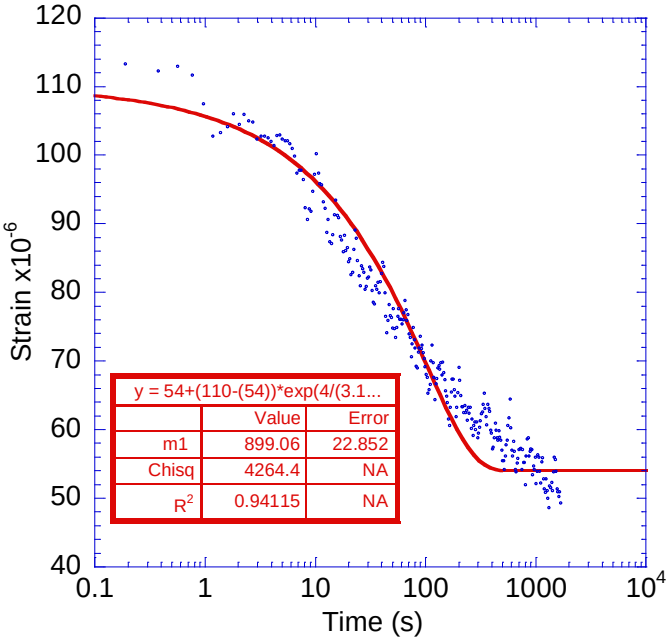

Figure B- 15: The strain versus time results for a 0.6 water to cement ratio specimen at an age of 33 days. The specimen was tested in water. Compressive strain is positive.

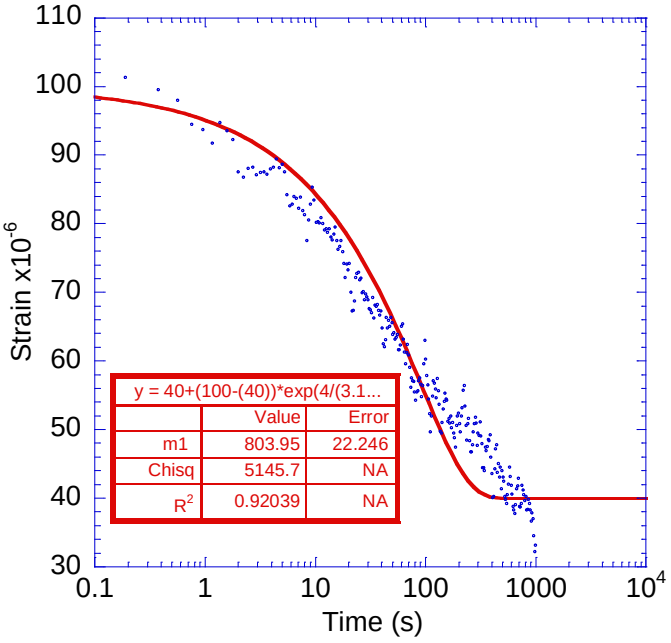

Figure B- 16: The strain versus time results for a 0.6 water to cement ratio specimen at an age of 33 days. The specimen was tested in water. Compressive strain is positive.

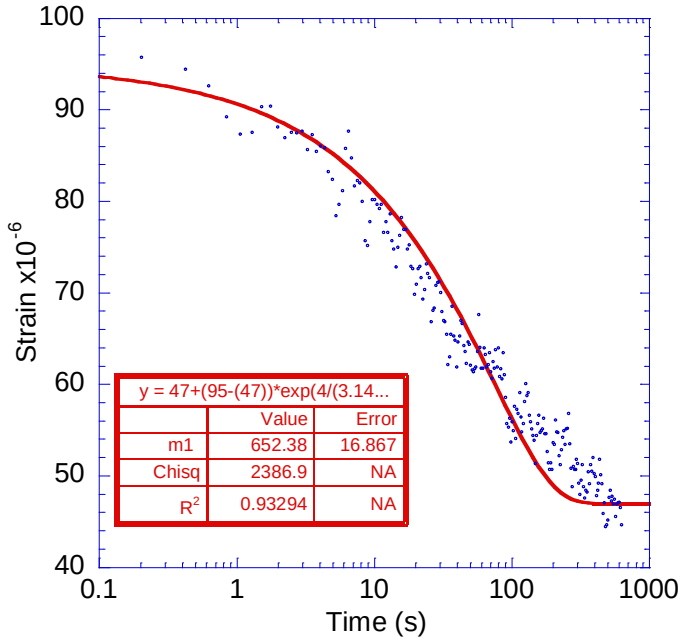

Figure B- 17: The strain versus time results for a 0.6 water to cement ratio specimen at an age of 33 days. The specimen was tested in water. Compressive strain is positive.

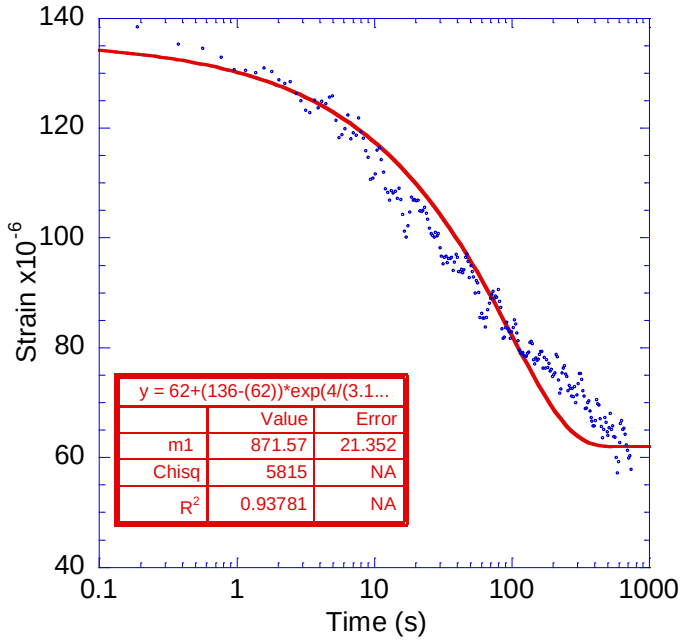

Figure B- 18: The strain versus time results for a 0.6 water to cement ratio specimen at an age of 33 days. The specimen was tested in water. Compressive strain is positive.

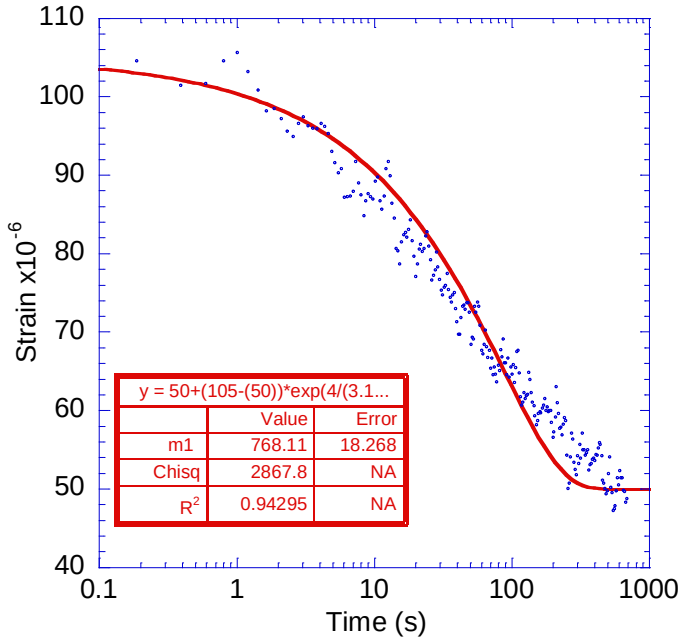

Figure B- 19: The strain versus time results for a 0.6 water to cement ratio specimen at an age of 33 days. The specimen was tested in water. Compressive strain is positive.

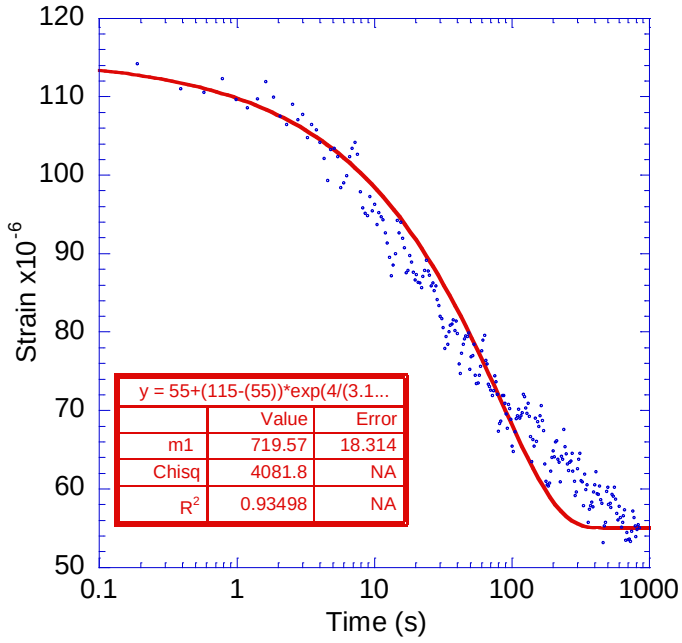

Figure B- 20: The strain versus time results for a 0.6 water to cement ratio specimen at an age of 33 days. The specimen was tested in water. Compressive strain is positive.

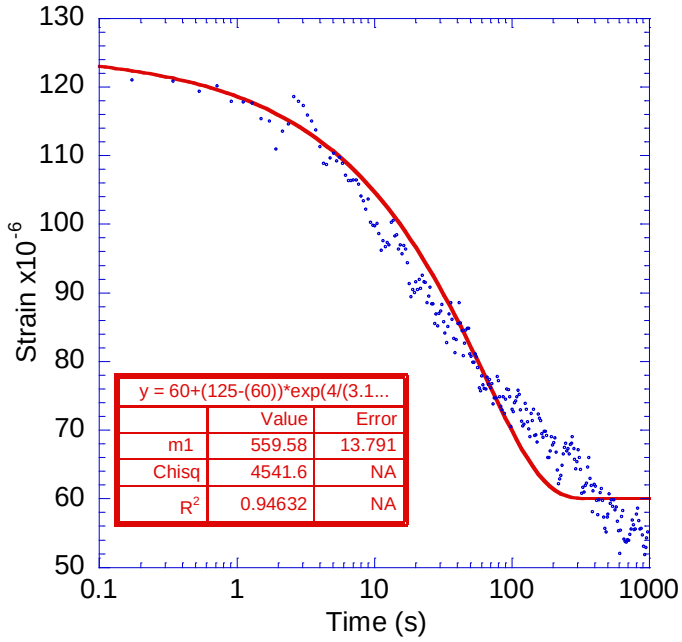

Figure B- 21: The strain versus time results for a 0.6 water to cement ratio specimen at an age of 33 days. The specimen was tested in water. Compressive strain is positive.

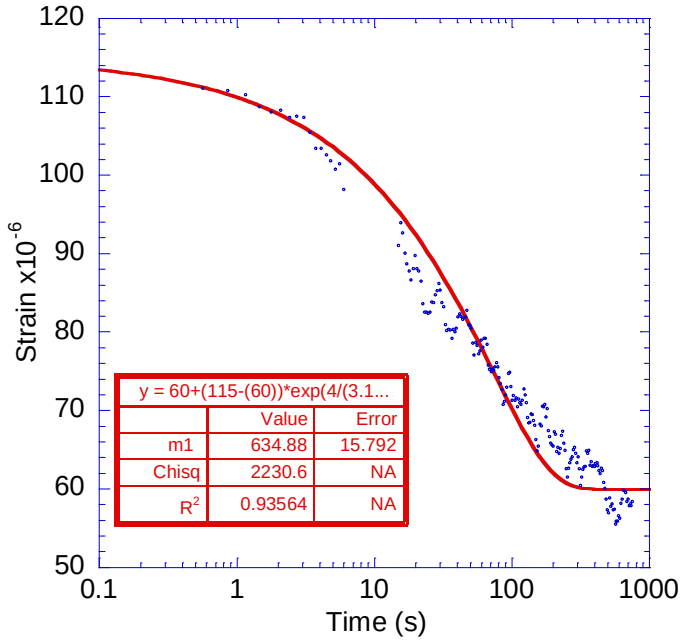

Figure B- 22: The strain versus time results for a 0.6 water to cement ratio specimen at an age of 33 days. The specimen was tested in water. Compressive strain is positive.

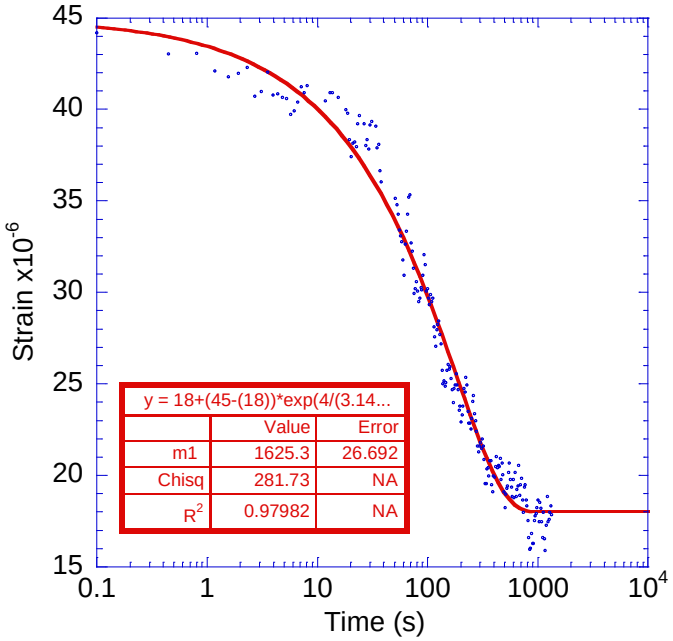

Figure B- 23: The strain versus time results for a 0.5 water to cement ratio specimen at an age of 96 hours. The specimen was tested in water. Compressive strain is positive.

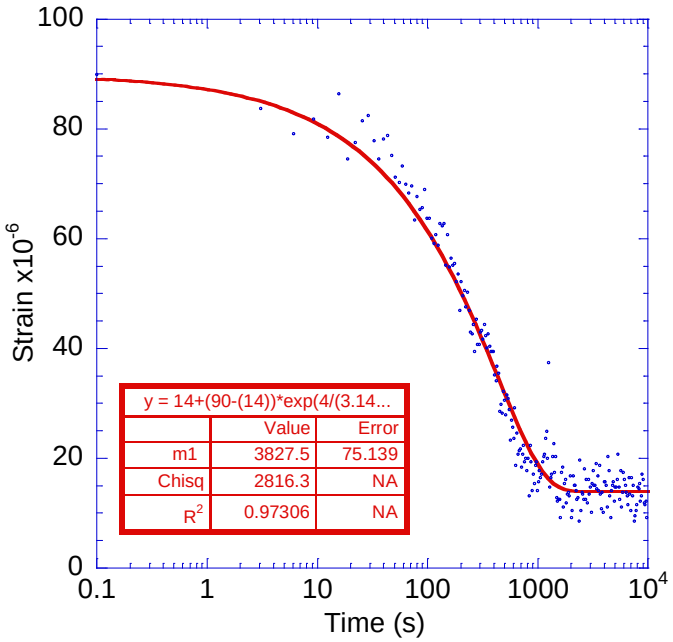

Figure B- 24: The strain versus time results for a 0.5 water to cement ratio specimen at an age of 99 hours. The specimen was tested in water. Compressive strain is positive.

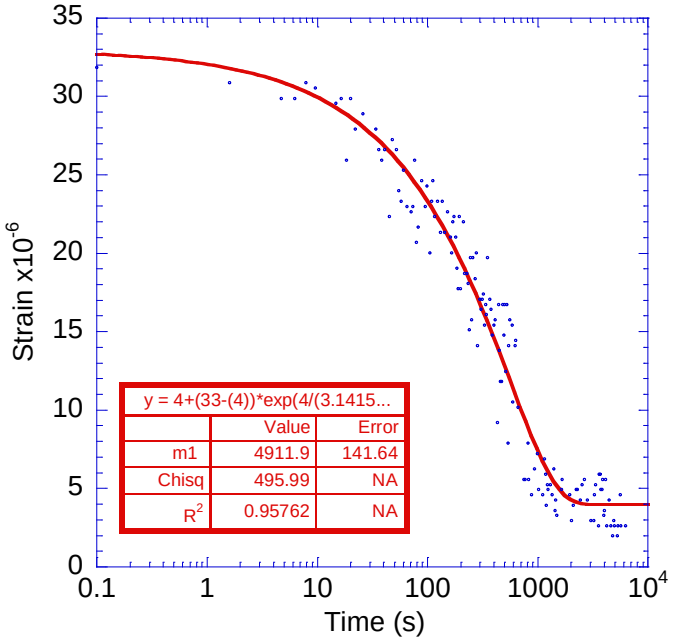

Figure B- 25: The strain versus time results for a 0.5 water to cement ratio specimen at an age of 115 hours. The specimen was tested in water. Compressive strain is positive.

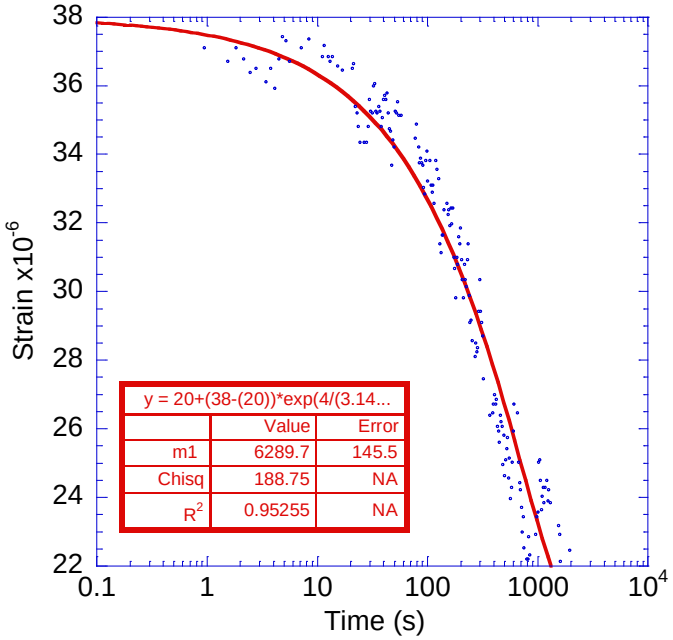

Figure B- 26: The strain versus time results for a 0.5 water to cement ratio specimen at an age of 117 hours. The specimen was tested in water. Compressive strain is positive.

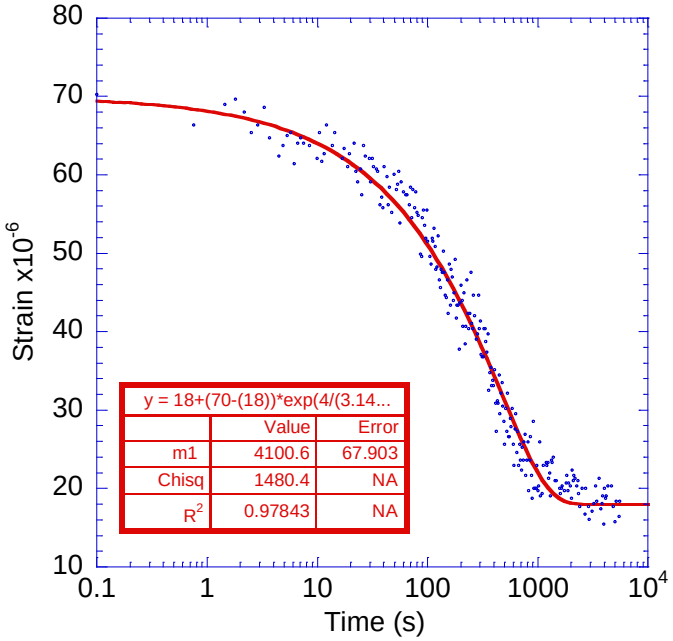

Figure B- 27: The strain versus time results for a 0.5 water to cement ratio specimen at an age of 119 hours. The specimen was tested in water. Compressive strain is positive.

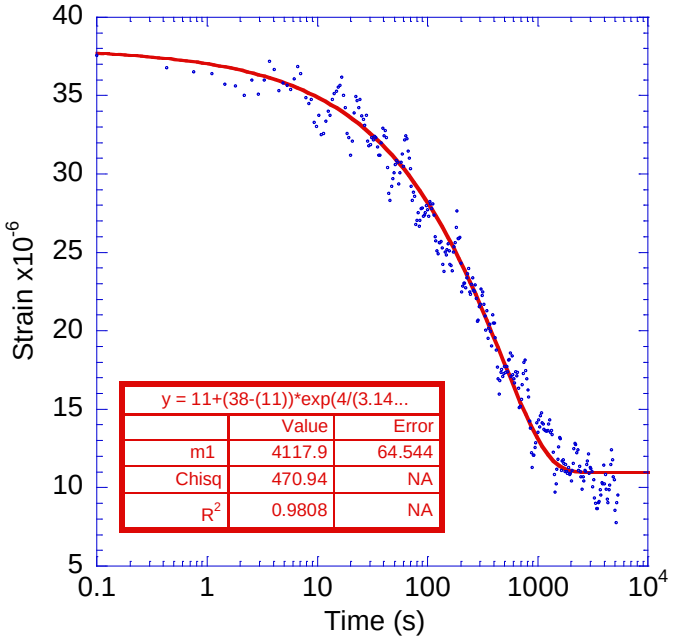

Figure B- 28: The strain versus time results for a 0.5 water to cement ratio specimen at an age of 121 hours. The specimen was tested in water. Compressive strain is positive.

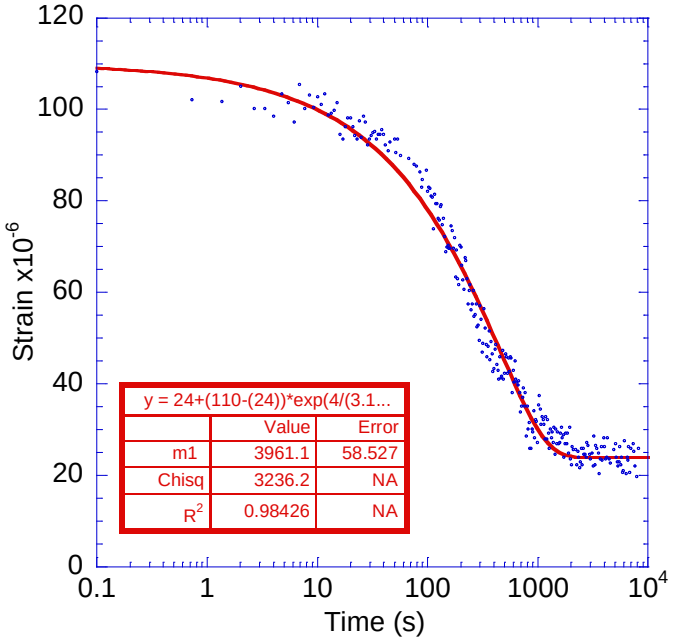

Figure B- 29: The strain versus time results for a 0.5 water to cement ratio specimen at an age of 122 hours. The specimen was tested in water. Compressive strain is positive.

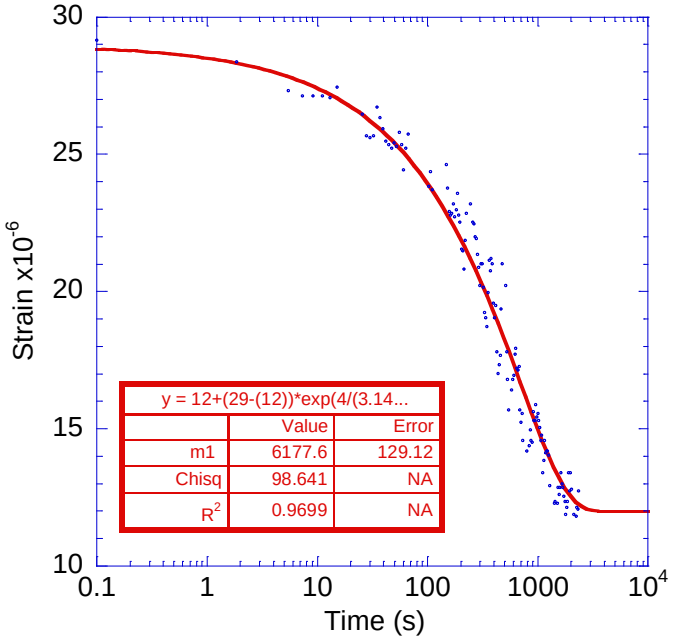

Figure B- 30: The strain versus time results for a 0.5 water to cement ratio specimen at an age of 139 hours. The specimen was tested in water. Compressive strain is positive.

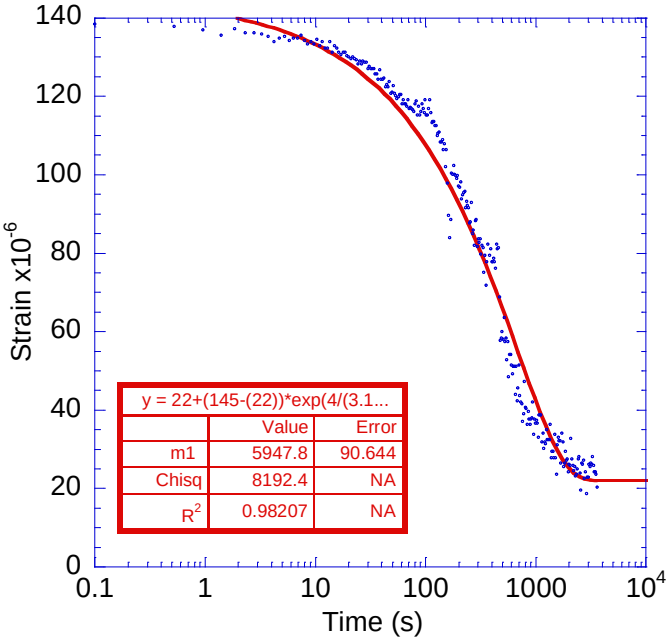

Figure B- 31: The strain versus time results for a 0.5 water to cement ratio specimen at an age of 140 hours. The specimen was tested in water. Compressive strain is positive.

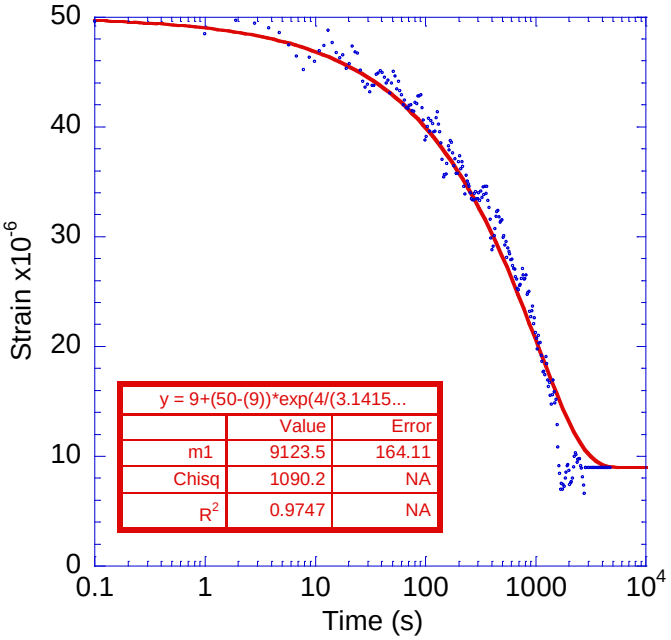

Figure B- 32: The strain versus time results for a 0.5 water to cement ratio specimen at an age of 141 hours. The specimen was tested in water. Compressive strain is positive.

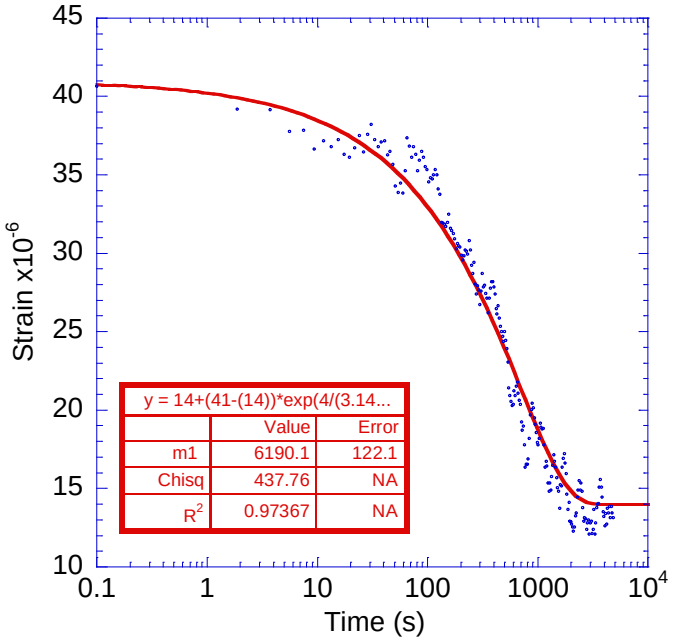

Figure B- 33: The strain versus time results for a 0.5 water to cement ratio specimen at an age of 142 hours. The specimen was tested in water. Compressive strain is positive.

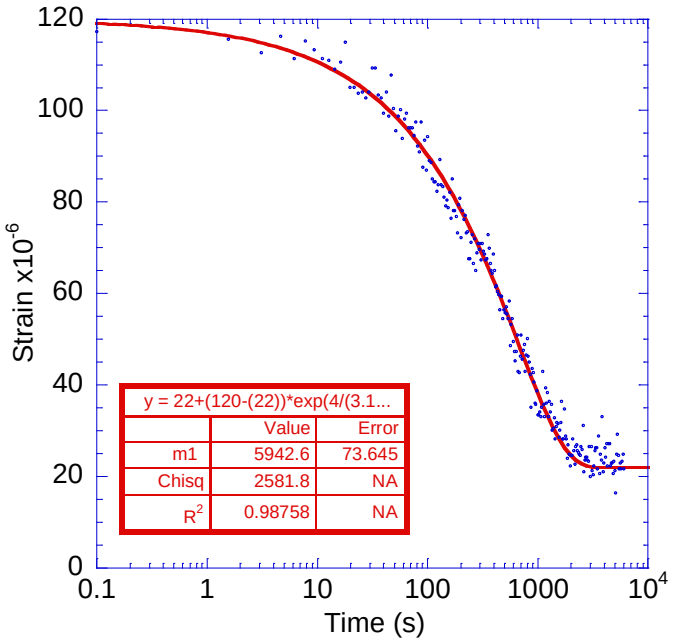

Figure B- 34: The strain versus time results for a 0.5 water to cement ratio specimen at an age of 143 hours. The specimen was tested in water. Compressive strain is positive.

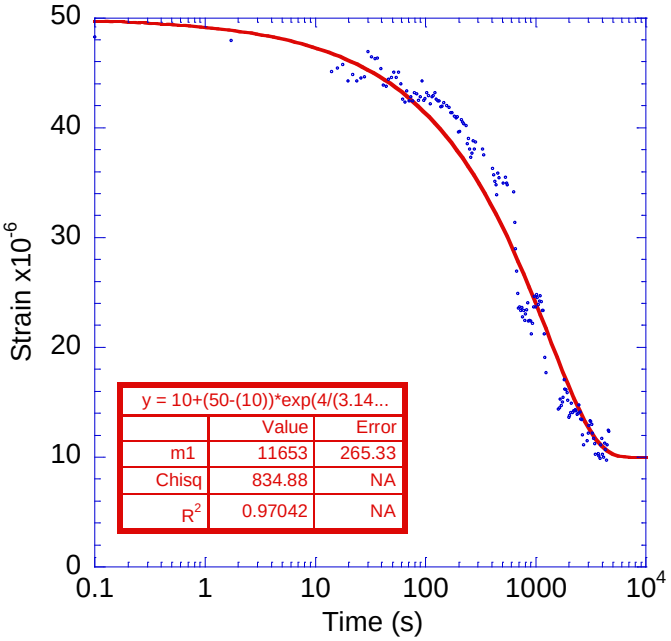

Figure B- 35: The strain versus time results for a 0.5 water to cement ratio specimen at an age of 145 hours. The specimen was tested in water. Compressive strain is positive.

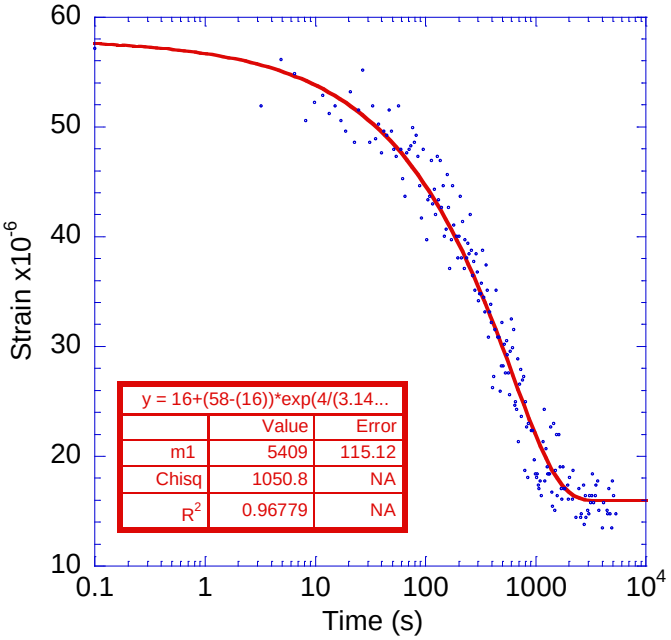

Figure B- 36: The strain versus time results for a 0.5 water to cement ratio specimen at an age of 147 hours. The specimen was tested in water. Compressive strain is positive.

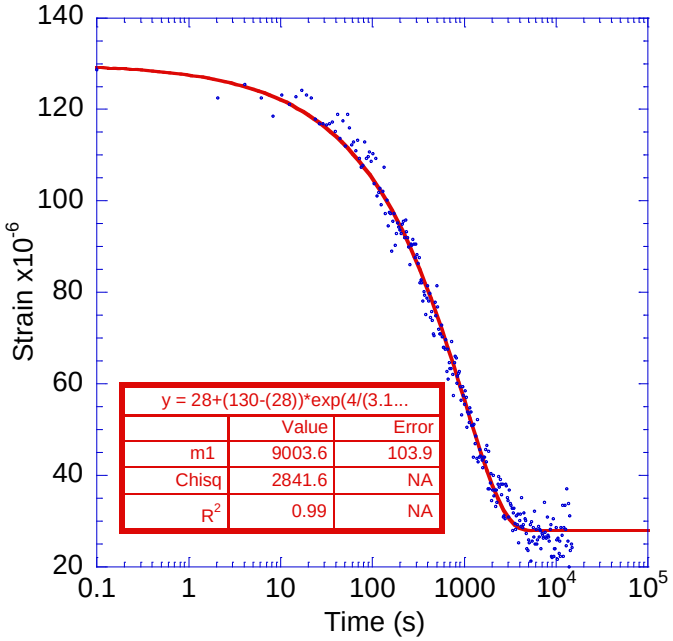

Figure B- 37: The strain versus time results for a 0.5 water to cement ratio specimen at an age of 163 hours. The specimen was tested in water. Compressive strain is positive.

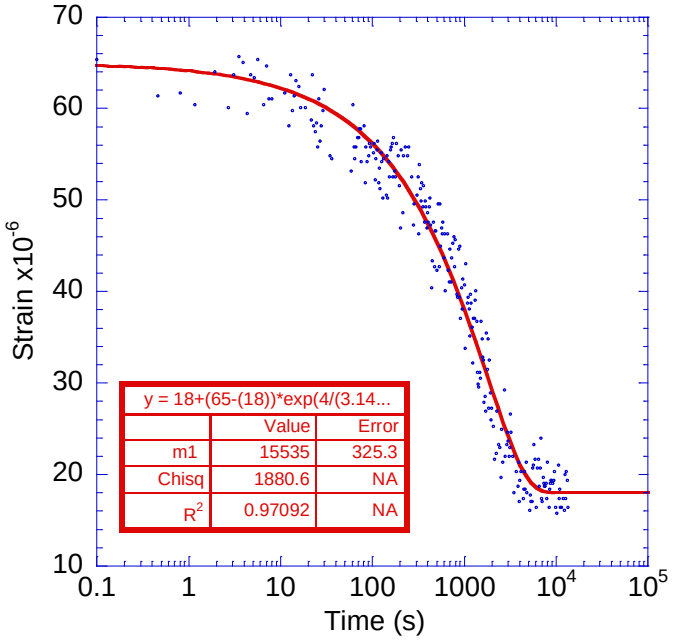

Figure B- 38: The strain versus time results for a 0.5 water to cement ratio specimen at an age of 167 hours. The specimen was tested in water. Compressive strain is positive.

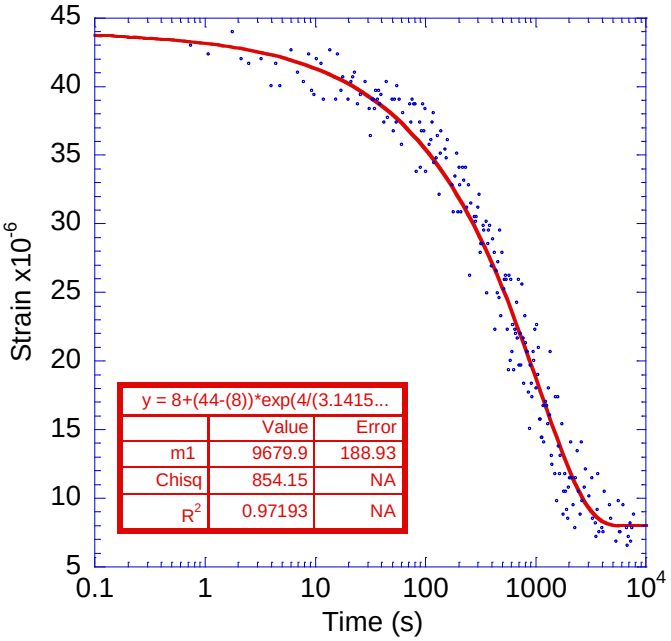

Figure B- 39: The strain versus time results for a 0.5 water to cement ratio specimen at an age of 171 hours. The specimen was tested in water. Compressive strain is positive.

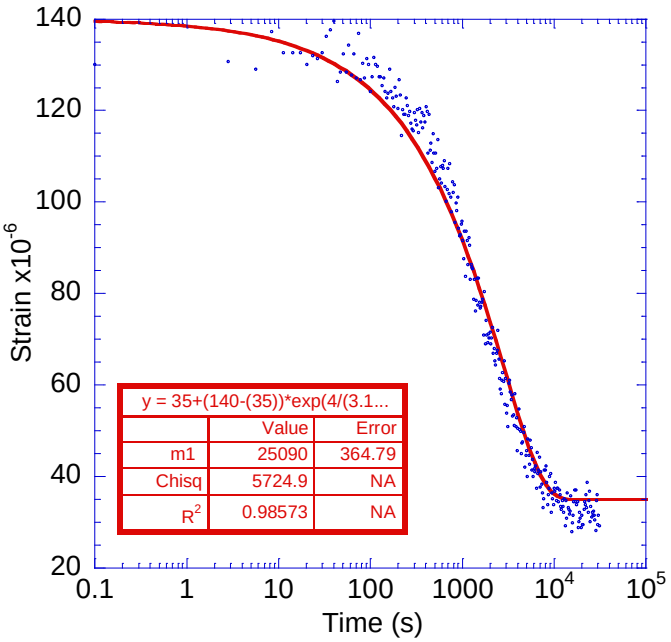

Figure B- 40: The strain versus time results for a 0.5 water to cement ratio specimen at an age of 235 hours. The specimen was tested in water. Compressive strain is positive.

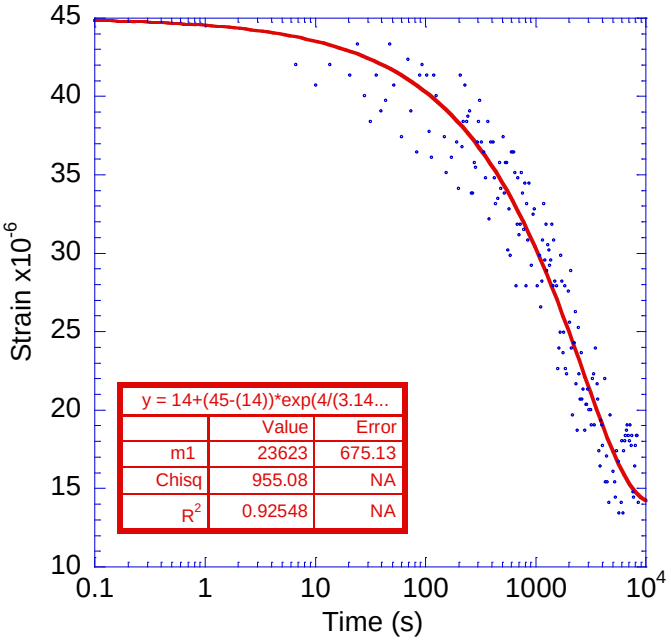

Figure B- 41: The strain versus time results for a 0.5 water to cement ratio specimen at an age of 258 hours. The specimen was tested in water. Compressive strain is positive.

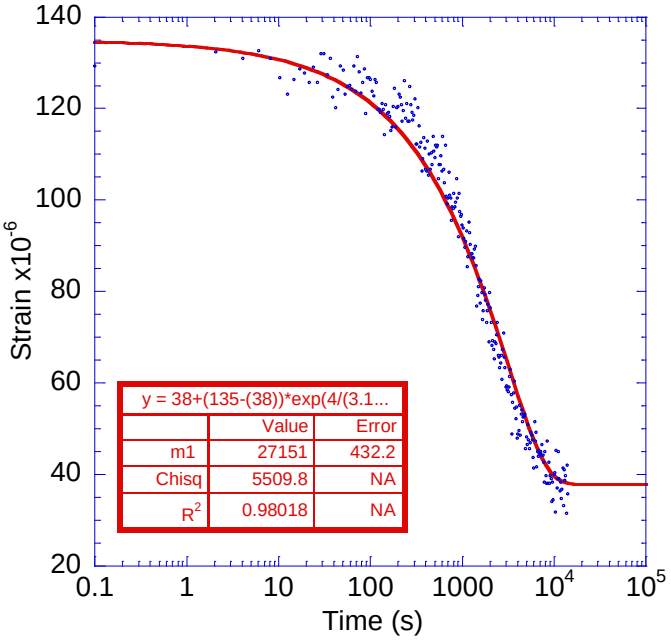

Figure B- 42: The strain versus time results for a 0.5 water to cement ratio specimen at an age of 263 hours. The specimen was tested in water. Compressive strain is positive.

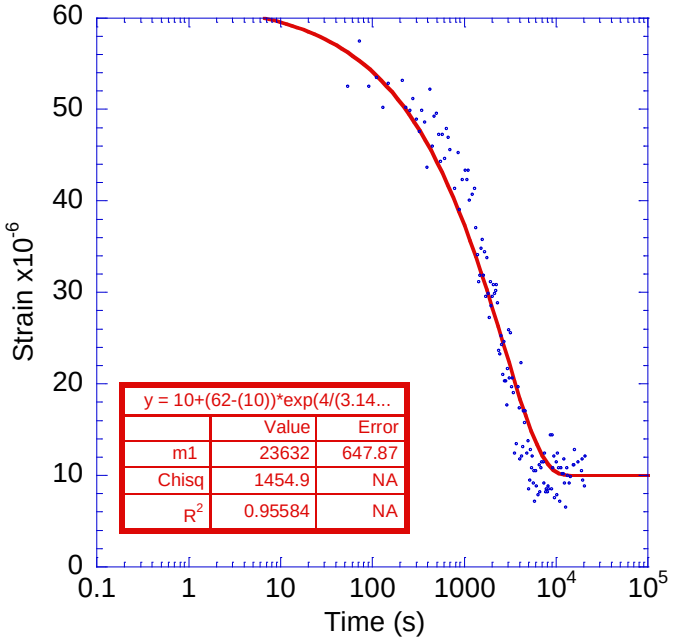

Figure B- 43: The strain versus time results for a 0.5 water to cement ratio specimen at an age of 267 hours. The specimen was tested in water. Compressive strain is positive.

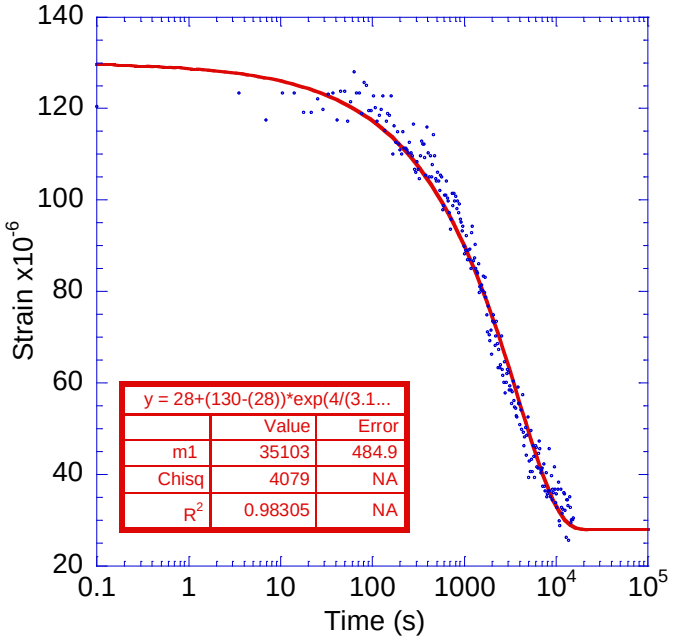

Figure B- 44: The strain versus time results for a 0.5 water to cement ratio specimen at an age of 286 hours. The specimen was tested in water. Compressive strain is positive.

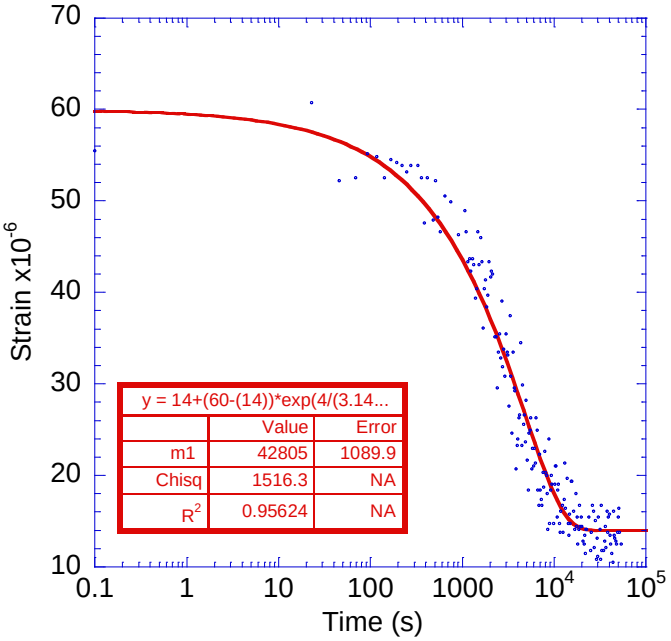

Figure B- 45: The strain versus time results for a 0.5 water to cement ratio specimen at an age of 291 hours. The specimen was tested in water. Compressive strain is positive.

Cement Paste Solid Dynamic Pressurization Plots

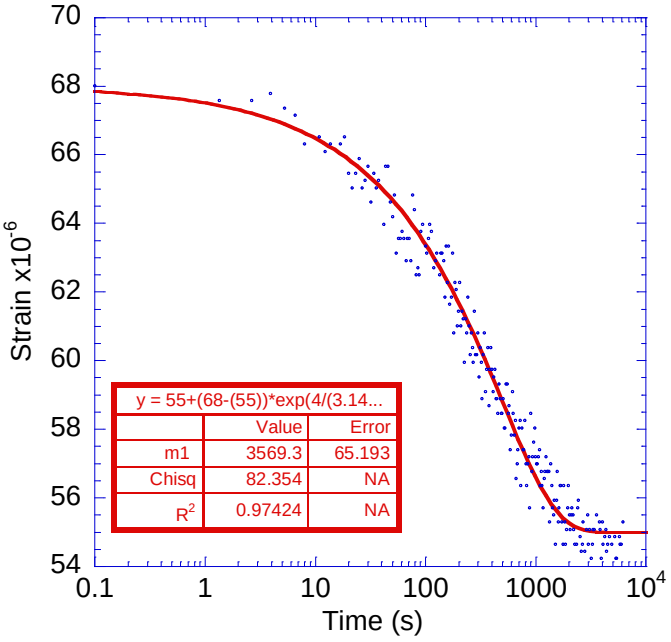

Figure B- 46: The strain versus time results for a 0.5 water to cement ratio specimen at an age of 94 hours. The specimen was tested in water. Compressive strain is positive.

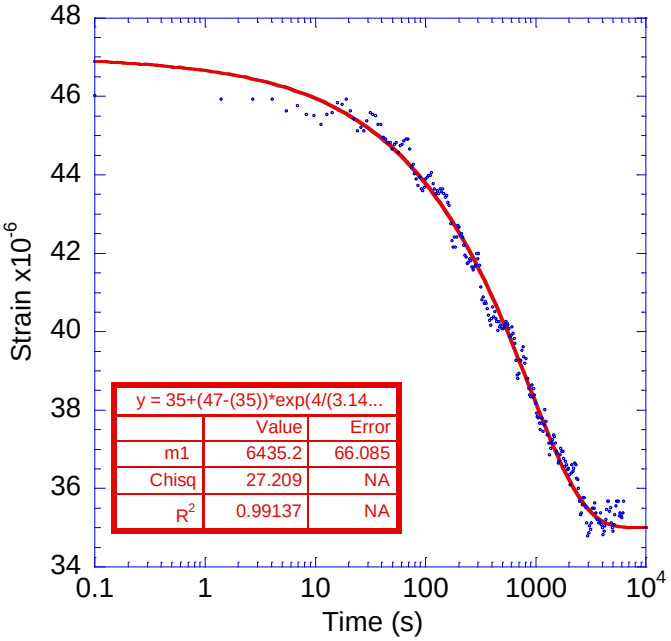

Figure B- 47: The strain versus time results for a 0.5 water to cement ratio specimen at an age of 115 hours. The specimen was tested in water. Compressive strain is positive.

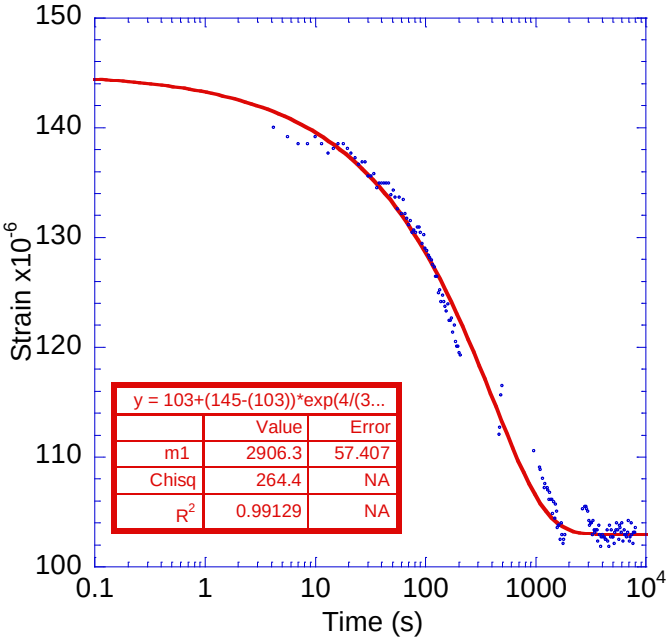

Figure B- 48: The strain versus time results for a 0.5 water to cement ratio specimen at an age of 117 hours. The specimen was tested in water. Compressive strain is positive.

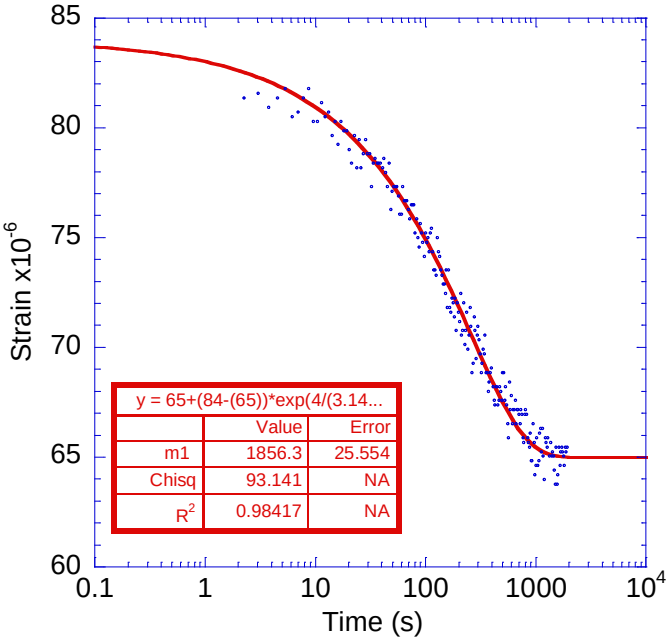

Figure B- 49: The strain versus time results for a 0.5 water to cement ratio specimen at an age of 121 hours. The specimen was tested in water. Compressive strain is positive.

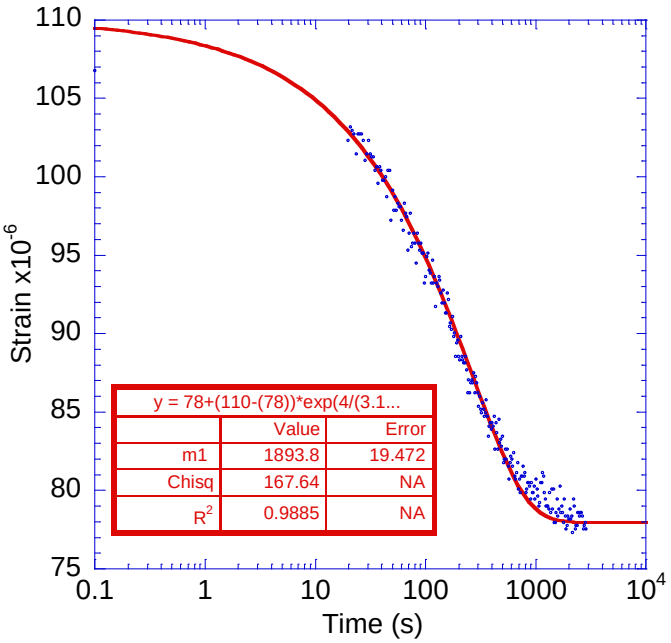

Figure B- 50: The strain versus time results for a 0.5 water to cement ratio specimen at an age of 139 hours. The specimen was tested in water. Compressive strain is positive.

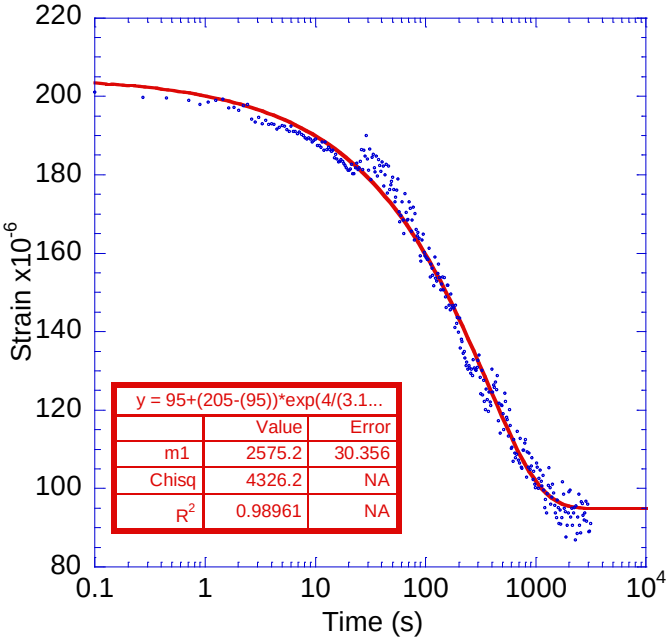

Figure B- 51: The strain versus time results for a 0.5 water to cement ratio specimen at an age of 140 hours. The specimen was tested in water. Compressive strain is positive.

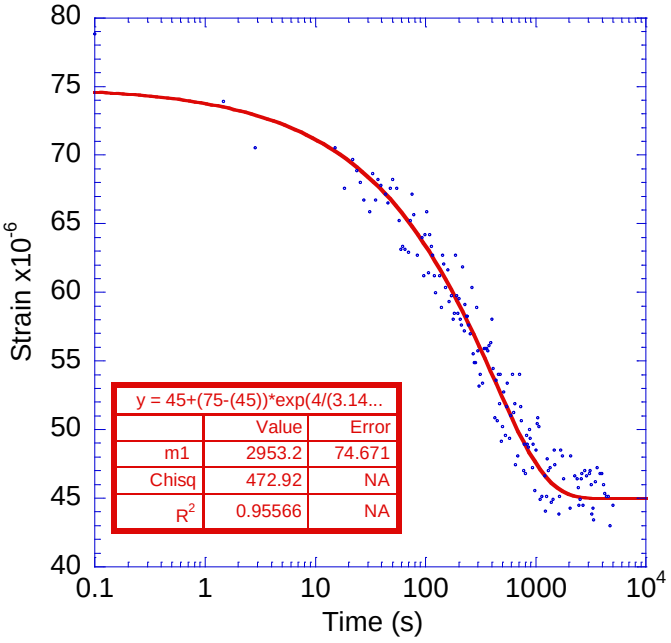

Figure B- 52: The strain versus time results for a 0.5 water to cement ratio specimen at an age of 142 hours. The specimen was tested in water. Compressive strain is positive.

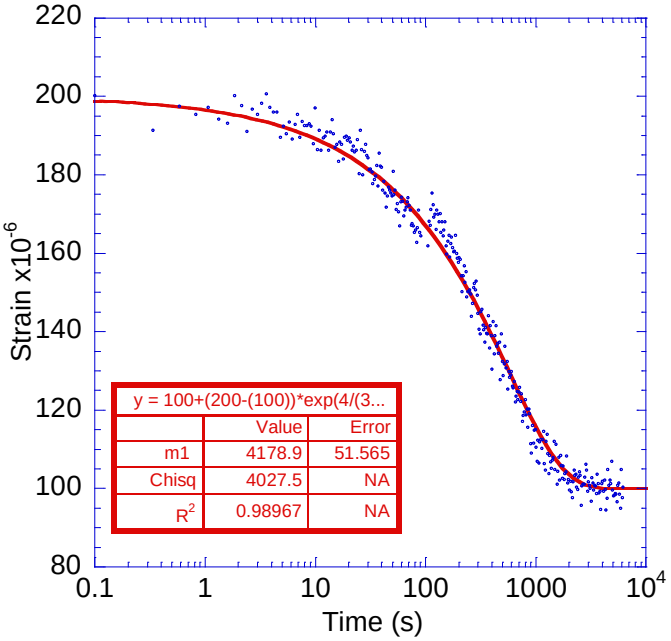

Figure B- 53: The strain versus time results for a 0.5 water to cement ratio specimen at an age of 143 hours. The specimen was tested in water. Compressive strain is positive.

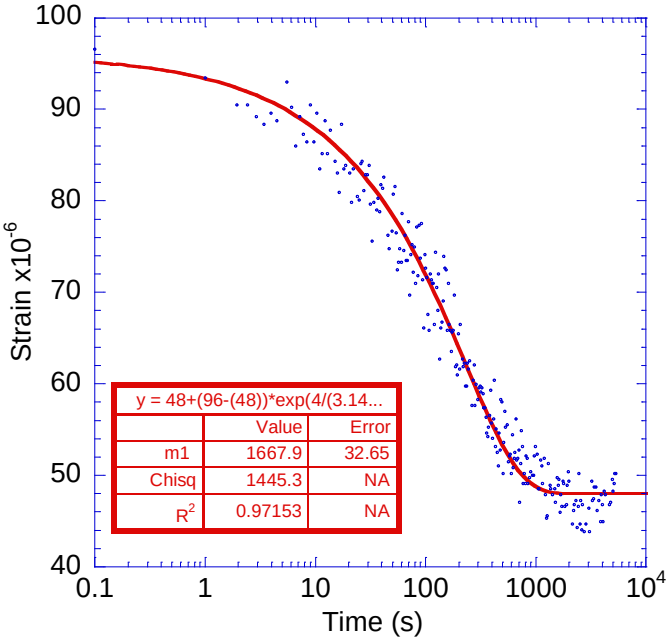

Figure B- 54: The strain versus time results for a 0.5 water to cement ratio specimen at an age of 145 hours. The specimen was tested in water. Compressive strain is positive.

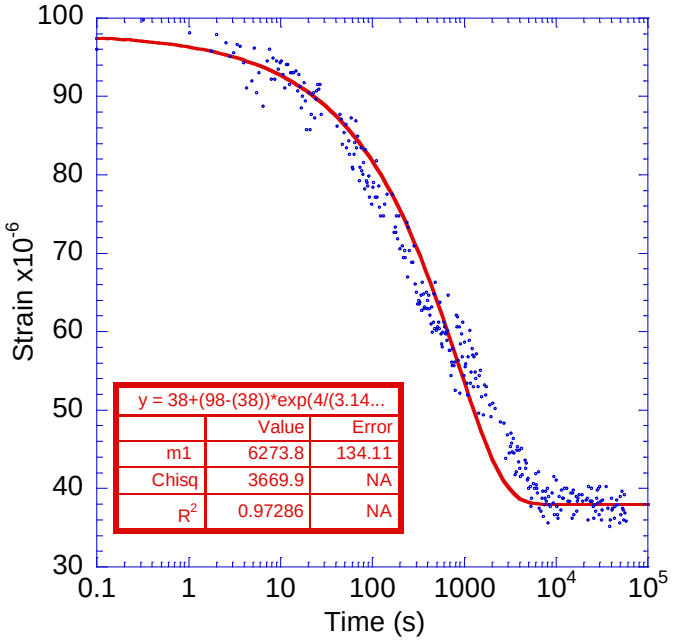

Figure B- 55: The strain versus time results for a 0.5 water to cement ratio specimen at an age of 146 hours. The specimen was tested in water. Compressive strain is positive.

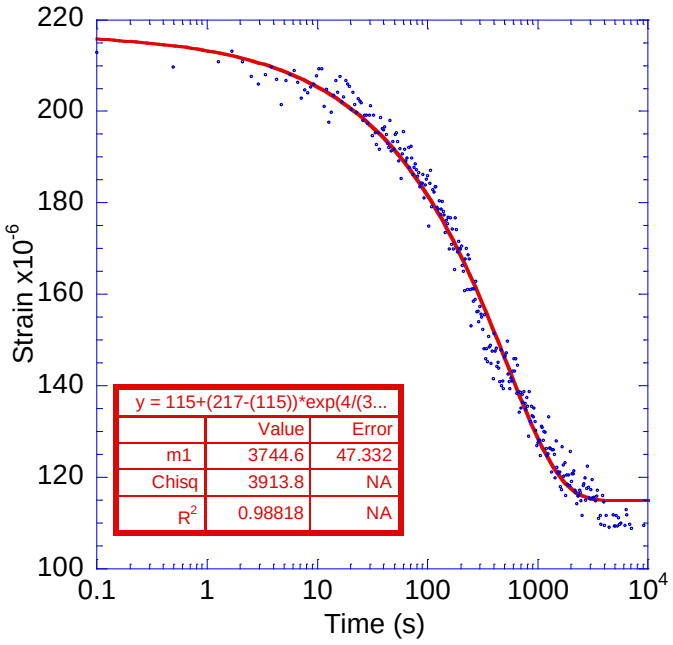

Figure B- 56: The strain versus time results for a 0.5 water to cement ratio specimen at an age of 163 hours. The specimen was tested in water. Compressive strain is positive.

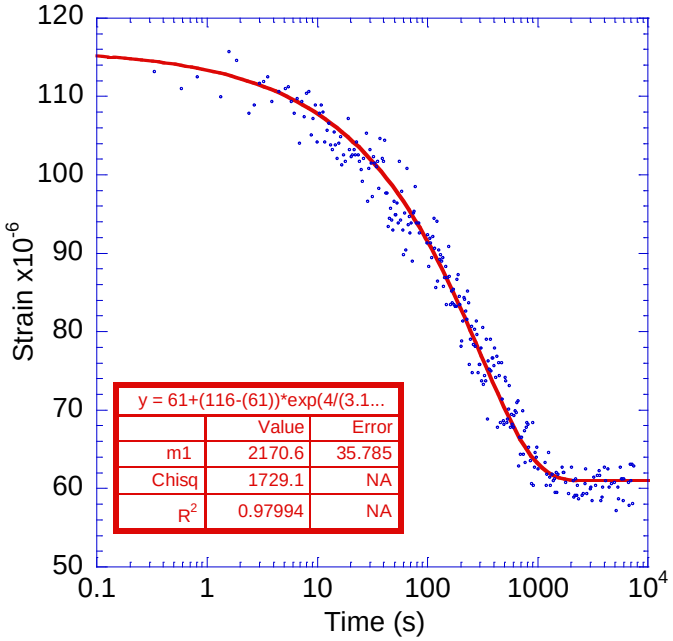

Figure B- 57: The strain versus time results for a 0.5 water to cement ratio specimen at an age of 167 hours. The specimen was tested in water. Compressive strain is positive.

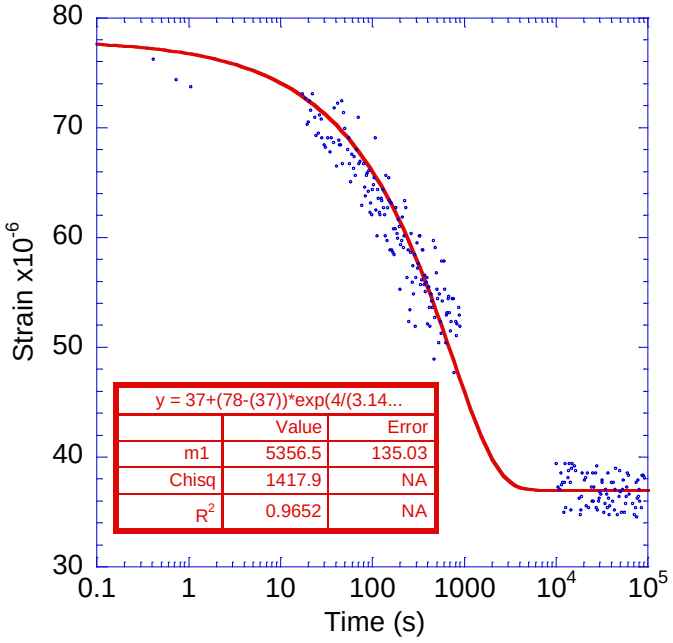

Figure B- 58: The strain versus time results for a 0.5 water to cement ratio specimen at an age of 171 hours. The specimen was tested in water. Compressive strain is positive.

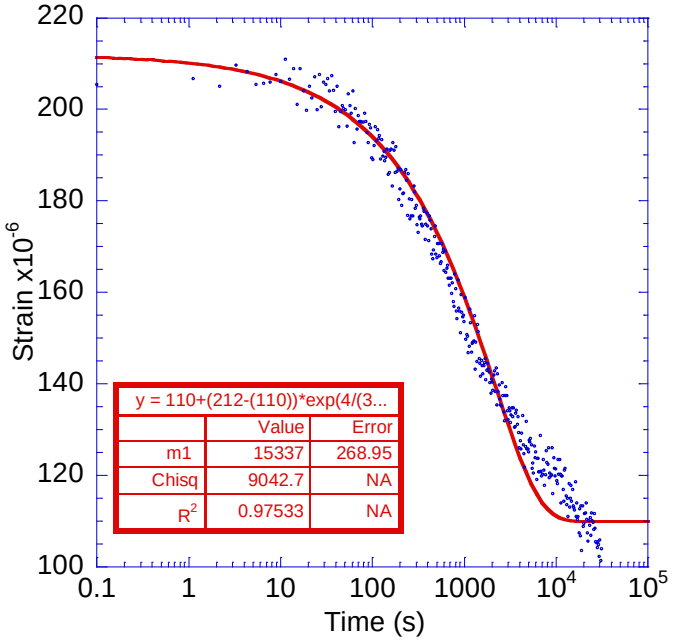

Figure B- 59: The strain versus time results for a 0.5 water to cement ratio specimen at an age of 235 hours. The specimen was tested in water. Compressive strain is positive.

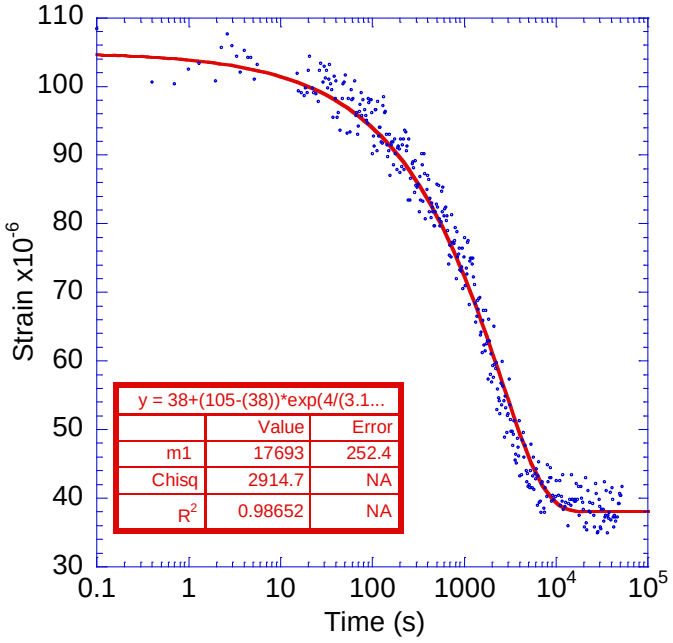

Figure B- 60: The strain versus time results for a 0.5 water to cement ratio specimen at an age of 244 hours. The specimen was tested in water. Compressive strain is positive.

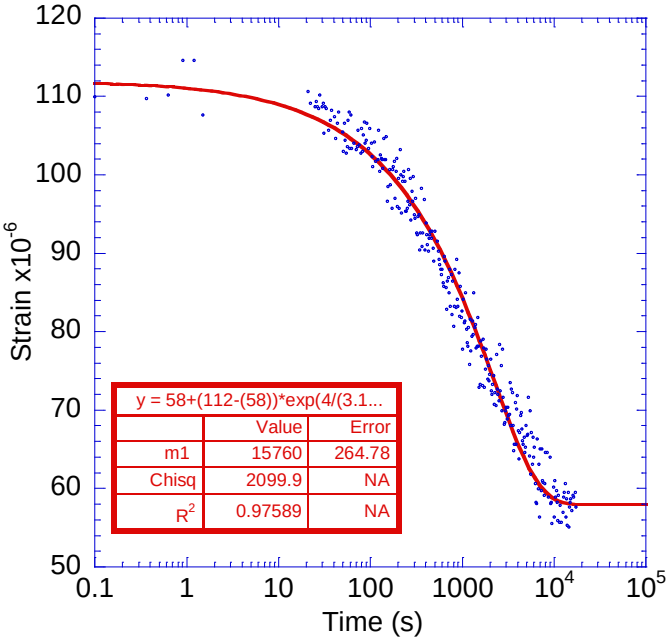

Figure B- 61: The strain versus time results for a 0.5 water to cement ratio specimen at an age of 258 hours. The specimen was tested in water. Compressive strain is positive.

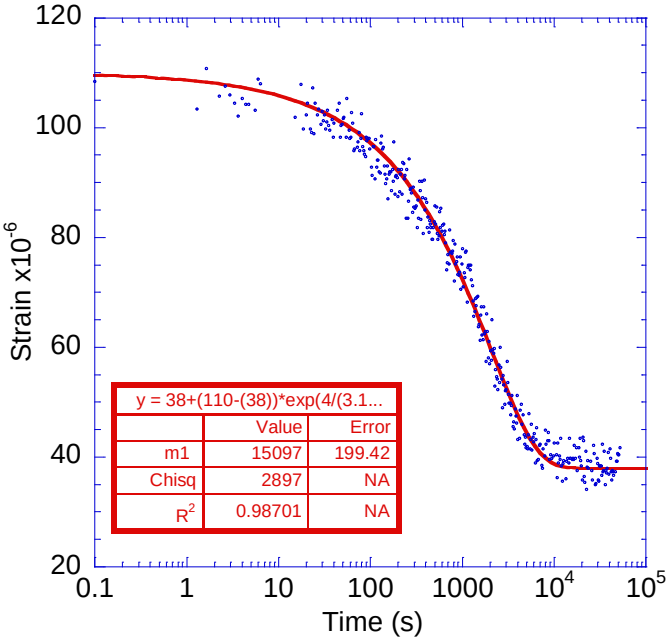

Figure B- 62: The strain versus time results for a 0.5 water to cement ratio specimen at an age of 263 hours. The specimen was tested in water. Compressive strain is positive.

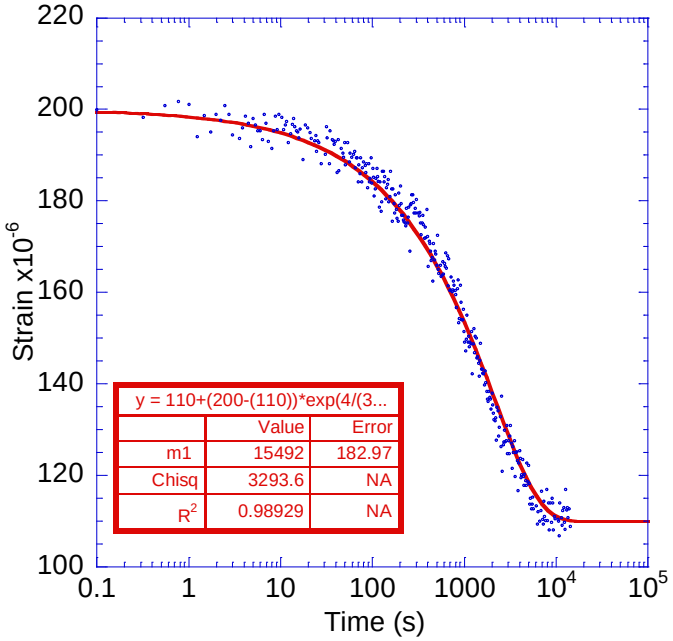

Figure B- 63: The strain versus time results for a 0.5 water to cement ratio specimen at an age of 267 hours. The specimen was tested in water. Compressive strain is positive.

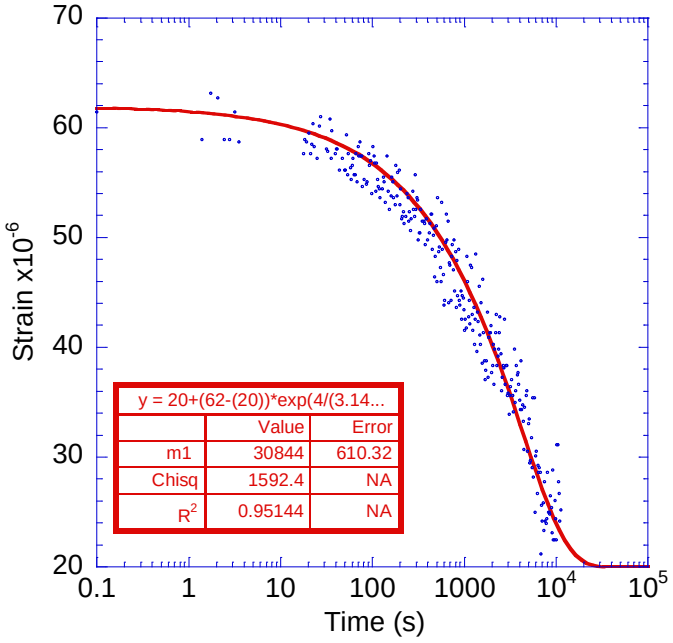

Figure B- 64: The strain versus time results for a 0.5 water to cement ratio specimen at an age of 283 hours. The specimen was tested in water. Compressive strain is positive.

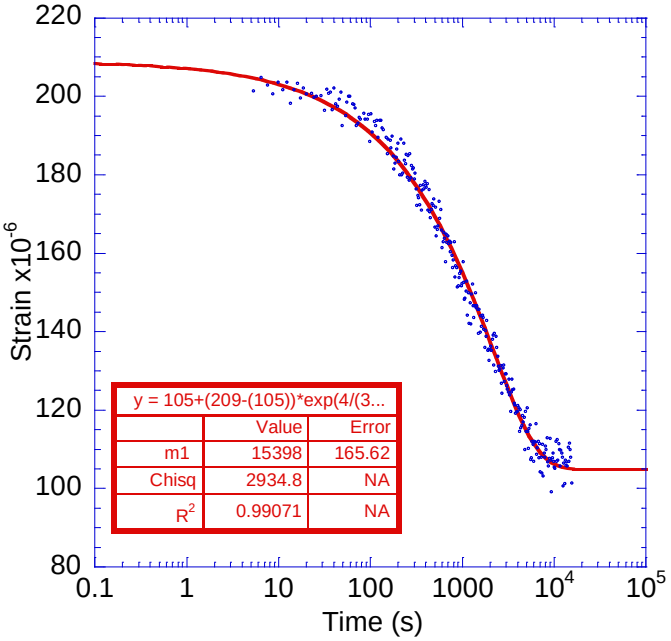

Figure B- 65: The strain versus time results for a 0.5 water to cement ratio specimen at an age of 286 hours. The specimen was tested in water. Compressive strain is positive.

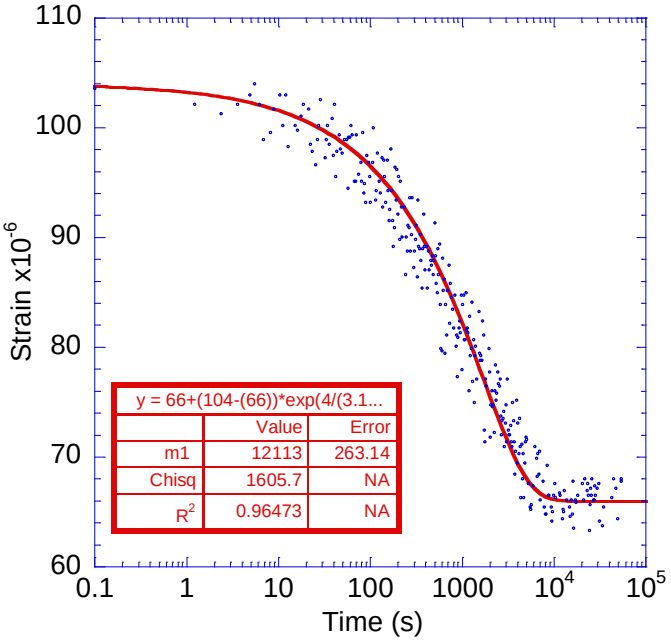

Figure B- 66: The strain versus time results for a 0.5 water to cement ratio specimen at an age of 291 hours. The specimen was tested in water. Compressive strain is positive.

VITA

Christopher Andrew Jones was born in Corpus Christi, Texas. After graduating from W.B. Ray High School in 2001, he enrolled in the 3-2 Dual Degree Engineering Program at Southwestern University in Georgetown, Texas. Once he completed his three years at Southwestern, Christopher enrolled as a student at Texas A&M University in College Station, Texas where he graduated with a B.S. in civil engineering in December of 2006. At this point Christopher was also awarded his B.A. in physical science from Southwestern. While working on his master's degree Christopher was supported by the Transportation Scholars Program through the Federal Highway Administration. He will graduate with his Master of Science in August of 2008. Christopher will continue at A&M and start work on his Ph.D.

Christopher A. Jones

8413 Alison Ave.

College Station, Texas 77845